



Modelica models of PV elements
For system-level
Simulation and Control studies

MAGED MAHROUS ABDELSATTAR MAHROUS
matricola / 798430

Supervised by Professor Alberto Leva

Master of Science Thesis in Automation Engineering
Scuola di Ingegneria dell' Informazione
Politecnico di Milano
A.Y. 2014/2015

CONTENTS

ACKNOWLEDGEMENT

ABSTRACT

CHAPTER ONE: INTRODUCTION

1. 1	Overview of the problem	2
1. 2	Brief Literature review	4
1. 3	Motivation	6
1. 4	Objectives of the study	7
1. 5	Outline of the Dissertation	8

CHAPTER TWO: MODEL COMPONENTS

2. 1	Photovoltaic cell	11
2. 2	Battery	21
2. 3	Inverter	29

CHAPTER THREE: MODELICA IMPLEMENTATION

3. 1	Photovoltaic Cells	40
3. 2	Battery	58
3. 3	Inverter	68

CHAPTER FOUR: SIMULATION EXAMPLES

4. 1	Controller	79
4. 2	Islanded load simulation example	99
4. 3	Grid connected simulation example	106

CHAPTER FIVE: CONCLUSION AND FUTURE WORKS

5.	CONCLUSION AND FUTURE WORKS	112
----	-----------------------------	-----

LIST OF FIGURES

REFERENCES

To my father, mother, and brother;
without whom, I would not be the person I am today.
I dedicate this work as a small exchange
for your love and support.

Also I would like to mention my appreciation for all my colleagues
and Professors for all what I learned during my Masters and
especially Prof. Alberto Leva for his support and guidance through
all the steps to deliver this thesis.

Thank you.

ABSTRACT

As the renewable energy became essential and competitive source of energy, new simulation models are needed to help comparing the feasibility of using renewable energy sources with the grid and discuss its connection and energy optimization problems in a simple and clear way. This thesis presents a number of models for modelling, simulation and control of a photovoltaic system, equipped with battery and inverter to be connected to AC loads directly or to be synchronized with the electric network. The models are realized in Modelica, in order to create a useful library that compare the technical issues related to PV systems in connection with the grid and also can be integrated with similar Modelica models developed in the future. After an introduction to describe the problem, explain the work motivation and discussing the basis of modelling of each component, the approximations done were explained and justified in order to give a reasonable balance between the modelling details and computational time. Some simulation examples were applied and commented to justify the results and confirm the objectives of the models were achieved.

SOMMARIO

La crescente importanza e competitività delle fonti energetiche rinnovabili richiede modelli di simulazione adatti alla valutazione del loro impiego nel contesto delle reti in modo affidabile e computazionalmente efficiente. Questa tesi presenta modelli siffatti per i principali elementi dei sistemi fotovoltaici, con particolare riferimento a pannelli, batterie e inverter, atti allo studio di sistemi sia isolati che connessi alla rete elettrica. I modelli sono realizzati in Modelica e pensati per ampliare di una libreria di dimensioni più ampie, rendendola adatta a studiare le maggiori questioni tecniche relativi ai sistemi fotovoltaici in rete e mantenendola flessibile a fronte di sviluppi futuri. Dopo un'introduzione che descrive il problema, motiva il lavoro e discute le basi della modellistica di ciascuno dei componenti trattati, le approssimazioni introdotte vengono discusse e giustificate nell'ottica di un ragionevole bilanciamento tra complessità ed efficienza computazionale. Si riportano e si commentano alcuni esempi di simulazione per dimostrare la correttezza dei risultati e l'ottenimento degli obiettivi modellistici prefissati.

1

CHAPTER ONE

INTRODUCTION AND BRIEF
LITERATURE REVIEW

1.1

OVERVIEW OF THE PROBLEM

With increasing concerns about fossil fuel deficit, skyrocketing oil prices, global warming, and damage to environment and ecosystem, the promising incentives to develop alternative energy resources with high efficiency and low CO₂ emissions are of great importance.

Among the renewable energy resources, the energy through the photovoltaic (PV) effect can be considered the most essential and prerequisite sustainable resource because of the ubiquity, abundance, and sustainability of solar radiant energy. Regardless of the intermittency of sunlight, solar energy is widely available and completely free of cost. Recently, photovoltaic array system is likely recognized and widely utilized to the forefront in electric power applications. It can generate direct current electricity without environmental impact and contamination when is exposed to solar radiation. Being a semiconductor device, the PV system is static, quite, and free of moving parts, and these make it have little operation and maintenance costs. Even though the PV system is posed to its high capital fabrication cost and low conversion efficiency, the skyrocketing oil prices make solar energy naturally viable energy supply with potentially long-term benefits.

PV module represents the fundamental power conversion unit of a PV generator system. The output characteristics of PV module depends on the solar insolation, the cell temperature and output voltage of PV module. Since PV module has nonlinear characteristics, it is necessary to model it for the design and simulation of maximum power point tracking (MPPT) for PV system applications. ^[1]

Battery technologies represent a key power source used in many domains of our daily life. Nowadays, they are essential for the utilization of renewable energy by matching and compensating for any electrical variation between the source and the load.

In order to improve the existing battery technologies, engineers need to understand better the functionality, the behaviour, and the properties of multiple types of batteries under different circumstances. For that matter, many research projects were conducted to simulate the physical battery using a variety of theoretical models, like the electrochemical, the stochastic, the analytical, and the electrical circuit models.

Also most of renewable energy technology produces a DC power output. An inverter is needed to convert the DC electric energy from the renewable energy source into AC electric energy. The inverters are either stand-alone, or grid-connected, In case of grid-connected inverter, the inverter output voltage and frequency should be the same as that of the grid voltage and frequency. Consequently, the control of the inverter should be improved to meet the requirements for grid interconnection. ^[2]

Modelica is an open source software, object oriented and equation based modelling language, which can be used to build models and simulate it easily.

1.2

BRIEF LITERATURE REVIEW

PV systems have been the subject of a long-term research effort, see e.g. [4-5].

In recent years, the increasing importance of these systems has been reflecting into control problems that before were of scarce – if any – importance, especially for what concerns the combined power and frequency control, see e.g. [9-15].

As a result, many techniques were proposed, and many models for PV system components were presented in the literature, see e.g. [1-3] for cells, [2-3-6] for batteries, [8] for inverters, and so forth.

However, many of these models are either too complex for studying a network with tens or even hundreds of components, or not easy to parameterize with information available on data sheets, or any combination thereof, see [8-9-13-14].

Hence, despite the impressive development of research over the years, the need for models suited to system studies and easy enough to parameterize even at early stages of a project, is still a not totally answered question. This thesis aims at providing a contribution in the direction just sketched.

Modelica is used for the models' development because of its popularity in academia and research models as it supports the object oriented model approach, solve all components

sequentially and extend the functionality with regard to dynamic systems optimization, see [16-17].

1.3

MOTIVATION

The mathematical PV models used in computer simulation have been built for over the past four decades ^[4-5]. Almost all well-developed PV models describe the output characteristics mainly affected by the solar insolation, cell temperature, and load voltage. However, the Modelica library package doesn't offer yet power system and renewable energy sources electric components like PV cells, battery and inverter models to integrate together forming a small electrical network. Thus, it is difficult to simulate and analyse in the generic modelling of PV power system in connection with islanded loads or grid tied through inverter. This motivates me to develop a generalized model for PV cell, battery, inverter and a generalized control scheme to analyse the behaviour and optimize the efficiency of small electrical network using Modelica.

1.4

OBJECTIVES OF THE STUDY

The main contribution of this thesis is the implementation of a generalized PV cell, battery, inverter and general control scheme models in the form of simple masked blocks, which have user-friendly icons and dialogs in the same way of Modelica block libraries or other object oriented-based simulation software packages.

The modelling of the PV system is based on modular blocks, as illustrated in FIG.1.4.1. The modular structure facilitates the modelling of the other system structures and replacing of elements, for instance a DC load instead of an AC load or connection to the grid. [3]

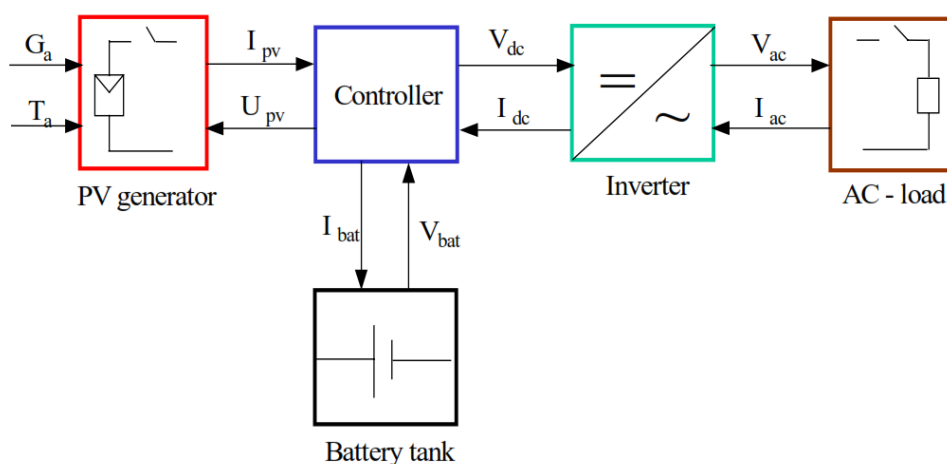


FIG.1.4.1 - Block diagram of a general control scheme of PV system

1.5

OUTLINE OF THE DISSERTATION

Chapter 1 is a general introduction about the concepts of used models and the objective of the thesis.

Chapter 2 is a comprehensive description for the modelled systems;

part 2.1 is the PV cell including how it works, the equivalent model, equations, discussing the characteristic curves, the effect of temperature and solar radiation change on the IV curve, the maximum power point concept and how modules and arrays are formed.

Part 2.2 is a battery model and main factors affecting it, the equivalent circuit and the modelling approaches.

Part 2.3 is the inverter model operation, control techniques, space phasor modulation, grid synchronization and simulation of grid connected inverter.

Chapter 3 covers the implemented PV cells, battery and inverter models using Modelica language also showing some simulation results to verify the models used.

Chapter 4 is about using some simulation examples to verify the usage of all the models connected together;

Part 4.1 includes an introduction about optimization and control of the PV module in case of islanded load and grid connected.

Part 4.2 is about a Modelica simulation example verifying the islanded load case scenario.

Part 4.3 is about a Modelica simulation example verifying the grid connected case scenario.

Chapter 5 includes the thesis conclusion and the proposed future work ideas.

Chapter 6 is the reference list.

2

CHAPTER TWO

MODEL

COMPONENTS

2.1

PHOTOVOLTAIC CELL

Solar cell is basically a p-n junction fabricated in a thin layer of semiconductor. The electromagnetic radiation of solar energy can be directly converted electricity through photovoltaic effect. Being exposed to the sunlight, photons with energy greater than the band-gap energy of the semiconductor are absorbed and create some electron-hole pairs proportional to the incident irradiation. Under the influence of the internal electric fields of the p-n junction, these carriers are swept apart and create a photocurrent which is directly proportional to solar insolation. PV system naturally exhibits a nonlinear I-V and P-V characteristics which vary with the radiant intensity and cell temperature. ^[1]

A photovoltaic PV generator is the whole assembly of solar cells, connections, protective parts, supports etc. In the present modelling, the focus is only on cell/module/array.

2.1.1 Solar cell model

During darkness, the solar cell is not an active device; it works as a diode, i.e. a p-n junction. It produces neither a current nor a voltage. However, if it is connected to an external supply (large voltage) it generates a current I , called diode current or dark current.

A solar cell is usually represented by an electrical equivalent one-diode model, as shown in FIG.2.1.1.

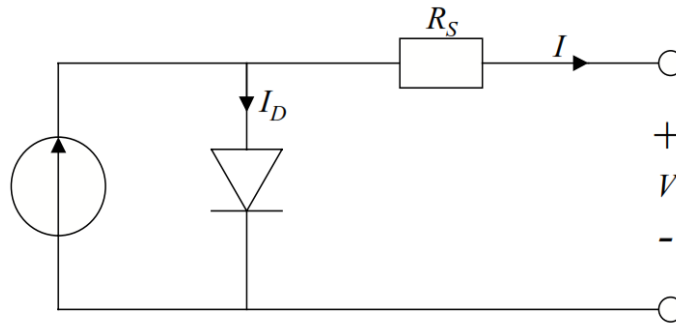


FIG.2.1.1 – Model for a single solar cell

The model contains a current source I_{ph} , one diode and a series resistance R_s , which represents the resistance inside each cell and in the connection between the cells. The net current is the difference between the photocurrent I_{ph} and the normal diode current I_D :

$$I = I_{ph} - I_D = I_{ph} - I_0 \left(\exp \frac{e(V + IR_s)}{mKT_c} - 1 \right)$$

Where m is idealising factor, k is Boltzmann's gas constant, T_c is the absolute temperature of the cell, e is the electronic charge and V is the voltage imposed across the cell. I_0 is the dark saturation current and it is strongly depending on temperature. ^[3]

FIG.2.1.2.a shows the I-V characteristic curves of a photovoltaic cell at a constant ambient temperature but different radiation levels.

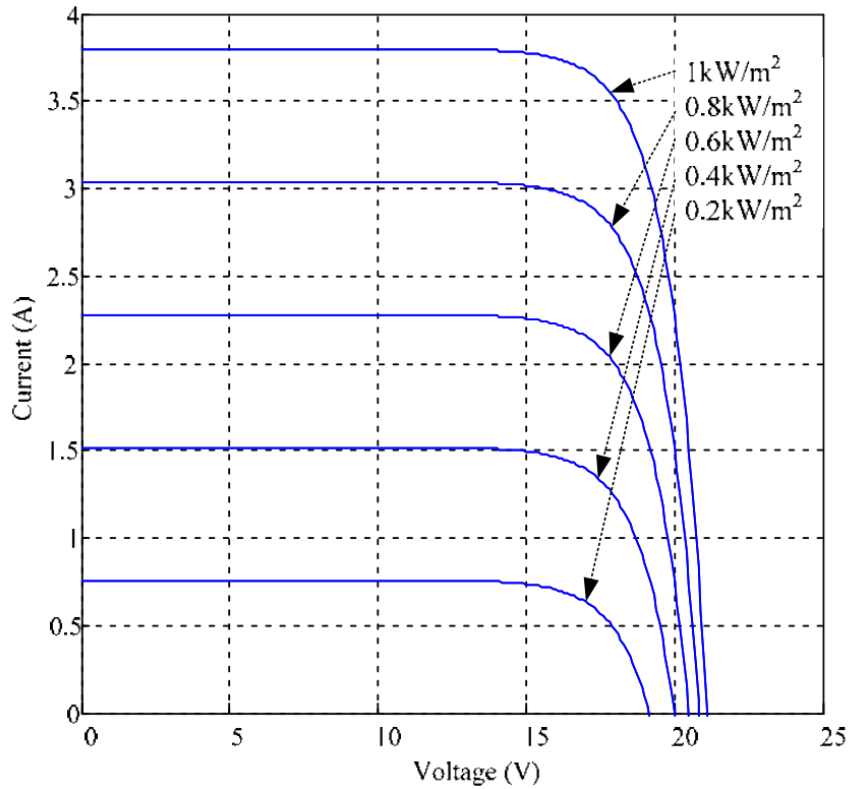


FIG.2.1.2.a – PV cell I-V curve at different solar radiation ^[1]

While FIG.2.1.2.b shows the I-V characteristic curves of a photovoltaic cell at a constant solar radiation but different ambient temperature levels.

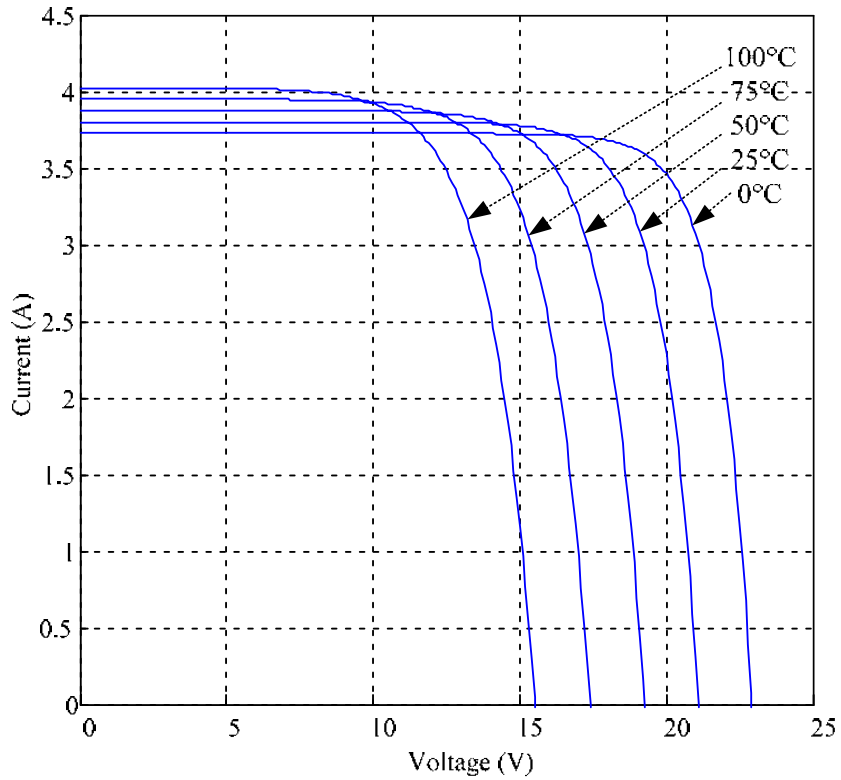


FIG.2.1.2.b – PV cell I-V curve at different temperature [1]

FIG.2.1.3 shows the I-V characteristic of the solar cell for a certain ambient irradiation G_a and a certain fixed cell temperature T_c .

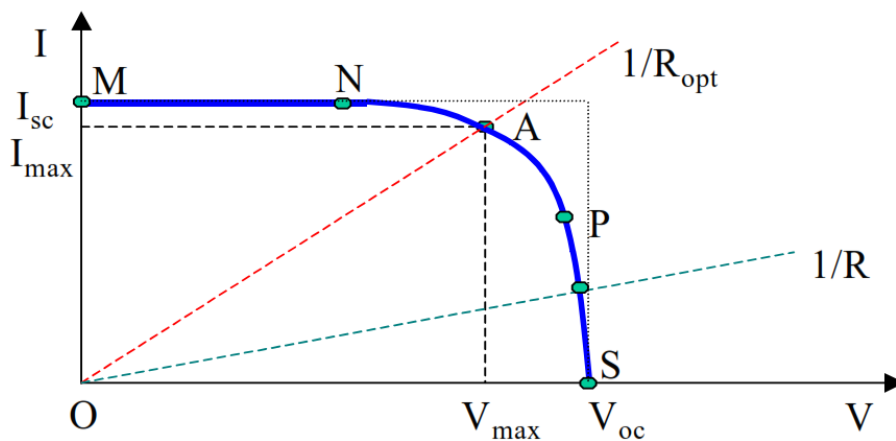


FIG.2.1.3 - Typical solar cell I-V curve

In the representation of I - V characteristic, a sign convention is used, which takes as positive the current generated by the cell when the sun is shining and a positive voltage is applied on the cell's terminals.

If the cell's terminals are connected to a variable resistance R , the operating point is determined by the intersection of the I - V characteristic of the solar cell with the load I - V characteristic - see FIG2.1.3. For a resistive load, the load characteristic is a straight line with a slope $I/V=1/R$. It should be pointed out that the power delivered to the load depends on the value of the resistance only.

However, if the load R is small, the cell operates in the region MN of the curve, where the cell behaves as a constant current source, almost equal to the short circuit current. On the other hand, if the load R is large, the cell operates on the region PS of the curve, where the cell behaves more as a constant voltage source, almost equal to the open-circuit voltage.

A real solar cell can be characterised by the following fundamental parameters, which are also sketched in FIG2.1.3:

Short circuit current: $I_{sc} = I_{ph}$. It is the greatest value of the current generated by a cell. It is produced under short circuit conditions: $V=0$.

Open circuit voltage corresponds to the voltage drop across the diode (p-n junction), when it is traversed by the photocurrent I_{ph} (namely $I_D = I_{ph}$), namely when the generated current is $I=0$. It reflects the voltage of the cell in the night and it can be mathematically expressed as:

$$V_{oc} = \frac{mKT_c}{e} \ln\left(\frac{I_{ph}}{I_0}\right) = V_t \ln\left(\frac{I_{ph}}{I_0}\right)$$

Where $V_t = \frac{mKT_c}{e}$ is known as thermal voltage and T_c is the absolute cell temperature.

Maximum power point is the operating point A (V_{max} , I_{max}) in FIG.2.1.3, at which the power dissipated in the resistive load is maximum: $P_{max} = I_{max} V_{max}$.

Maximum efficiency is the ratio between the maximum power and the incident light power:

$$\eta = \frac{P_{max}}{P_{in}} = \frac{I_{max} V_{max}}{AG_a}$$

Where G_a is the ambient irradiation and A is the cell area.

Fill factor is the ratio of the maximum power that can be delivered to the load and the product of I_{sc} and V_{oc} :

$$FF = \frac{P_{max}}{V_{oc} I_{sc}} = \frac{V_{max} I_{max}}{V_{oc} I_{sc}}$$

The fill factor is a measure of the real I - V characteristic. Its value is higher than 0.7 for good cells. The fill factor diminishes as the cell temperature is increased.

In FIG.2.1.3, an I - V characteristic of a solar cell for only a certain ambient irradiation G_a and only a certain cell temperature T_c is illustrated. The influence of the ambient irradiation G_a and the cell temperature T_c on the cell characteristics is presented in FIG.2.1.4.

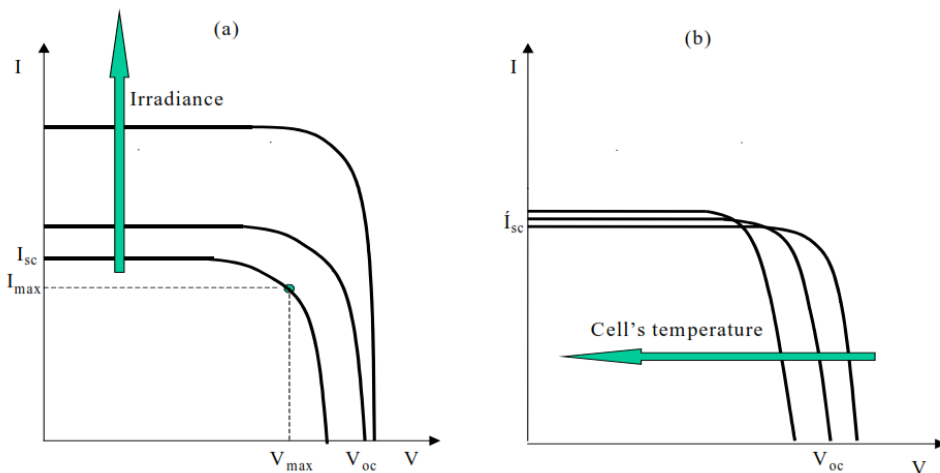


FIG.2.1.4 – Influence of ambient radiation (a) and cell temperature (b) on the cell characteristics

FIG.2.1.4 (a) shows that the open circuit voltage increases logarithmically with the ambient irradiance, while the short circuit current is a linear function of the ambient irradiance. The arrow shows in which sense the irradiance and the cell temperature, respectively, increase. The influence of the cell temperature on the I-V characteristics is illustrated in FIG.2.1.4 (b). The dominant effect with increasing cell's temperature is the linear decrease of the open circuit voltage, the cell being thus less efficient. The short circuit current slightly increases with cell temperature.

For practical use, solar cells can be electrical connected in different ways: Series or parallel. FIG.2.1.5 presents how the I-V curve is modified in the case when two identical cells are connected in series and in parallel.

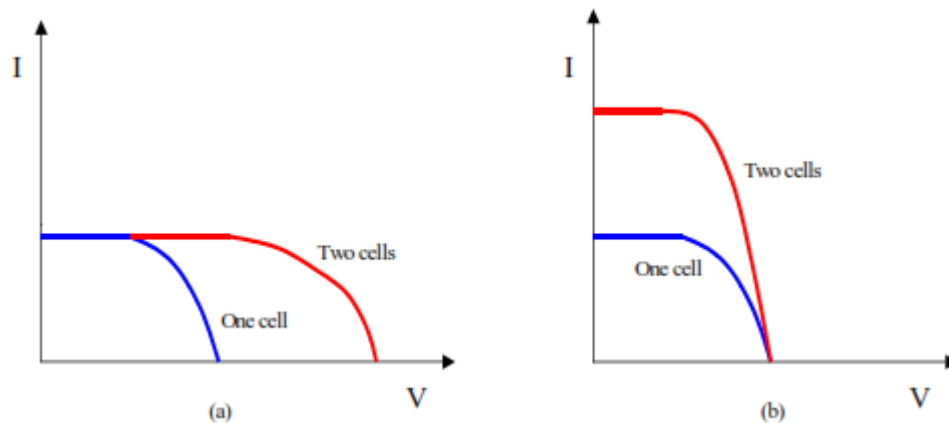


FIG.2.1.5 – Series (a) and parallel (b) connection of identical cells

It is seen that I-V characteristics of series interconnected cells can be found by adding, for each current, the different voltages of the individual cells. On the other hand, for parallel cells the currents of the individual cells must be added at each voltage in order to find the overall I-V curve.

2.1.2 Module model

Cells are normally grouped into “modules”, which are encapsulated with various materials to protect the cells and the electrical connectors from the environment. The manufacturers supply PV cells in modules, consisting of N parallel branches, each with N solar cells in series, as shown in FIG.2.1.6.

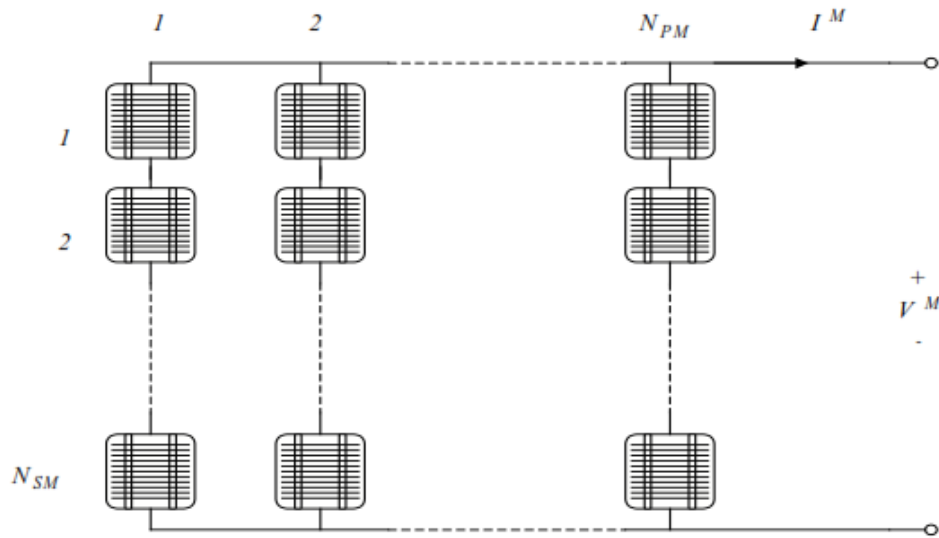


FIG.2.1.6 – PV module consists of N_{PM} parallel branches, each of N_{SM} solar cells in series

In order to have a clear specification of which element (cell or module) the parameters in the mathematical model are regarding, the following notation is used from now on: the parameters with superscript "M" are referring to the PV module, while the parameters with superscript "C" are referring to the solar cell. Thus, the applied voltage at the module's terminals is denoted by V , while the total generated current by the module is denoted by I^M .

A model for the PV module is obtained by replacing each cell in FIG.2.1.6, by the equivalent diagram from FIG.2.1.1. In the following, the mathematical model of a PV module is briefly reviewed. The advantage of this model is that it can be established applying only standard manufacturer supplied data for the modules and cells. The PV module's current I under arbitrary operating conditions can thus be described as:

$$I^M = I_{sc}^M \left[1 - \exp\left(\frac{V^M - V_{oc}^M + R_s^M \cdot I^M}{N_{SM} V_t^C}\right) \right]$$

The expression of the PV module's current I^M is an implicit function, being dependent on:

- The short circuit current of the module, which is $I_{sc}^M = N_{PM} I_{sc}^C$
- The open circuit voltage of the module, which is $V_{oc}^M = N_{SM} V_{oc}^C$
- The equivalent serial resistance of the module, which is

$$R_s^M = \frac{N_{SM}}{N_{PM}} R_s^C$$

- The thermal voltage in the semiconductor of a single solar cell, which is $V_t^C = \frac{mKT^C}{e}$

In current practice, the performance of a module or another PV device is determined by exposing it at known conditions.

The module characteristics supplied by the manufacturer are usually determined under special conditions, as for example nominal or standard conditions, see FIG.2.1.7. [3]

Nominal conditions	Standard conditions
Irradiation: $G_{a,ref}=800 \text{ W/m}^2$	Irradiation: $G_{a,0}=1000 \text{ W/m}^2$
Ambient temperature: $T_{a,ref} = 20^\circ \text{ C}$	Cell temperature: $T_0^C = 25^\circ \text{ C}$
Wind speed: 1 m/s	

FIG.2.1.7 – Nominal and standard conditions

2.2

BATTERY

Another important element of a stand-alone PV system is the battery. Batteries are a collection of electrochemical cells. The main characteristic of the electrochemical cell is the transduction of chemical energy into electrical energy and its reverse, thus enabling rechargeable energy storage. The battery is necessary in such a system because of the fluctuating nature of the output delivered by the PV arrays. Thus, during the hours of sunshine, the PV system is directly feeding the load, the excess electrical energy being stored in the battery. During the night, or during a period of low solar irradiation, energy is supplied to the load from the battery.

Different types of batteries exist such as the Lead-acid, Lithium ion, Nickel Cadmium, etc. The cell of any type is characterized by its open-circuit voltage, its lifetime and a cut-off voltage under which the battery will stop operating.

General notions for battery

Before a mathematical model for the battery is presented, some fundamental concepts of the battery are briefly reviewed:

Nominal capacity C_{max} is the number of ampere-hours (Ah) that can maximally be extracted from the battery, under predetermined discharge conditions.

State of charge SOC is the ratio between the present capacity and the nominal capacity C_{max} : $SOC=C/C_{max}$. Obviously $0 \leq SOC \leq 1$. If $SOC=1$ the battery is totally charged, otherwise if $SOC=0$ the battery is totally discharged.

Charge (or discharge) regime is the parameter which reflects the relationship between the nominal capacity of a battery and the current at which it is charged (or discharged).

It is expressed in hours; for example, discharge regime is 30 h for a battery 150 Ah that is discharged at 5A.

Efficiency is the ratio of the charge extracted (Ah or energy) during discharge divided by the amount of charge (Ah or energy) needed to restore the initial state of charge. It is depending on the state of charge **SOC** and on the charging and discharging current.

Lifetime is the number of cycle's charge/discharge the battery can sustain before losing 20% of its nominal capacity.

Over the years a number of battery models have been developed (Facinelli, 1983), (Hyman et al., 1986), (Manwell & McGowan, 1993), (Manwell et al., 1994). Most of these models can be defined as phenomenological, namely they are based on observable quantities such as voltage, current and time, and do not depend on the internal structure of the system (Manwell et al., 1994). Other models are based on physical or electrochemical processes. ^[3]

In general, the battery models view the battery as a voltage source E in series with an internal resistance, as shown in FIG.2.2.1.

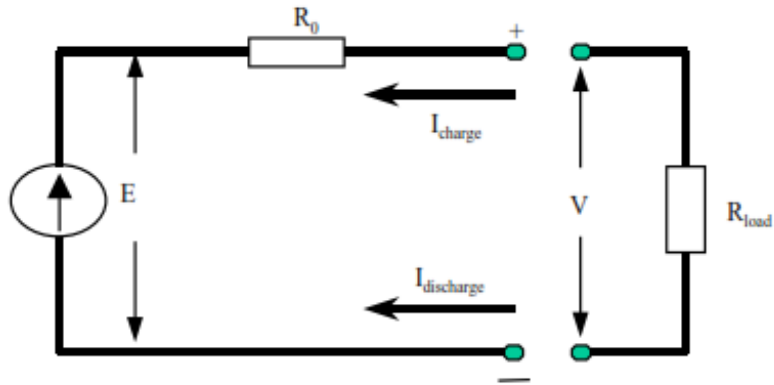


FIG.2.2.1 – battery schematic diagram

The terminal voltage V is given by:

$$V = E - I R_0. \quad [3]$$

There are three main sources of voltage drops ^[7] within the passive components in the electrochemical cell:

- Internal resistance (IR) drop: the voltage drop due to flow of charge across the cell internal resistance;
- Activation polarization: due to the resistance faced by the charge at the surface of the electrodes and the electrolyte, and other factors inherent to the kinetics of an electrochemical reaction; and
- Concentration polarization: the retarding factor due to the transfer of charge ions across the electrolyte (from one electrode to another).

There are different models characterizing the internal parameters of batteries but four different modelling approaches are usually adopted to study the behaviour of a rechargeable electrochemical battery cell:

- Electrochemical modelling of the inner battery cell behaviour;
- Stochastic modelling, in which the battery behaviour is modelled using a discrete-time transient stochastic process.
- “black-box” based modelling, in which the system behaviour is analytically described using a set of mathematical equations, using fuzzy logic, or artificial neural networks.
- Use of electric equivalent network models (also called equivalent circuit models) , where the battery is modelled as a network of electrical components.

Although all the four approaches are common, the first approach is predominantly followed by battery manufacturers and battery chemistry researchers and is not very useful for electrical engineers and system integrators who need easy-to-use models which are expressed in terms of quantities they are accustomed to, such as voltages and currents.

Consequently, they prefer the fourth approach, which is easier to use, for modelling battery cells. This approach mixed with the black box approach is adopted for this thesis.

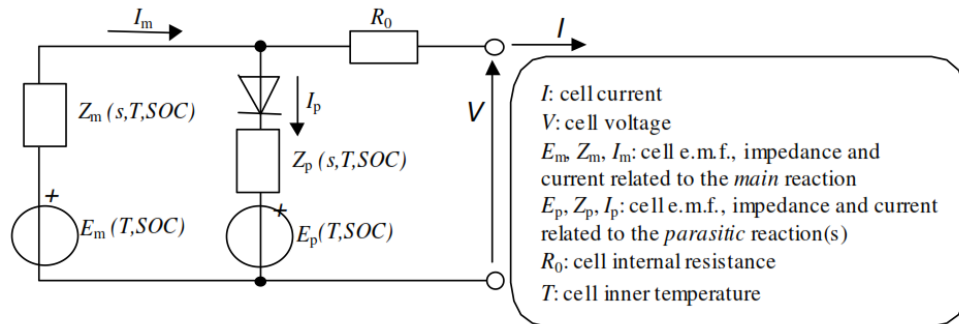


FIG.2.2.2 – general electric equivalent network model of a cell taking into consideration parasitic reactions

A general representation of an electrochemical accumulator cell in the equivalent circuit model is shown in FIG.2.2.2.

In this figure:

- The branch containing the cell electromotive force E_m , represents the main reversible reaction of the cell: the charge stored in the cell during the charge process is the time integral of the current I_m entering that branch. The electromotive force E_m is a function of the cell SOC, and the inner cell temperature (assumed to be uniform), T .

The branch containing the cell electromotive force E_p , represents the parasitic reactions inside the cell that are not associated with charge accumulation inside the cell. For example, in lead-acid cells, the parasitic reaction is constituted by the water electrolysis that occurs at the end of the charge process. The diode indicates that the energy always flows out of the parasitic branch. Again, the electromotive force E_p is a function of the cell SOC, and the inner cell temperature (assumed to be uniform), T .

The impedances are represented as functions of the laplacian transform variable s , since in this way a single $Z(s)$ can be

representative of any network of resistor and/or capacitor and/or inductor components. For instance, the network containing a resistor in series with multiple resistor-capacitor blocks, constitutes an expansion of the laplacian impedance $Z(s)$. Both the laplacian impedances, $Z_m(s)$ and $Z_p(s)$ are functions of the cell SOC, and the inner cell temperature (assumed to be uniform), T .

In large regions of battery cell operation, the parasitic reaction effects can be neglected. For instance, in the case of lead-acid batteries it can be neglected during the discharge process and during the initial stages of charging ^[12]. Parasitic reaction effects are much more negligible in lithium cells, as it is clear from the very high *coulombic efficiency*¹ they show. For this reason, the simplified model of the kind shown in FIG.2.2.3 can be used for cells that exhibit a very high coulombic efficiency.

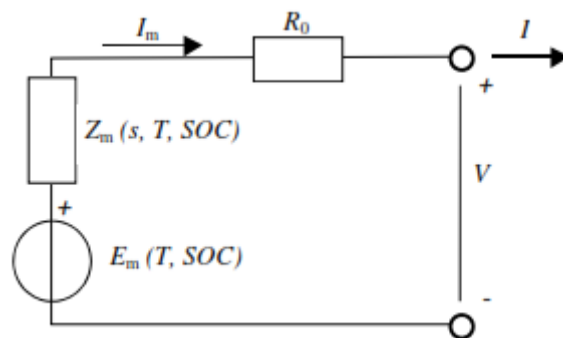


FIG.2.2.3 – A simplified electric equivalent network model of a cell (neglecting the parasitic reactions) ^[6]

End note:

¹ The *coulombic efficiency* of a battery is the ratio of the charge that the battery delivers, starting from fully-charged condition, and the charge that is delivered back to the battery for recharging it, up to fully charged condition.

Black box approach

Modelling of dynamic systems is also referred to as System Identification. The Black box modelling approach is a well-established technique in modelling dynamic systems. Quite a number of books have been written on this subject, e.g. (Box & Jenkins, 1976), (Soderstrom & Stoica, 1989), (Ljung.L, 1999), (Madsen, 1995). Therefore, only a short introduction to this time discrete approach is presented below and essential keywords are introduced.

A first step in the modelling of a dynamic system is to select a proper model description for the system to be modelled. Different model structures exist with respect to parametric, spectral and correlation model descriptions. Next step is to select an appropriate estimation method – depending on the selected model type – and to estimate the parameters. Finally, the model performance must be validated in order to decide whether the model can model the system.

In this modelling approach a linear state space structure (parametric model) is applied for the following reasons:

- 1) It is assumed that given knowledge on the present state of the battery at time t_0 is available. This knowledge combined with knowledge on future input signals and disturbances will unambiguously determine the state of the battery at $t \geq t_0$. This property is related to a Markov process property, which justifies the use of a state space structure. Moreover, the state space structure will reveal knowledge about the underlying dynamics, if the states can be interpreted.

- 2) The model structure is assumed to be linear as it makes the estimation method less complex compared to non-linear estimation methods.
- 3) The description is chosen parametric as it makes comparisons to the KiBaM battery model more feasible.

An advantage of using a Black box modelling approach compared to e.g. a Grey box modelling approach is that no prior system knowledge is necessary. However, it is usually difficult to interpret the estimated parameters (at model orders higher than 3) by equivalent physical parameters. On the other hand, if the system is fairly well known, it would be more advantageous to apply a Grey box modelling approach, see e.g. (Hansen, 1997), where estimation of continuous time parameters in non-linear models is performed. ^[3]

2.3

INVERTER

As known, the PV arrays produce DC power and therefore when the stand-alone PV system contains an AC load, as it is the case for the inverter tied to grid system, a DC/AC conversion is required. This is thus the reason why this part briefly presents the inverter.

An inverter is a converter where the power flow is from the DC to the AC side, namely having a DC voltage, as input, it produces a desired AC voltage, as out-put – see FIG.2.3.1.

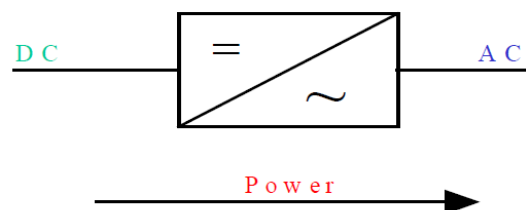


FIG.2.3.1 - Connection of the inverter

The inverter is characterized by a power dependent efficiency η . The role of the inverter is to keep on the AC side the voltage constant at the rated voltage 230V and to convert the input power P_{in} into the output power P_{out} with the best possible efficiency. The efficiency of the inverter is thus modelled as:

$$\eta = \frac{P_{out}}{P_{in}} = \frac{V_{ac}I_{ac} \cos \phi}{V_{dc}I_{dc}} \quad , \quad I_{dc} = \frac{V_{ac}I_{ac} \cos \phi}{V_{dc}\eta}$$

Where I_{dc} is the current required by the inverter from the DC side (for example, from the controller) in order to be able to keep the rated voltage on the AC side (for example on the load). V_{dc} is the input voltage for the inverter delivered by the DC side, for example by the controller. ^[3]

2.3.1 THE THEORY OF THE THREE-PHASE GRID-CONNECTED INVERTER

In order to control three-phase voltage-source inverters (VSI), there are two control strategies: current control and voltage control. The voltage-controlled VSI use the phase angle between the inverter output voltage and the grid voltage to control the power flow. In the current controlled VSI, the active and reactive components of the current injected into the grid are controlled using pulse width modulation (PWM) techniques. A current controller is less sensitive to voltage phase shifts and to distortion in the grid voltage. Moreover, it is faster in response. On the other hand, the voltage control is sensitive to small phase errors and large harmonic currents may occur if the grid voltage is distorted. Consequently, the current control is recommended in the control of grid-connected inverter.

The current controller of three-phase VSI plays an essential part in controlling grid-connected inverters. Consequently, the quality of the applied current controller largely influences the performance of the inverter system. Many control mechanisms have been proposed to regulate the inverter output current that is injected into the utility grid. Among these control mechanisms, three major types of current controller have evolved: hysteresis controller, predictive controller and linear proportional-integral (PI) controller. Predictive controller has a very good steady-state

performance and provides a good dynamic performance. However, its performance is sensitive to system parameters. The hysteresis controller has a fast transient response, non-complex implementation and an inherent current protection. However, the hysteresis controller has some drawbacks such as variable switching frequency and high current ripples. These cause a poor current quality and introduce difficulties in the output filter design.

The PI controller is the most common control algorithm used for current error compensation. A PI controller calculates an error value as the difference between a measured inverter output current and a desired injected current to the grid, then the controller attempts to minimize the error between them. The PI controller calculation algorithm involves two separate constant parameters, the proportional constant K_p and the integral constant K_i . The proportional term of the controller is formed by multiplying the error signal by a K_p gain. This tends to reduce the overall error with time. However, the effect of the proportional term will not reduce the error to zero, and there is some steady state error. The Integral term of the controller is used to fix small steady state errors. The Integral term integrates the error then multiplies it by a K_i constant and becomes the integral output term of the PI controller. This removes the steady state error and accelerates the movement of the process into the reference point.

The PI current control offers an excellent steady-state response, low current ripple, constant switching frequency, in addition to well-defined harmonic content. Moreover, the controller is insensitive to system parameters since the algorithm does not need system models. PI controllers can be applied either in the stationary ($\alpha\beta$) or in synchronous (dq) reference frame. When the

synchronous PI controller is used, the control variables become DC and the PI compensators are able to reduce the stationary error of the fundamental component to zero. This is not the case with PI controllers working in the stationary system, where there is an inherent tracking error of phase and amplitude. Therefore, current control in a synchronous (rotating) reference frame, using PI controllers is the typical solution in the three-phase grid-connected inverters.

According to the mathematical model of the grid-connected inverter, the output voltages of the inverter in the synchronous (dq) frame are given by

$$\begin{bmatrix} u_d \\ u_q \end{bmatrix} = L \frac{d}{dt} \begin{bmatrix} i_d \\ i_q \end{bmatrix} + R \begin{bmatrix} i_d \\ i_q \end{bmatrix} + \omega L \begin{bmatrix} -i_q \\ i_d \end{bmatrix} + \begin{bmatrix} e_d \\ e_q \end{bmatrix}$$

Where e_d and e_q are the components of the park transformation of the grid voltage. u_d and u_q are the components of the park transformation of the inverter output. ω is the angular frequency of the grid. L is the inductance between the grid-connected inverter and the grid. R is the resistance between the grid-connected inverter and the grid.

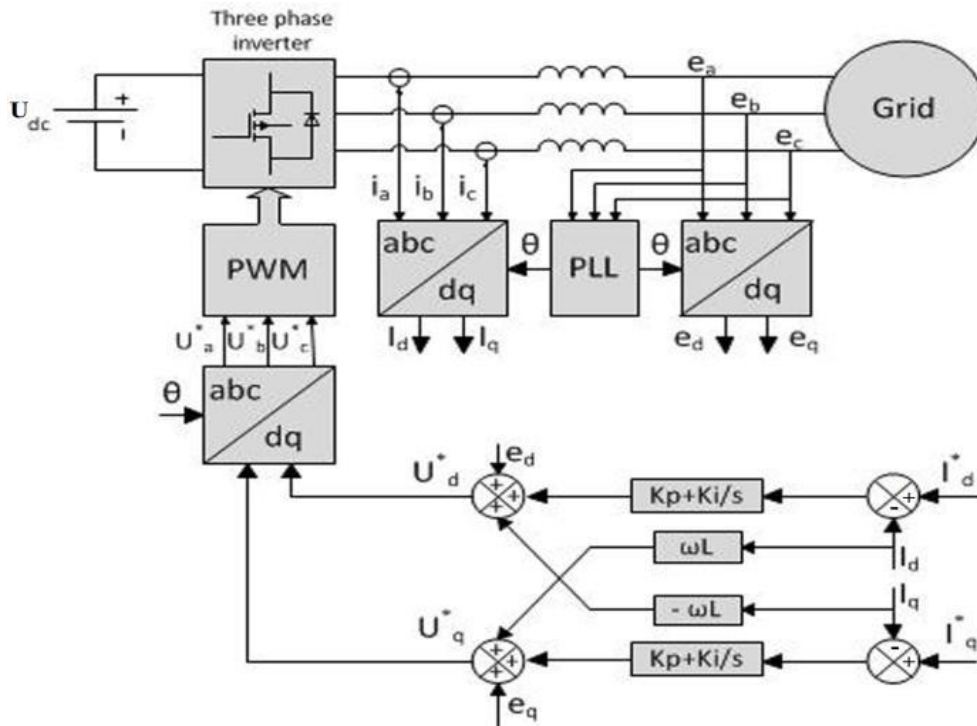


FIG.2.3.2 - General structure for synchronous controller [6].

The block diagram of the synchronous controller for the grid-connected inverter is represented in FIG.2.3.2. We see from the figure that the inverter has two PI controllers to compensate the current vector components that are defined in synchronous reference frame (dq). Because of coordinate transformations, i_q and i_d are DC components and therefore, PI compensators reduce the error(s) between the desired current I^*_d (I^*_q) and the actual current I_d (I_q) to zero. The output energy and power factor can be controlled via changing d-axis current and q-axis current. For improving the performance of PI controller in such a structure, cross-coupling terms and voltage feed forward are usually used.

2.3.1.1 Space vector modulation (SVM)

After calculating the three-phase reference voltages U^*_a , U^*_b and U^*_c by the current regulation algorithm, the gating pulses for individual inverter switches are generated using the PWM algorithm. Then the desired inverter voltage is generated.

Many PWM techniques have been developed and described during the last few decades. However, with microprocessor development, the space vector modulation (SVM) becomes popular and possibly the best PWM technique in three-phase PWM inverter. SVM has many advantages such as constant switching frequency, well-defined output harmonic spectrum, optimum switching patterns, and excellent DC-link voltage utilization.

SVM treats the three-phase inverter as a single unit. Specifically, in the case of a two-level inverter as shown in FIG.2.3.3, there are eight possible unique states, each of which determines a voltage space vector. As shown in FIG.2.3.4, six voltage space vectors shape the axis of a hexagon and divide the whole space into six sectors from 1 to 6. Moreover, there are two zero vectors, U_0 and U_7 which lie at the origin. The angle between any two adjacent non-zero vectors is 60° . Therefore, SVM is a digital modulating technique where the objective is to find an appropriate combination of active and zero vectors to approximate a given reference voltage.

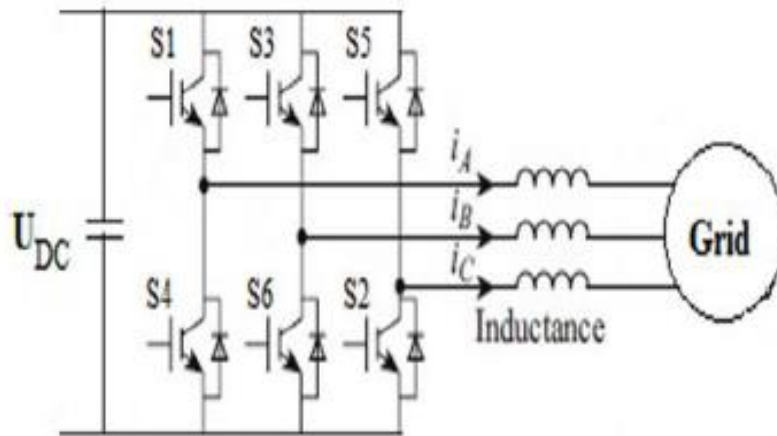


FIG.2.3.3 - Two-level three-phase inverter configuration

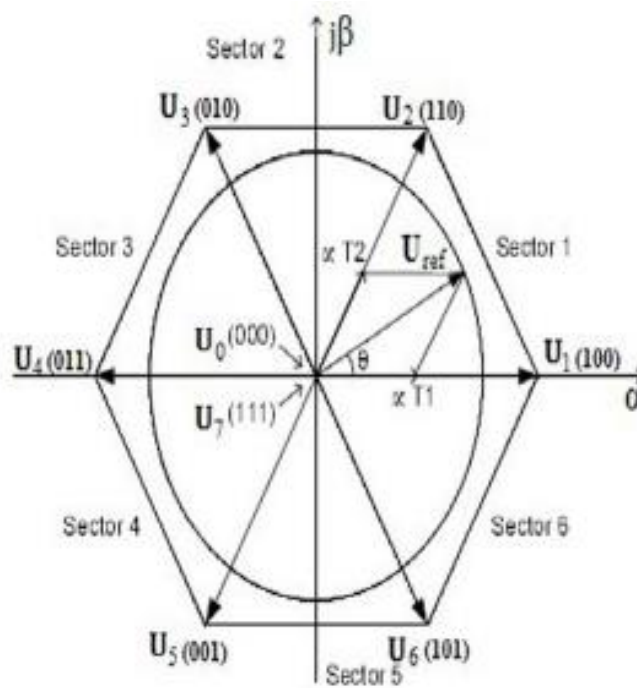


FIG.2.3.4 - Six active vectors and two null vectors in SVM

In SVM, the three-phase reference voltages U^*a , U^*b , and U^*c are mapped to the complex two-phase orthogonal ($\alpha\beta$) plane. This is known as the Clark's transformation.

$$\begin{bmatrix} U_\alpha \\ U_\beta \end{bmatrix} = \begin{bmatrix} 1 & -1/2 & -1/2 \\ 0 & \sqrt{3}/2 & -\sqrt{3}/2 \end{bmatrix} \begin{bmatrix} U_a^* \\ U_b^* \\ U_c^* \end{bmatrix}$$

The construction of any space vector U_{ref} which lies in the hexagon can be done by time averaging the adjacent two active space vectors and any zero vectors, as follows

$$U_{ref} = \frac{U_n T_1 + U_{n+1} T_2 + U_0 T_0 + U_7 T_7}{T_s}$$

Where U_n and U_{n+1} are the non-zero adjacent active vectors. U_0 and U_7 are the zero vectors. T_1, T_2, T_0, T_7 are time-shares of respective voltage vectors and T_s is the sampling period. SVM can be implemented through the following steps:

1. The Computation of reference voltage and angle (θ).

$$U_{ref} = \sqrt{U_\alpha^2 + U_\beta^2}$$

$$\theta = \tan^{-1} \frac{U_\beta}{U_\alpha}$$

2. Identification of sector number that is done by taking the angle computed from the last step, and then comparing it with angles range of each sector.

3. Calculate the modulation index (m) and the time duration T_1, T_2, T_0, T_7 .

$$m = \frac{U_{ref}}{U_{DC}/2}$$

$$T_1 = \frac{\sqrt{3}}{2} T_s m \sin\left(\frac{\pi}{3} - \theta\right)$$

$$T_2 = \frac{\sqrt{3}}{2} T_s m \sin(\theta)$$

$$T_0 + T_7 = T_s - T_1 - T_2$$

4. After T_1 , T_2 , T_7 , and T_0 are calculated; the SVM pulses can be generated. The arrangement of switching sequence must ensure minimum transition between one vector and the next. This method reduces the switching frequency and has fewer harmonics. For sector 1, one can use 01277210 for symmetry reasons as shown in FIG.2.3.5.

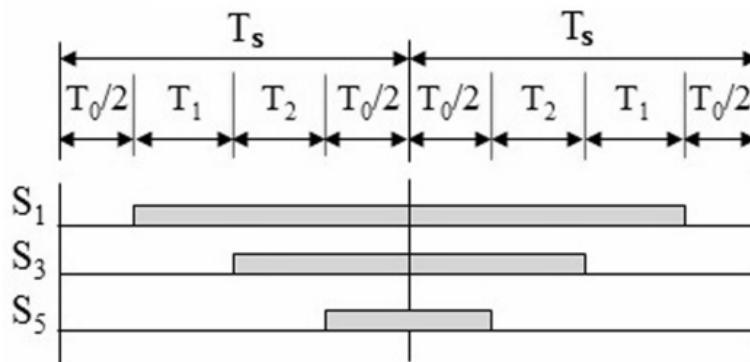


FIG.2.3.5 – SVM switching patterns for sector 1

2.3.2 Grid synchronization

The inverter output current that is injected into the utility network must be synchronized with the grid voltage. The objective the synchronization algorithm is to extract the phase angle of the grid voltage. The feedback variables can be converted into a suitable reference frame using the extracted grid angle. Hence, the detection of the grid angle plays an essential role in the control of the grid-connected inverter. The synchronization algorithms

should respond quickly to changes in the utility grid. Moreover, they should have the ability to reject noise and the higher order harmonics. Many synchronization algorithms have been proposed to extract the phase angle of the grid voltage such as zero crossing detection, and phase-locked loop (PLL).

The simplest synchronization algorithm is the zero crossing detection. However, this method has many disadvantages such as low dynamics. In addition, it is affected by noise and higher order harmonics in the utility grid. Therefore, this method is unsuitable for applications that require consistently accurate phase angle detection.

Nowadays, the most common synchronization algorithm for extracting the phase angle of the grid voltages is the PLL. The PLL can successfully detect the phase angle of the grid voltage even in the presence of noise or higher order harmonics in the grid.

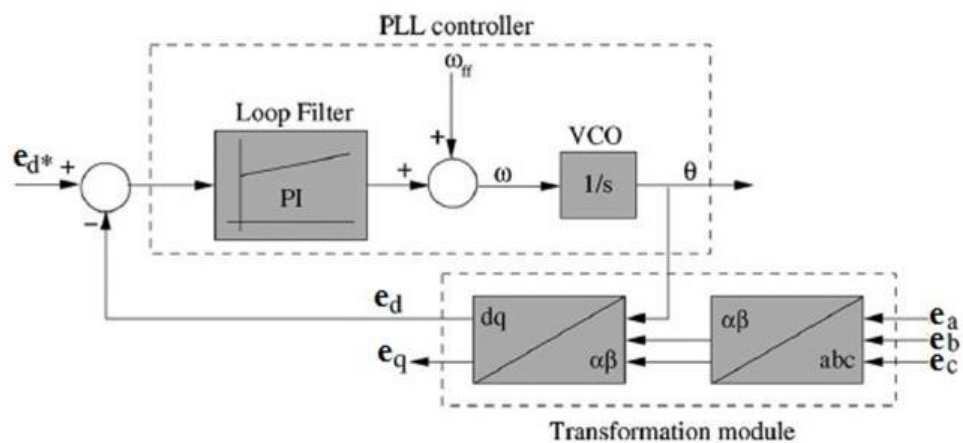


FIG.2.3.6 - Basic structure of a PLL system for grid synchronization

As shown in FIG.2.3.6, the PLL is implemented in synchronous (dq) reference frame. e_{abc} is the sensed grid voltage which is then transformed into DC components using park transformation abc-

dq. The PLL is locked by setting e_d^* to zero, which acts as a phase detector. A controller, usually PI, is used to control this variable, which brings the phase error to zero and acts as a loop filter. The ω_{ff} represents the utility nominal frequency that is added to the output of the regulator then outputted as the grid frequency. After the loop filter, whose output is the grid frequency, a voltage-controlled oscillator (VCO) is applied. This is usually an integrator, which gives the phase locked angle of the grid θ as output. [8]

3

CHAPTER THREE

MODELICA

IMPLEMENTATION

3.1

PHOTOVOLTAIC CELLS

The photovoltaic cell was simulated on three stages together to form the photovoltaic model simulation.

The first stage is TQ /IV curve; expressing the relation of the input temperature and sun radiation and converting them to the current and voltage generated accordingly and getting finally to construct the generated IV curve in this stage taking into consideration the main effect of change in temperature and sun radiation on the output results.

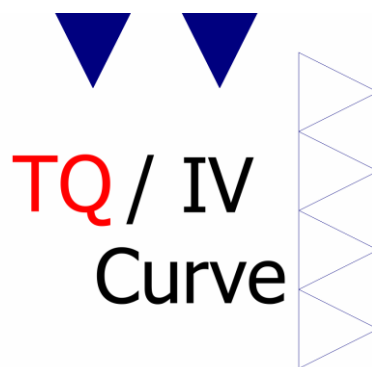


FIG 3.1.1 - TQ/IV curve Modelica icon

As shown in the FIG.3.1.1 the icon for the first stage of the photovoltaic model (TQ/IV curve) is formed by two blue triangles at the top representing the input values of ambient temperature and sun radiation, and other four white triangles at the right

representing the output values of the open circuit voltage, short circuit current, alpha and the corresponding voltage. The used graphical representation symbols in the icon are designed to give an introductive idea of the model in a simple significant way.

The internal structure of this part is very similar to the icon configuration as shown in the FIG.3.1.2

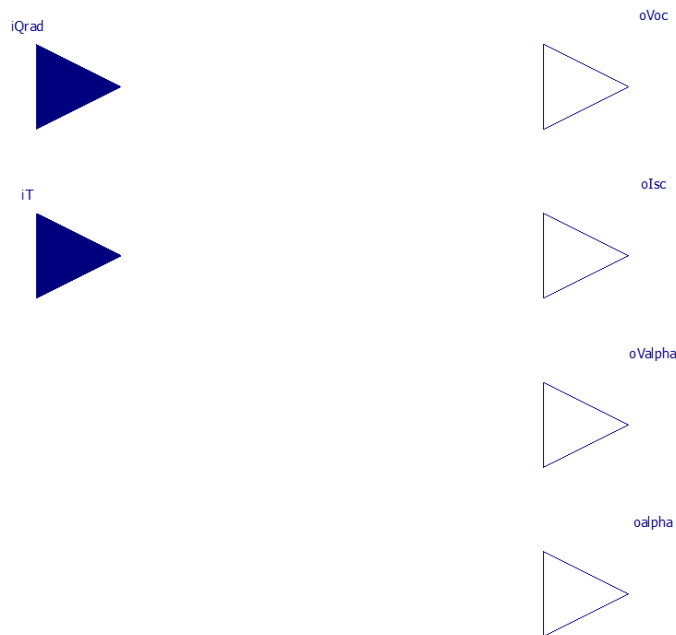


FIG 3.1.2 - TQ/IV curve Modelica diagram

The input temperature and sun radiation affects the generated output voltage and current of the photovoltaic cell respectively leading to the change of open circuit voltage and short circuit current values. The new values of the open circuit voltage and short circuit current constructs the new IV curve of the solar cell as described in the model equations below:

$$VOC = VOC_{nom.} - \Delta_{Voc} \times (iT - T_{nom.})$$

$$ISC = ISC_{nom.} \times (1 + \Delta_{ISC} \times (iT - T_{nom.}))$$

Where, the "Voc" and "Isc" are the new open circuit voltage and short circuit current values to be calculated corresponding to a new given temperature different from standard, "Voc_{nom.}" and "Isc_{nom.}" are the nominal open circuit voltage and nominal short circuit current given at standard temperature, " Δ_{Voc} " and " Δ_{Isc} " are the additive open circuit voltage factor per unit temperature and multiplicative short circuit current factor per unit temperature respectively, "iT" is the input ambient temperature and "T_{nom.}" is the nominal temperature at which the standard open circuit voltage and short circuit current were recorded.

The second stage is the cell 2 lines char, which is an intermediate stage connecting stage one temperature, solar radiation inputs and the main values calculated to represent the characteristics of the IV curve (open circuit voltage, short circuit current, alpha, and the corresponding voltage to alpha) with stage three and the main function of this stage is introducing the system power equilibrium of the solar radiation which is generating useful electrical power and also part of the solar radiation is not transformed to electricity resulting in thermal heat generation at the surface of the solar cell module and increase of the ambient temperature of the cell in general.

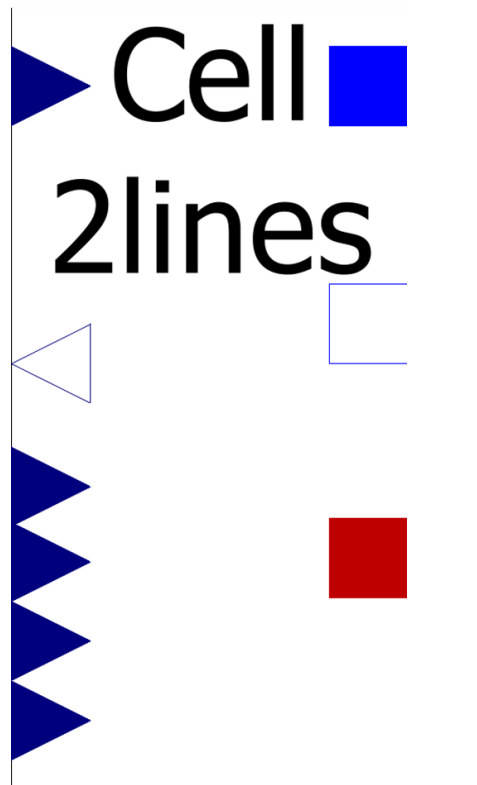


FIG 3.1.3 - Cell 2 lines Modelica icon

Here in this icon we can find all the mentioned elements of stage one plus the heat port expressed by the red square on the bottom right which is responsible for the heat transfer part between the module and the surrounding, in addition to the positive and negative pins expressed in the blue and white squares on the top right respectively which are implementing the electrical side as the generated voltage and current from the module can appear through these two pins.

Here also the internal structure is very similar to the icon configuration as shown in the fig.3.1.4

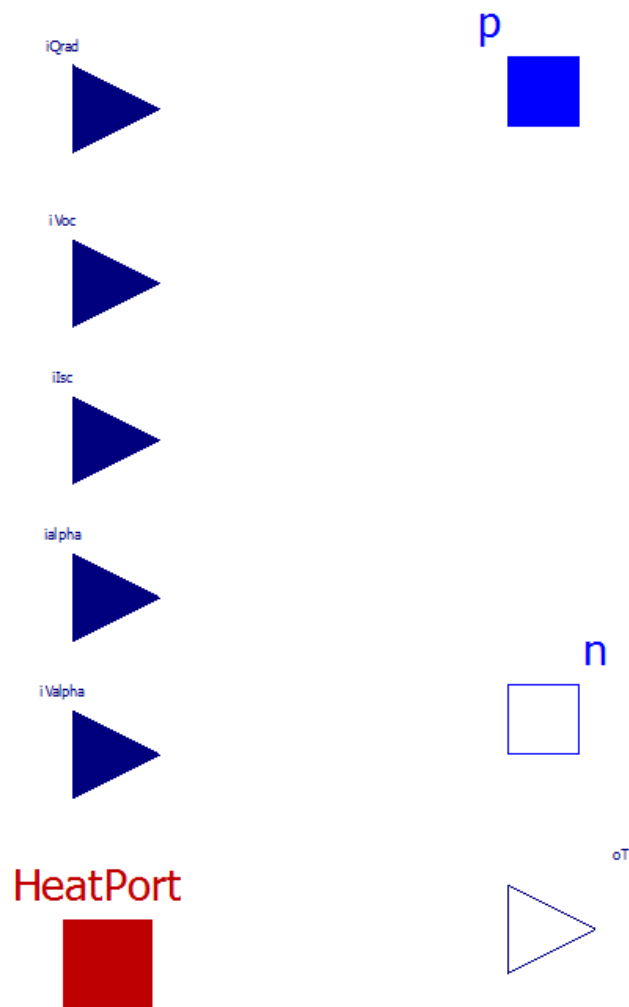


FIG 3.1.4 - Cell 2 lines char Modelica diagram

Using the outputs of stage one (open circuit voltage, short circuit current, alpha, and the corresponding voltage to alpha) as inputs to this stage also the input solar radiation while the temperature is taken as output through the heat port.

so the second stage is translating the characteristic curves of stage one into electrical voltage and current after defining the operating point voltage and current, and also takes in consideration the difference between input solar power and

output electrical power to calculate thermal power generated and use it again as a feedback to our system model as temperature change is one of the main factors affecting the overall efficiency of the PV cell module.

First the positive and negative pins are electrically defined through the following KCL equations:

$$p.i + n.i = 0$$

Where "P.i" is the electric current value at the positive pin, "n.i" is the electric current value at the negative pin

$$I = -p.i$$

In this equation the output current convention is introduced to define the positive direction of the output electric current "I".

$$V = p.v - n.v$$

Where "p.v" is the electric voltage value at the positive pin, "n.v" is the electric voltage value at the negative pin and the output voltage of the PV cell "V" is identified as the voltage difference between the positive and negative pins.

$$Q_e = V * I$$

Where "Qe" is the electrical power generated across the positive and negative pins

$$Q_{thloss} = -HeatPort.Q_{flow}$$

Where "Qthloss" is the thermal power loss in the form of heat and it is calculated through the Modelica heat port connection.

$$C_t * der(T) = iQ_{rad} - Q_e - Q_{thloss}$$

Where "Ct" is the heat capacity, "T" is the temperature and "iQrad" is the input solar radiation power. Through this equilibrium equation the exact power loss is known and the actual temperature is calculated.

$$(V_{tilde} - iVoc) / (iValpha - iVoc) = I / (ialpha * ilsc)$$

This is the equation describing the two straight lines approximating the IV curves. Where "Vtilde" is the maximum voltage corresponding to the short circuit current before it starts to decrease rapidly, "iVoc" is the open circuit voltage, "iValpha" is the voltage corresponding to the alpha short circuit current, "I" is the current, "ialpha" is the factor alpha which is multiplied by a, "iIsc" is the defined short circuit current of the IV curve.

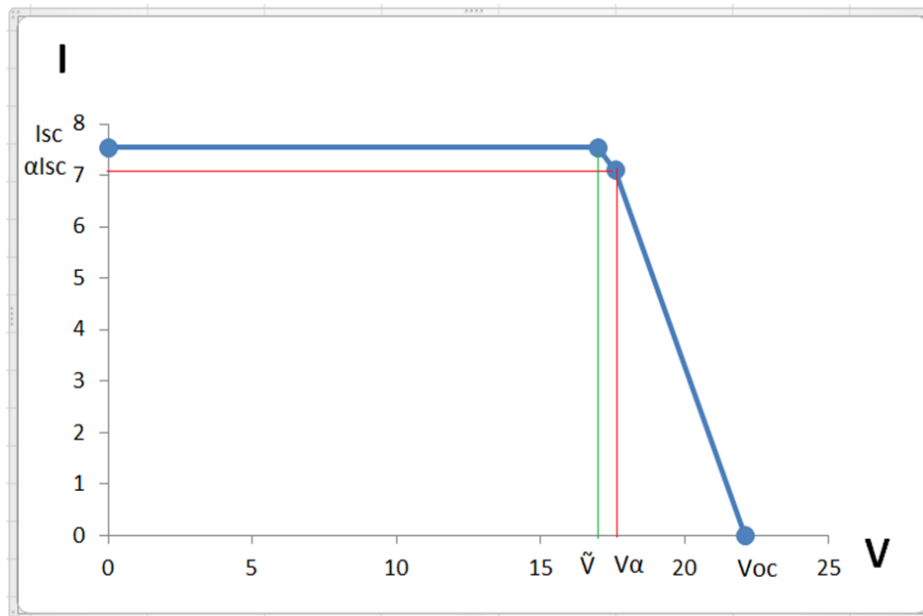


FIG. 3.1.5 - IV-Curve

if V < Vtilde then

$$I = i_{sc};$$

else

$$I = i_{alpha} * i_{sc} * (iV_{oc} - V) / (iV_{oc} - iV_{alpha});$$

end if;

And this if – else condition is used to complete filling the rest of points to complete drawing the approximated two lines of the original IV curve as follows:

If the value of the voltage is less than Vtilde then the current values corresponding are considered constant equals to the short circuit current value as a relevant approximation.

Otherwise the current value shall be decreasing following the straight line described by the second equation both these 2 approximations are relevant to describe the IV curve in a simple and easy modelling way and saves the efficiency of calculation time of the model.

The third stage is the cell 2 lines and it uses the data from the previous two stages and connecting them together to give the final model that represents the PV cell through the third stage block only, which contains directly the input values of the solar radiation, the input temperature and the output positive and negative pins hiding all the details inside the previous 2 stages.

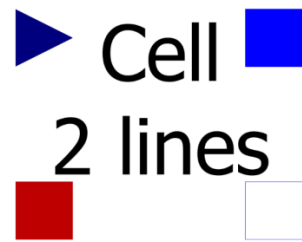


FIG. 3.1.6 - Cell 2 lines Modelica icon

Here in the above FIG.3.1.6 we can see only the input solar radiation as a blue triangle at the top left which has to be an input to the block, the heat port as red square at the bottom left that express the heat inside the PV cell and all heat transfer can be introduced through it, and the positive and negative pins as blue and white squares at the right that represent the electrical connection to the PV cell.

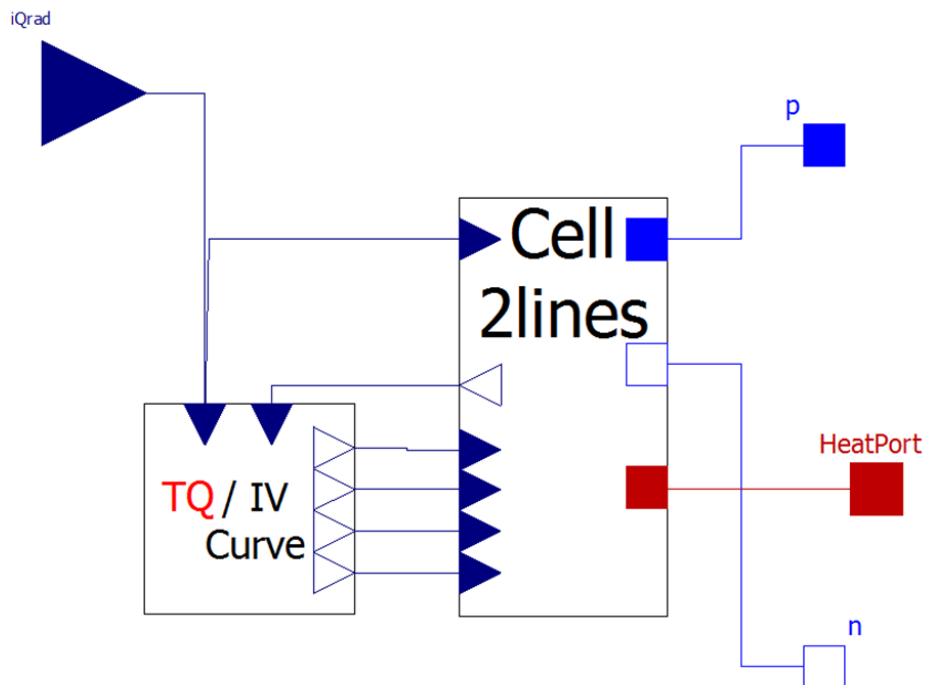


FIG. 3.1.7 - Cell 2 lines Modelica diagram

As shown in the above FIG.3.1.7 the third stage Modelica diagram connects stages one and two and gives at the end only the needed points to connect the PV cell with the outer world like amount of solar radiation intensity, thermal heat exchange through the heat port and other electrical systems through the positive and negative pins.

Now just few parameters need to be inserted before simulation of the model as shown in the following FIG.3.1.8.

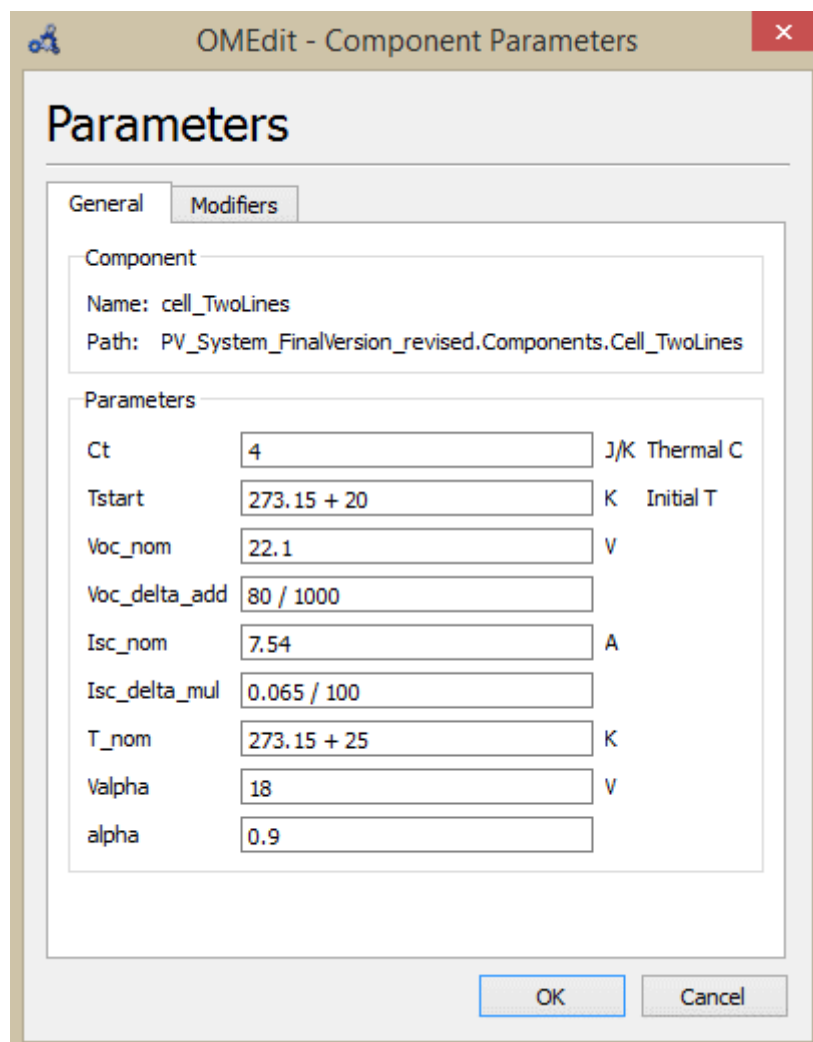


FIG. 3.1.8 – Cell 2 lines parameters

Since no real experiment was executed in this thesis, the values of parameters were found in the suitable literature sources. Through reading the BP solar data sheet of BP 3125 the parameters values were found as shown in the FIG.3.1.9 below.

Typical Electrical Characteristics	BP 3125
Maximum Power (P_{max})	125W
Warranted minimum power	119W
Voltage at P_{max} (V_{mp})	17.6V
Current at P_{max} (I_{mp})	7.1A
Short circuit current (I_{sc})	7.54A
Open circuit voltage (V_{oc})	22.1V
Temperature coefficient of I_{sc}	$(0.065 \pm 0.015)\%/K$
Temperature coefficient of V_{oc}	$-(80 \pm 10)mV/K$
Temperature coefficient of P_{max}	$-(0.5 \pm 0.05)\%/K$
NOCT (Air 20°C; Sun 0.8kW/m ² ; wind speed 1m/s)	$47 \pm 2^\circ C$
Maximum series fuse rating	15A (BP 3125S) / 20A (BP 3125U)
Maximum system voltage	1000V (IEC 61215 rating) 1000V (TÜV Rheinland rating)

Standard test conditions - irradiance of 1000W/m² at an AM1.5G solar spectrum and a temperature of 25°C.

FIG. 3.1.9 - BP 3125 datasheet

The configuration used for testing the Cell 2 lines module as shown in FIG.3.1.10 below.

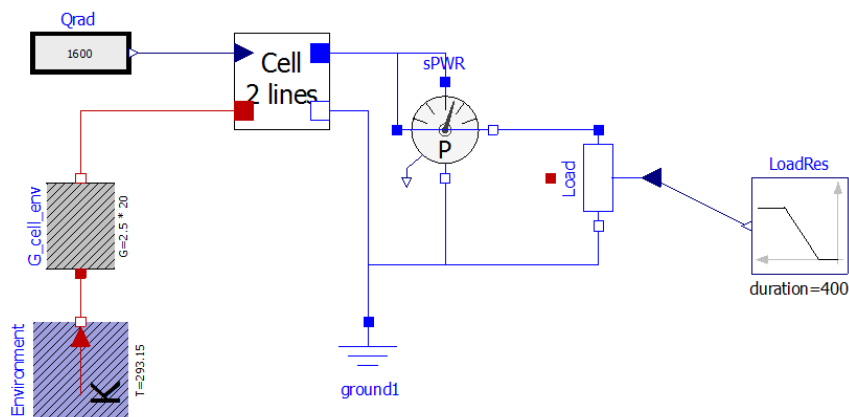


FIG. 3.1.10 - cell 2 lines test configuration

At a fixed solar radiation and temperature the cell was tested with variable load of ramp function.

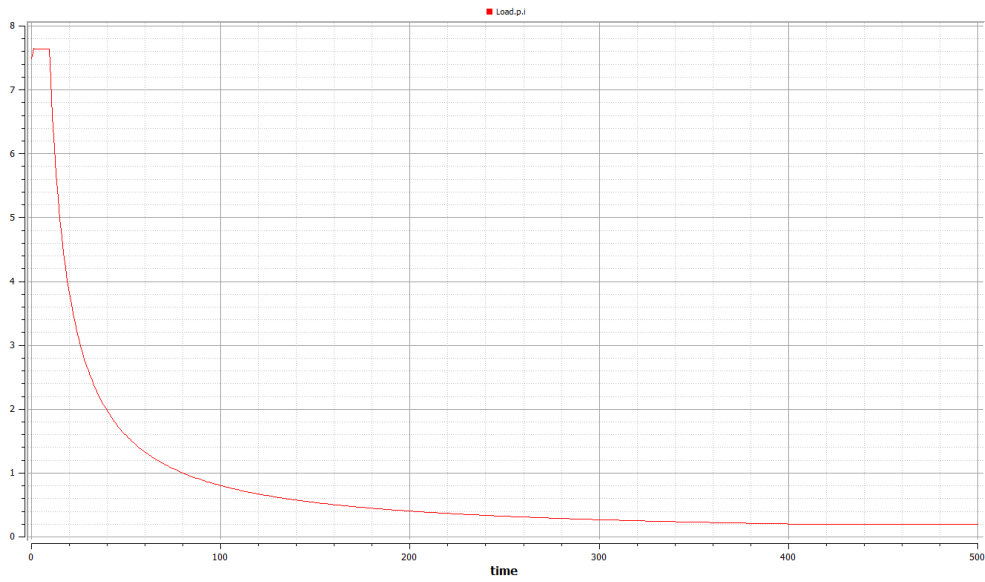


FIG.3.1.11 - Cell 2 lines output current

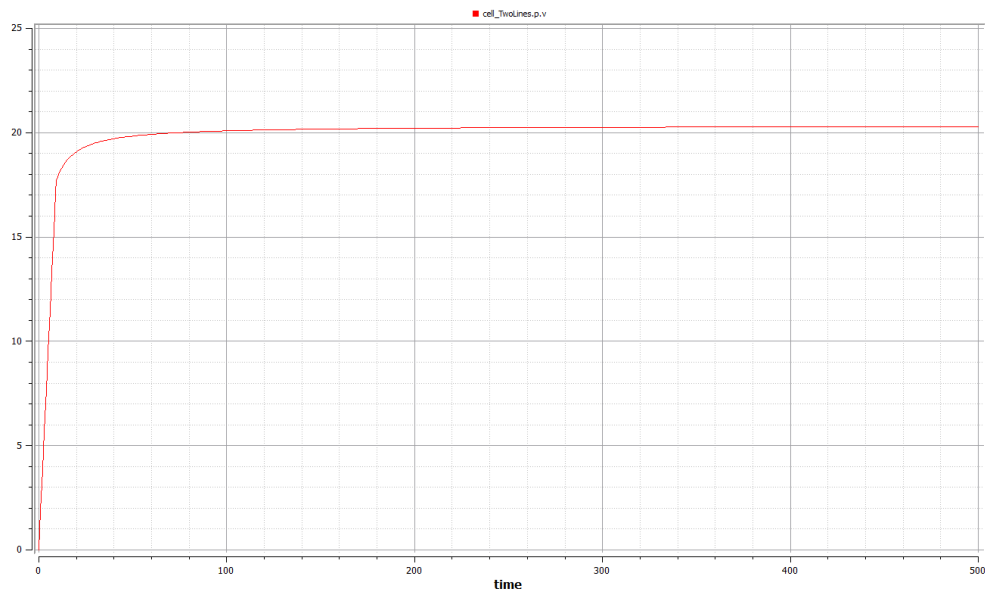


FIG.3.1.12 - Cell 2 lines output voltage

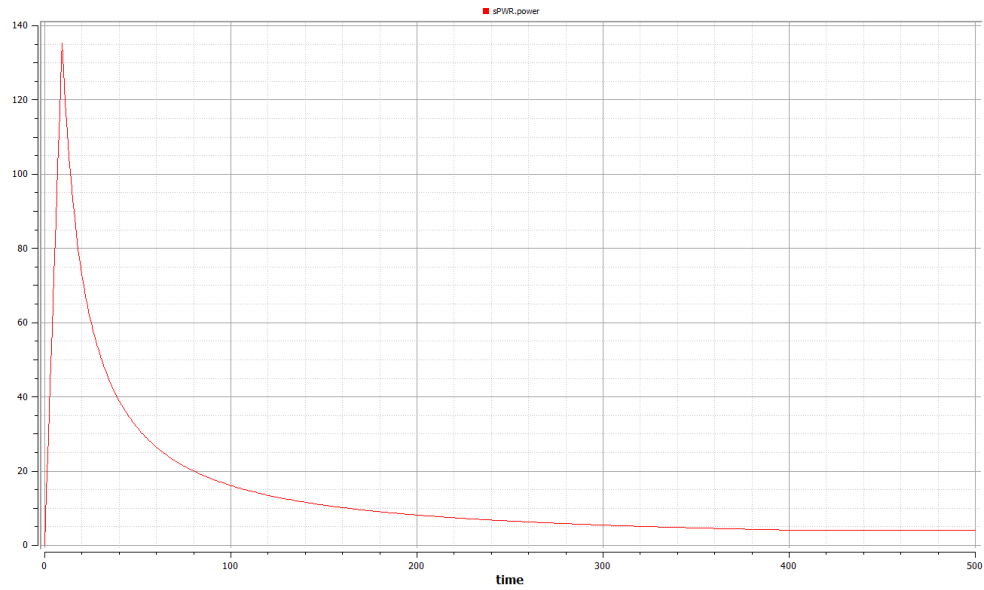


FIG.3.1.13 - Cell 2 lines output power

Series and parallel connections inside a module:

The power output of one cell is relatively small so usually they are connected in modules to be able to feed loads with different voltage and current so the cells are connected in series and parallel connections to form a module and according to the voltage and current needed to feed the load the connection is chosen as series or parallel. For series connection of several cells the overall voltage increase while the current stays the same and for the parallel connection of several cells the overall voltage stays the same of one cell while the current is multiplied by the number of cells existing in the parallel connection.

Series module:

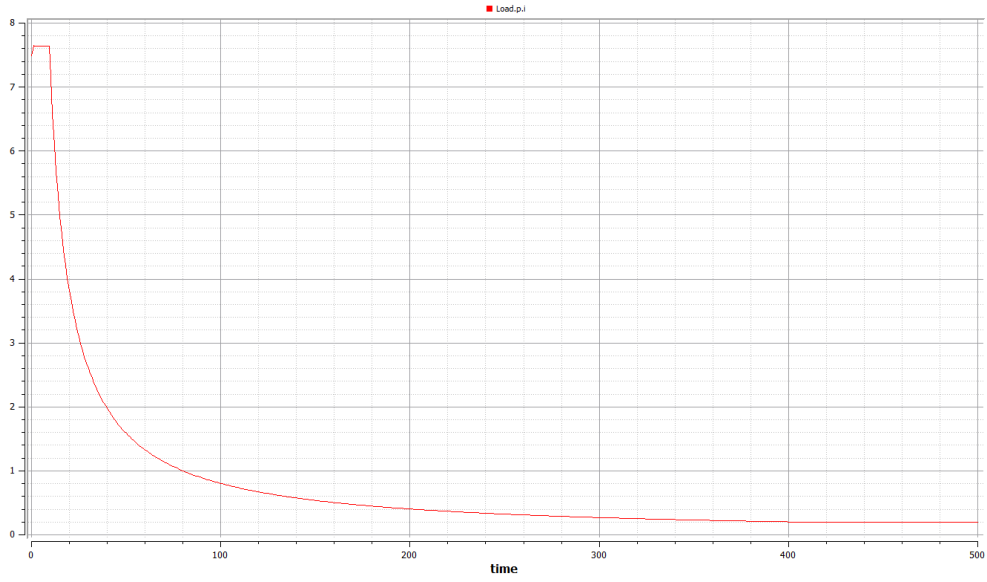


FIG.3.1.14 - Cell Series output current

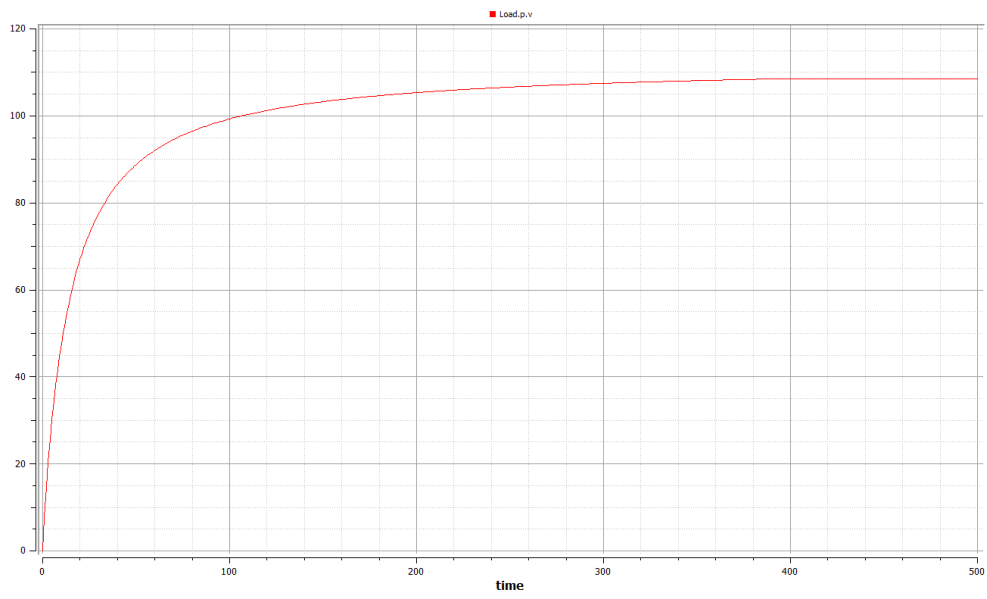


FIG.3.1.15 - Cell Series output voltage

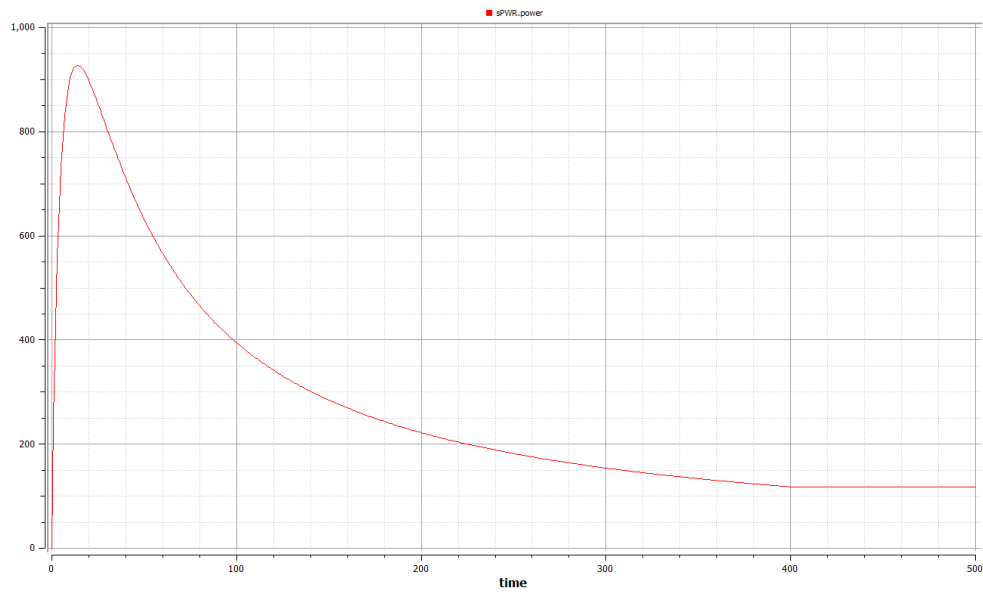


FIG.3.1.16 - Cell Series output power

In this model the voltage and the total power were multiplied 5 times while the current is not changed as it is composed of 5 cells connected in series

Parallel module:

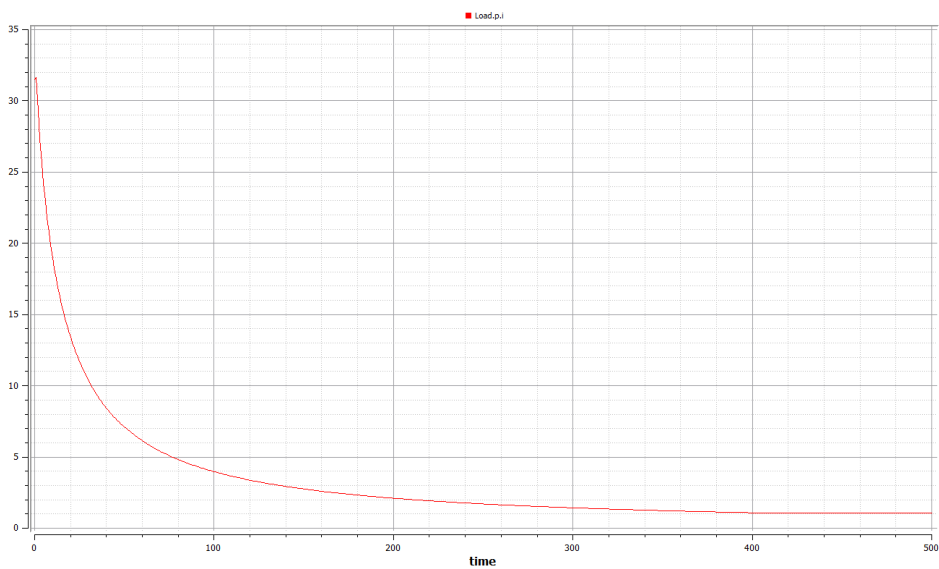


FIG.3.1.17 - Cell parallel output current

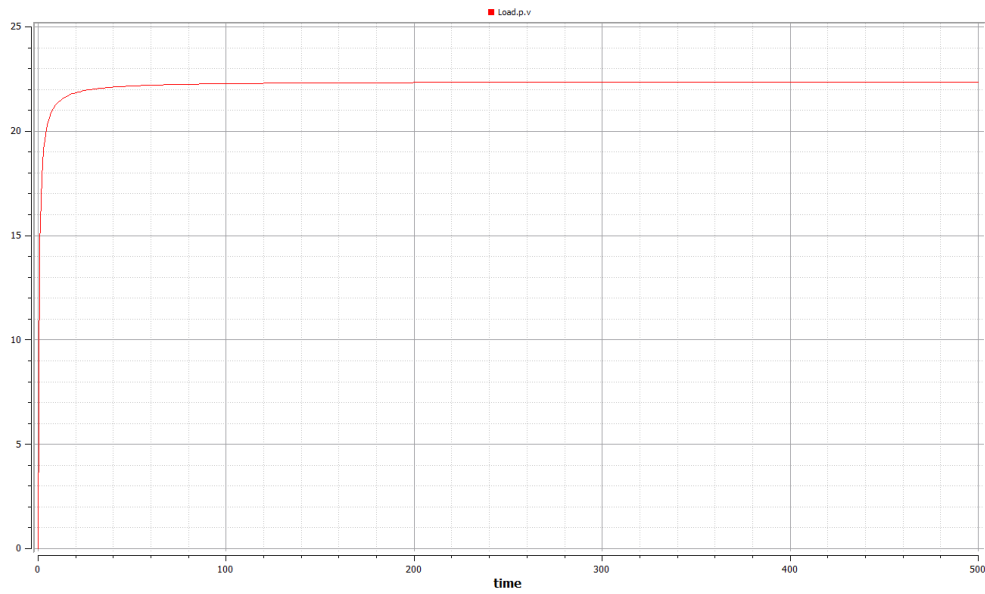


FIG.3.1.18 - Cell parallel output voltage

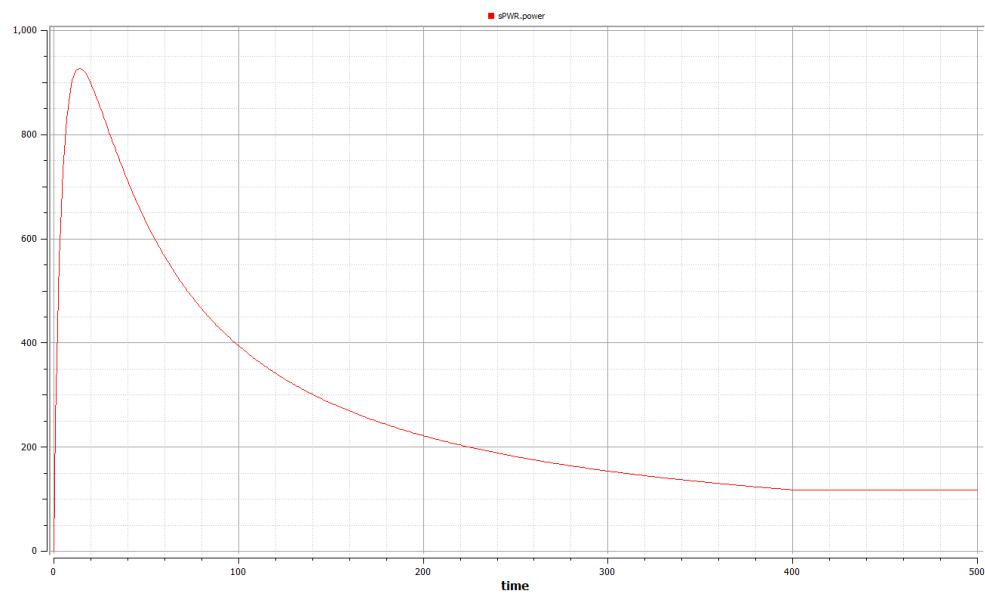


FIG.3.1.19 - Cell parallel output power

For the parallel model it is composed of 5 cells connected in parallel so the current and the total power were multiplied 5 times while the current is not changed.

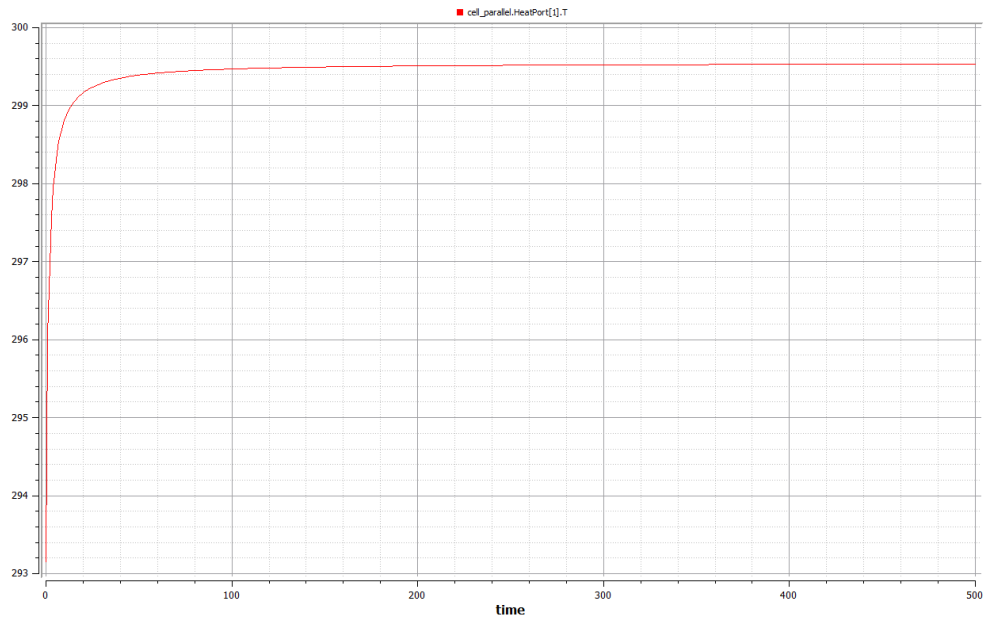


FIG.3.1.20 - Cell Heat port temperature

The heat response in FIG.3.1.20 shows that the temperature of the cell starts from ambient level and increases gradually due to the solar radiation heating and the power loss inside the PV cell then finally reaches a steady state.

3.2

BATTERY

For the output interface of the model only few things had to be in contact with the outer world so the battery icon was chosen simple as the FIG.3.2.1.

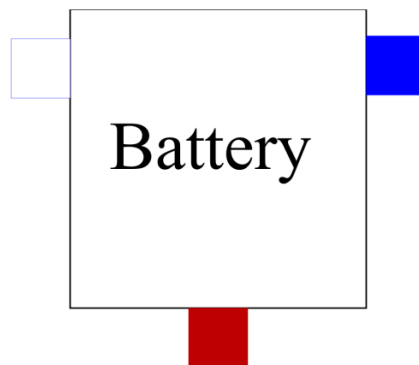


FIG.3.2.1 - Battery Modelica icon

In this icon the blue square at the top right represents the positive pin of the battery, the white square on the top left indicates the negative pin, and the red square at the bottom represents the heat port of the battery model.

These three parts represent the electrical connection of the battery expressed in the positive and negative pins, Plus the thermo-dynamic connection through the heat port.

And more details about the battery model are shown in the FIG.3.2.2 below

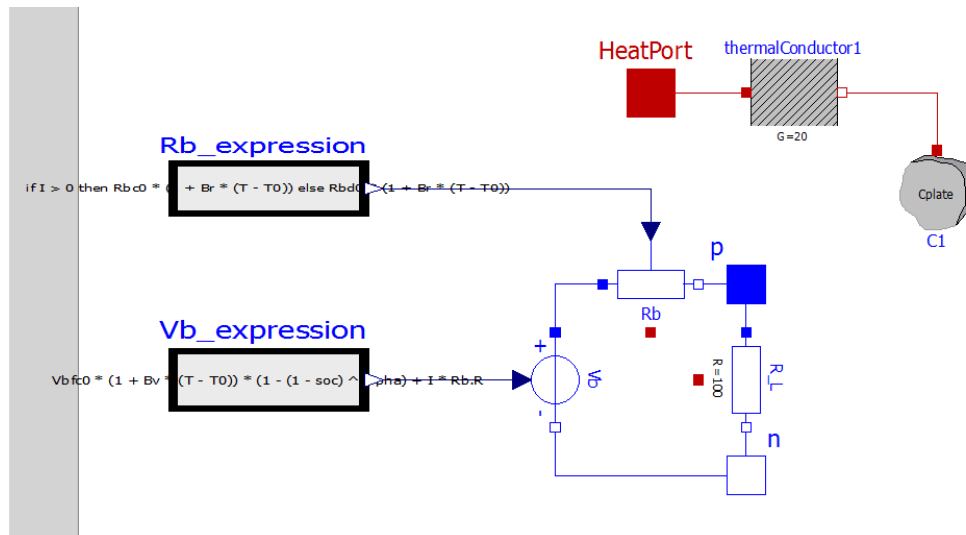


FIG.3.2.2 - Battery Modelica diagram

The internal construction of the battery is divided into two main parts; the electrical and thermal parts.

First the electrical part consists of the positive and negative pins as blue and white squares and they are the battery terminals to be connected to other electrical devices, two resistances R_b which expresses the variable internal resistance of the battery and R_L which expresses the parallel discharge resistance between the battery terminals that indicates the long-time discharge if no load was connected, are shown in white rectangles between the voltage source and positive pin for R_b and between the positive and negative pins for R_L , the last electrical component is the voltage generator which express the internal battery generated voltage.

While the thermal part is composed of the heat port this is also connected to the heat ports of both resistances of the model R_b and R_L to indicate the amount of heat generated inside the

model due to chemical reactions and represent the battery temperature to be connected through a thermal conductor to the temperature of the environment at the end which is expressed by the Cplate to simulate the heat transfer exchange effect.

Inside the battery model it was taken into consideration the real factors affecting the battery model behaviour "model variables" which are the internal resistance, Battery ampere hour capacity and voltage which are affected by change in temperature and state of charge. So the main variables of the battery model were selected to be: The battery internal resistance, voltage, current, charge and Temperature

The battery voltage keeps changing at every different state of charge of the battery giving the highest voltage corresponding to battery fully charged state, as shown in the FIG. 3.2.3 below

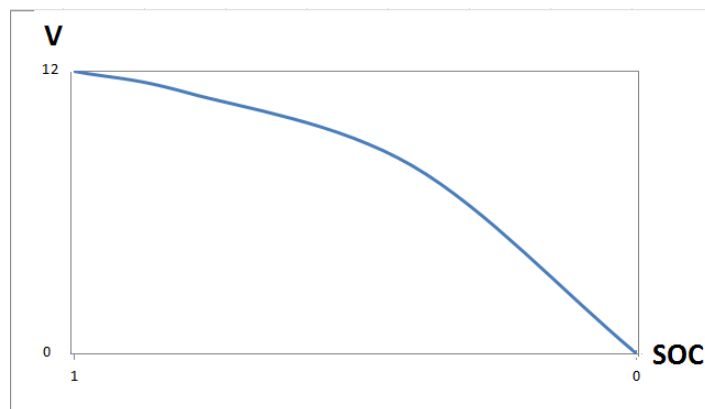


FIG. 3.2.3 - V-SOC-curve

Accordingly the characteristic curves of battery voltage vs state of charge can be interpreted as in the following equation:

$$Vb(t) \times (1 - (1 - soc)^{\alpha}) \quad , \text{for } \alpha > 1$$

Where, "soc" is the state of charge, "Vb(t)" is the change in battery voltage as a function of time, "a": represents the order of the polynomial which was selected in this model for model simplicity as second order polynomial.

The parameters "Bv, Br, Bmax" were driven from datasheets characteristic curves representing the relation between temperature change versus voltage, internal resistance, and battery maximum capacity respectively.

And was used in the equations to calculate the value of voltage, internal resistance and battery maximum capacity each in its equation:

$$Vb = Vbfc0 * (1 + Bv * (T - T0))$$

Where, "Vb": represents the battery voltage, "Vbfc0": represents the battery open circuit voltage, "Bv": represents the voltage coefficient corresponding to the change in temperature from ambient, "T": represents the working temperature, "T0": represents the standard working temperature.

$$Rb = [charging * Rbc0 + (1 - charging) * Rbd0] * [1 + Br * (T - T0)]$$

Where, "Rb" is the battery internal resistance, charging: represents the charging state of the battery "Rbc0" is the battery charging resistance coefficient, "Rbd0" is the battery discharging resistance coefficient, "Br" is the resistance coefficient corresponding to the change in temperature from ambient, "T" is the working temperature, "T0" is the standard working temperature.

$$Cmax = 3600 * ratedAH0 * (1 + Bmax * (T - T0))$$

Where, "Cmax" is the battery maximum ampere-hour capacity, "ratedAH0" is the battery ampere-hour capacity in standard working temperature, "Bmax" is the maximum ampere-hour capacity coefficient corresponding to the change in temperature from ambient, "T" is the working temperature, "T0" is the standard working temperature.

And the state of charge "soc" was expressed by the ratio of the battery charge at a given instant "C" compared to the battery maximum capacity "Cmax" as in the equation:

$$soc = C / Cmax$$

Other variables that were used in the model are:

"CurrentDir" which is defined as a real value of zero or one to express the current direction, if current "I" has value greater than zero then "CurrentDir=1" otherwise "CurrentDir=0", beside the variable "charging" has values from zero to one and is used to account for the non-instantaneous transition between charging and discharging states of the battery through the equation:

$$Charging + Taw_c * der(Charging) = CurrentDir$$

And finally the parameters needed for the model simulation are in the FIG.3.2.4

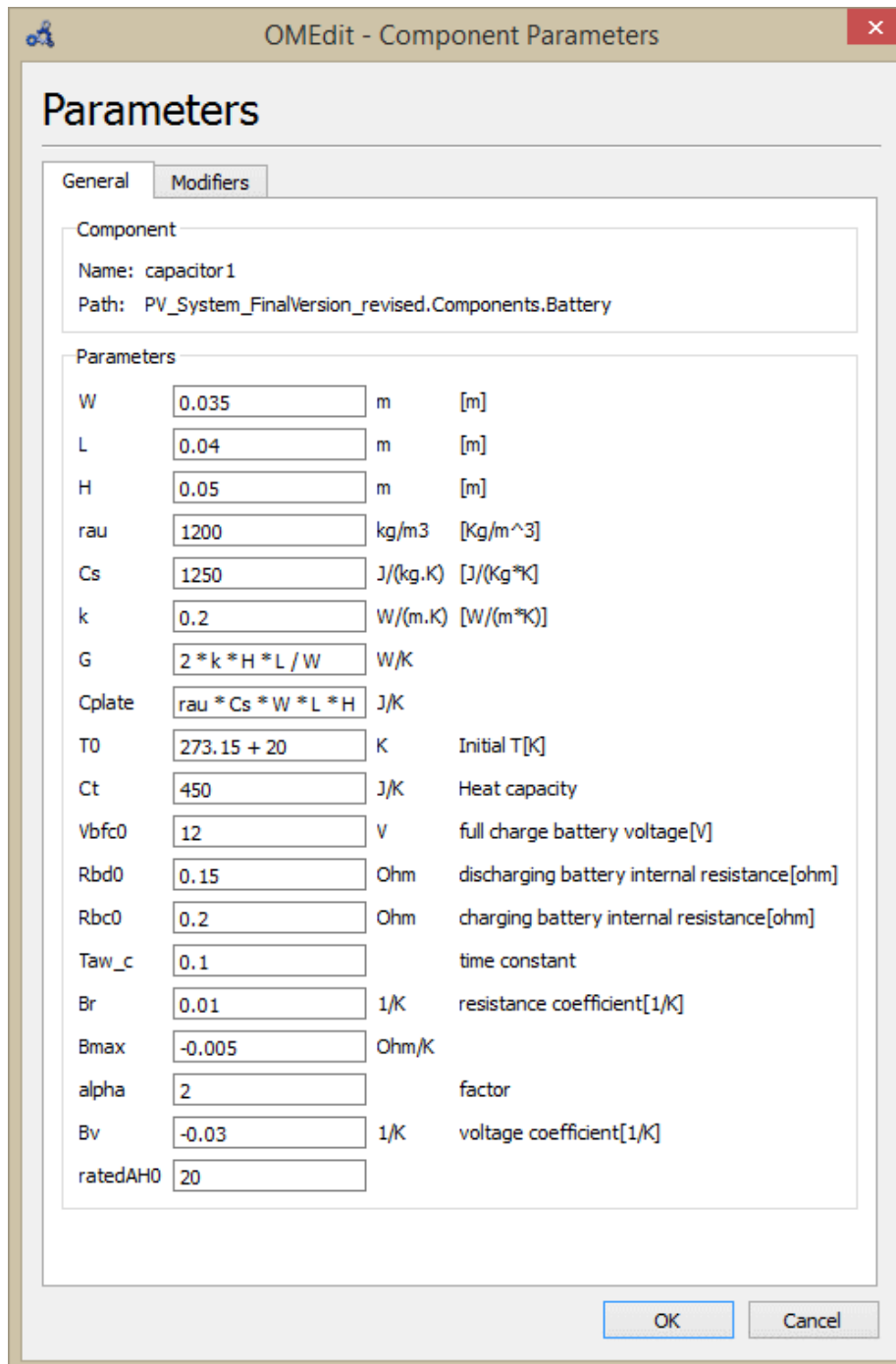


FIG.3.2.4 – Battery Parameters

As no experiments were done in this thesis the parameters values were deduced from datasheets and temperature curves

Capacity vs. Operating Temperature

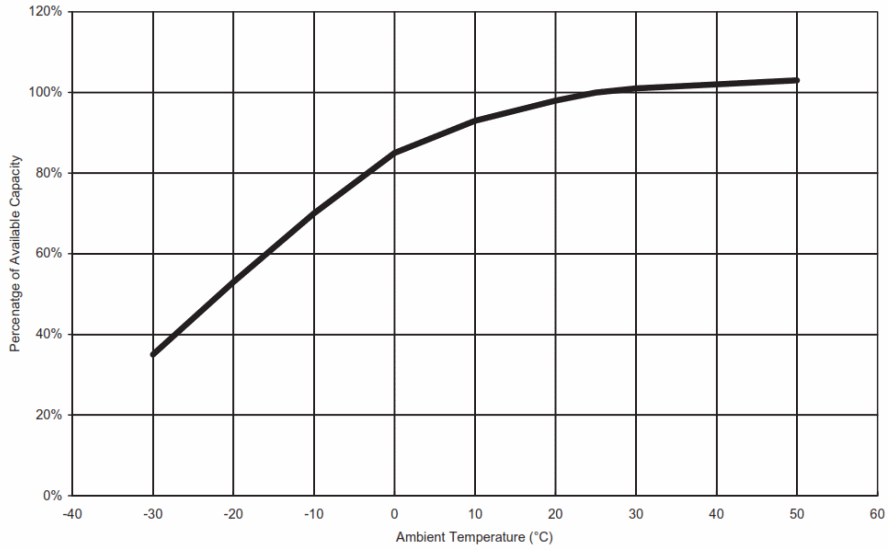


FIG.3.2.5 – Battery capacity vs temperature

Constant Charging Voltage

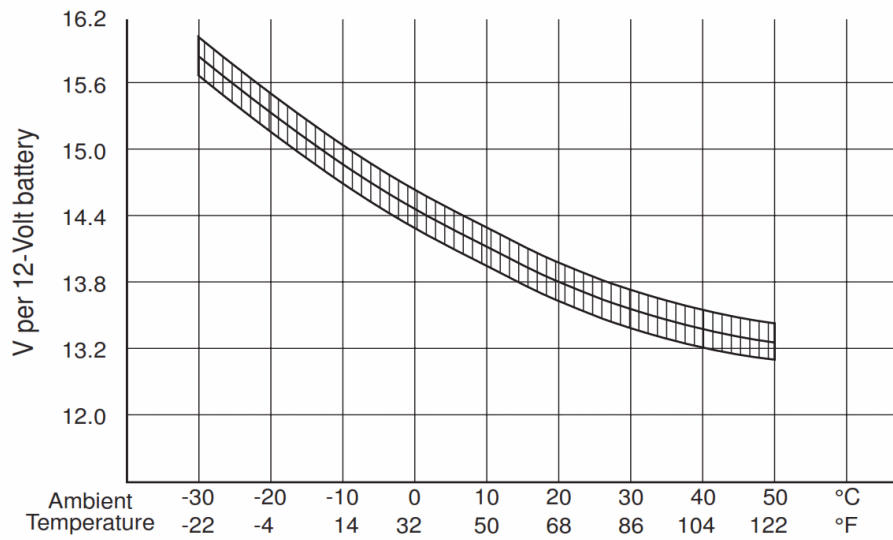


FIG.3.2.6 – Battery voltage vs temperature

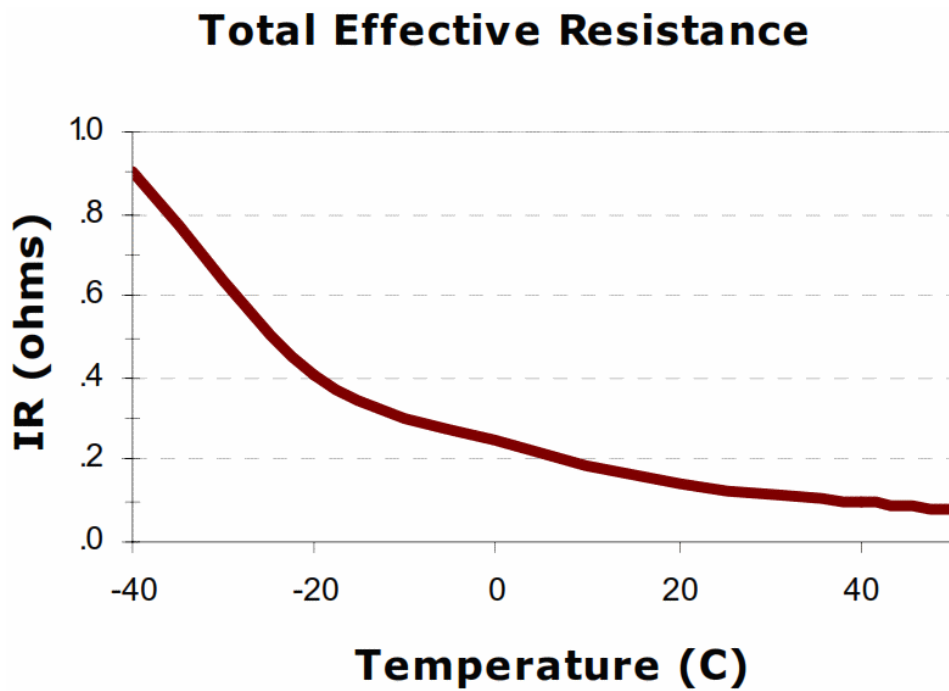


FIG.3.2.7 – Battery internal resistance vs temperature

From the previous figures 3.2.5,6,7 the factors B_v , B_{max} and B_r were deduced to be relevant realistic model.

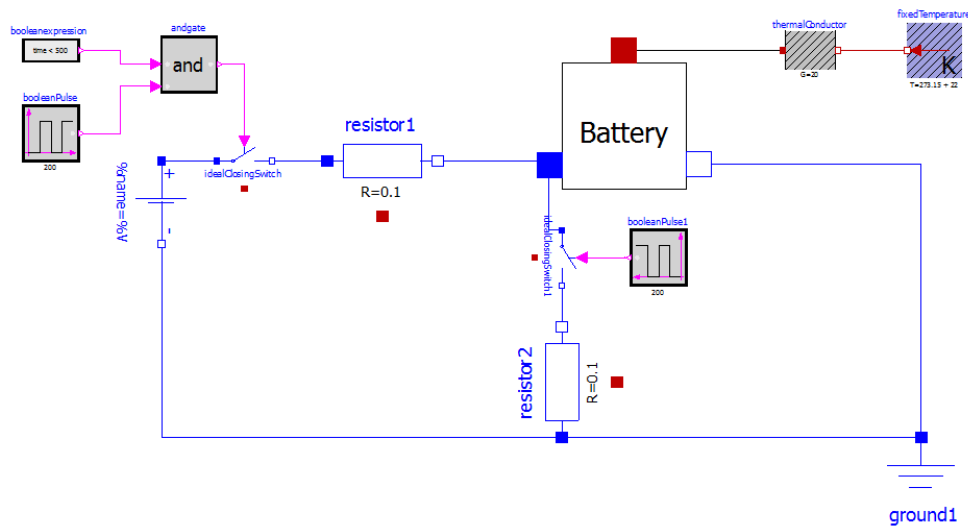


FIG.3.2.8 – Battery test configuration

The test configuration of the battery model in Fig.3.2.8 consists of a DC voltage source representing the input from PV cell and it charges the battery through resistor1, the heat port of the battery is connected to a thermal connector and a fixed temperature source representing the environment temperature, and the resistor2 exists to discharge the battery when its switch is closed. For charging of the battery, resistor1 switch is closed and resistor2 switch is open through a Boolean input signal to the switches and vice versa shall be done for discharge.

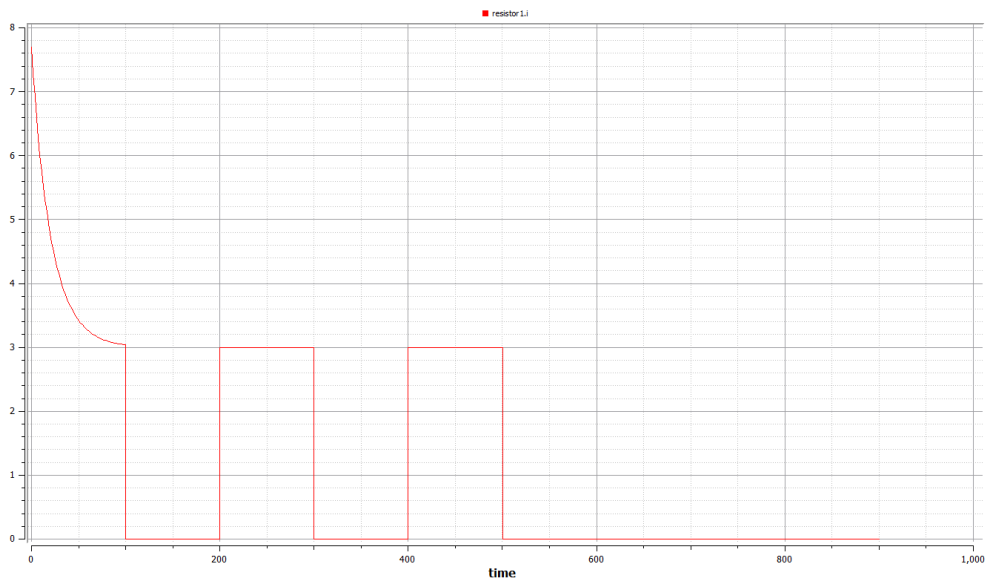


FIG.3.2.9 – Battery charging current

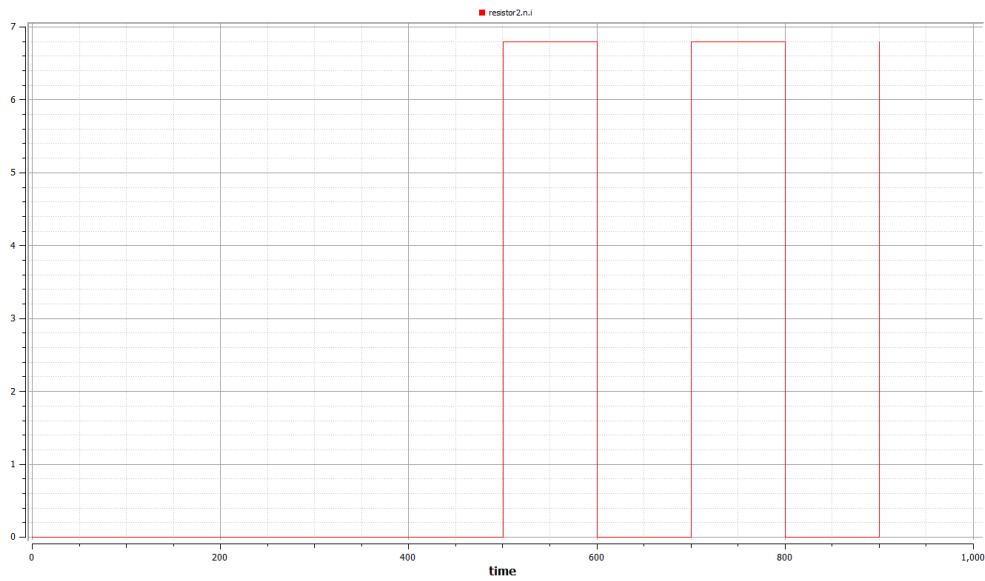


FIG.3.2.10 – Battery discharging current

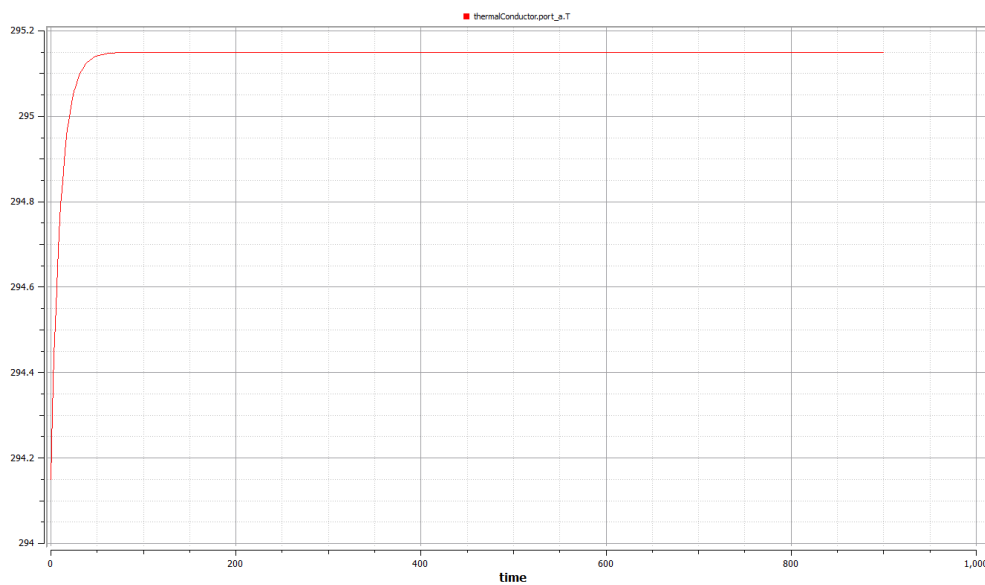


FIG.3.2.11 – Battery heat port temperature

Also the temperature of the battery model appearing in the heat port as shown in FIG.3.2.11 increases gradually above ambient then reaches a steady state value finally.

3.3

INVERTER

Phasor pins concept:

Pins are used as connectors in the Modelica language and they are necessary elements to construct any electrical model. The pins in the MSL are consisted of two variables, the potential at the pin, the voltage and the flowing variable, the current. The pins carry the information related to the complex quantities in the rectangular form. Given a pin labeled as "a", "a.Vre" stands for the real part of the complex potential, "a.Vim" stands for the imaginary part of the complex potential in the pin. "a.Ire" carries the information of the real part of the complex current which is a flow variable whereas "a.Iim" is the imaginary counterpart of the complex current.

In order to represent the AC power in our model, a phasor pin was used which defined internally through a separate interface model equations to play the role of a real and imaginary pins together and applying the calculations were considered on the real values and imaginary values separately but still included in one interface component replacing the normal positive and negative pins with the phasor positive and negative pins in case of using AC power to be able to take into consideration the phasor representation of the complex voltage and current relationships.



FIG.3.3.1 – Phasor pins

In each phasor pin model interface the imaginary and real values of voltage and current are declared as the pin variables as shown in the FIG.3.3.2 below to be used easily later in the complex AC models:

phasor positive pin

Contents

Type	Name	Description
Voltage	Vre	V phasor,real part [V]
Voltage	Vim	V phasor,imaginary part [V]
flow Current	Ire	I phasor,real part [A]
flow Current	Iim	I phasor,imaginary part [A]

FIG.3.3.2 –Phasor pins variables'

Then these pins were used to create new phasor models of resistors, inductors, capacitors, sine voltage source, ground and commutating switch to be able to use the new models directly with phasor representation.



FIG.3.3.3 – inverter Modelica icon

As shown in the FIG.3.3.3 the Inverter icon is composed of positive and negative pins represented by blue and white squares on the left as DC side circuit terminals of the inverter, positive and negative phasor pins represented by Blue and red squares on the right as AC output terminals of the inverter, and also two blue triangles on top to represent the control inputs of the inverter which are the phase angle "delta" and the output voltage amplitude "Vac_amplitude" that are used to define the desired output voltage of the inverter.

These icons were chosen for convenient and simple representation of the model to be easily understood and used in connection with other models.

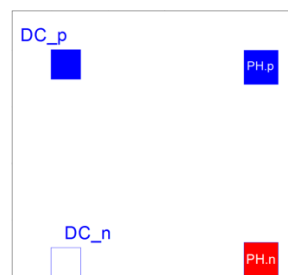


FIG.3.3.4 – inverter Modelica diagram

The model diagram in FIG.3.3.4 is done in a simple way to express the relation between input DC power and output AC power including the efficiency of the inverter.

$$P_{ac} = P_{dc} \times \eta$$

Then the Power on each side was declared in details, in the DC side power is a relationship of the variable DC current and voltages

$$P_{dc} = V_{dc} \times I_{dc}$$

While at AC side the power is a function of imaginary and real voltages and currents defined in the phasor pins as described through the equations:

$$P_{ac} = V_{re} \times I_{re} + V_{im} \times I_{im}$$

Where, V_{re} is the real voltage, I_{re} is the imaginary voltage, V_{im} is the imaginary voltage, I_{im} is the imaginary current.

Then the relation between control inputs to form the AC output voltage is described through the equations:

$$V_{re} = V_{ac} \times \cos\delta + (R + 2\pi fL) \times \sqrt{I_{re}^2 + I_{im}^2} \times \cos\left(\arctan\left(\frac{X}{R}\right) + \frac{\pi}{2}\right)$$

$$V_{im} = V_{ac} \times \sin\delta + (R + 2\pi fL) \times \sqrt{I_{re}^2 + I_{im}^2} \times \sin\left(\arctan\left(\frac{X}{R}\right) + \frac{\pi}{2}\right)$$

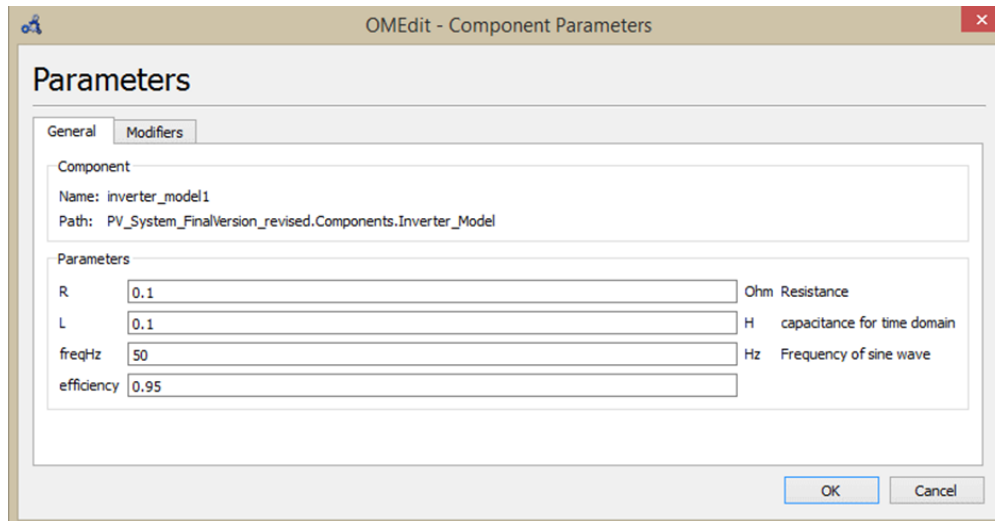


FIG.3.3.5 – inverter parameters

For completing the model simulation more parameter values are needed to be assigned for R and L that were chosen of small values (0.1) as the Inverter has very low impedance, while Frequency was fixed to 50 Hz and Efficiency as 0.95 %.

Inverter test islanded case:

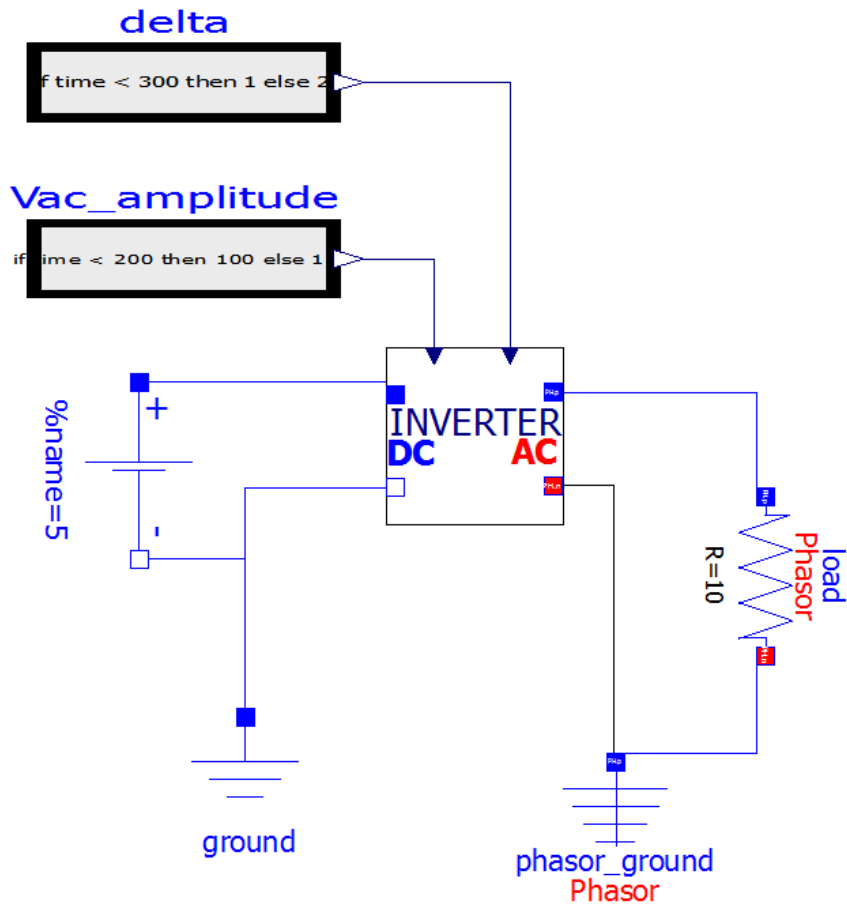


FIG.3.3.6 – inverter test islanded case configuration

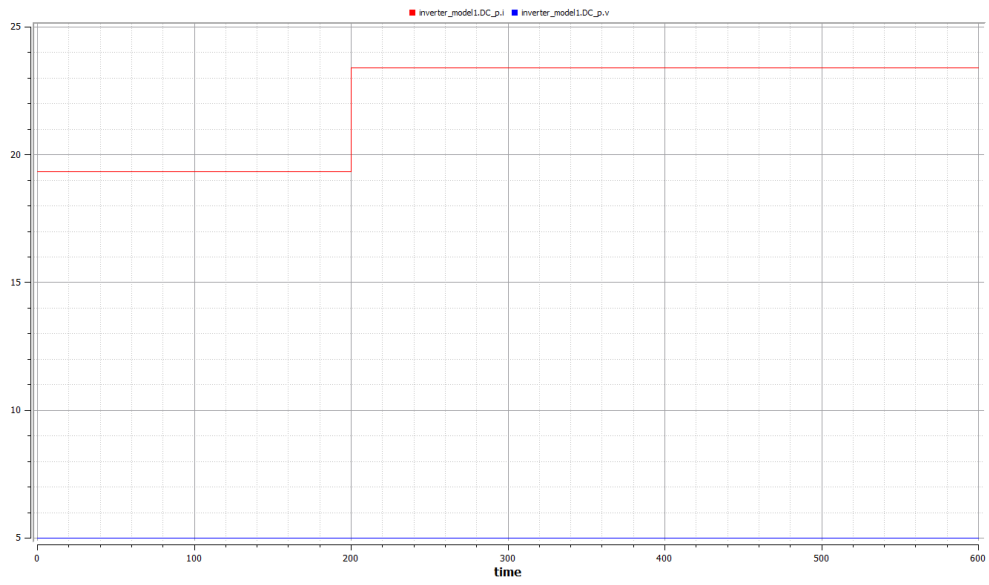


FIG.3.3.7 – inverter test islanded case DC input

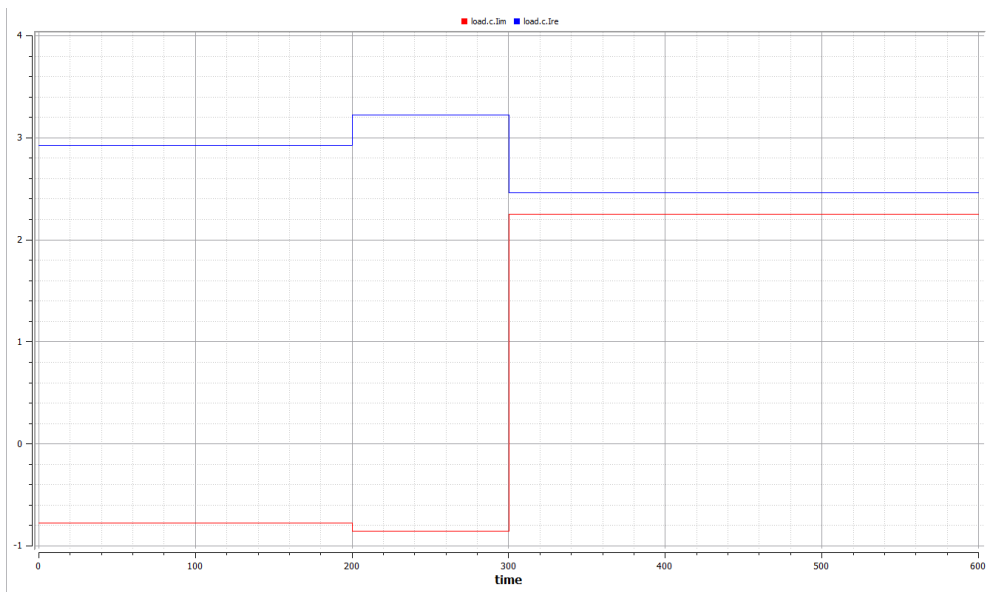


FIG.3.3.8 – inverter test islanded case AC current

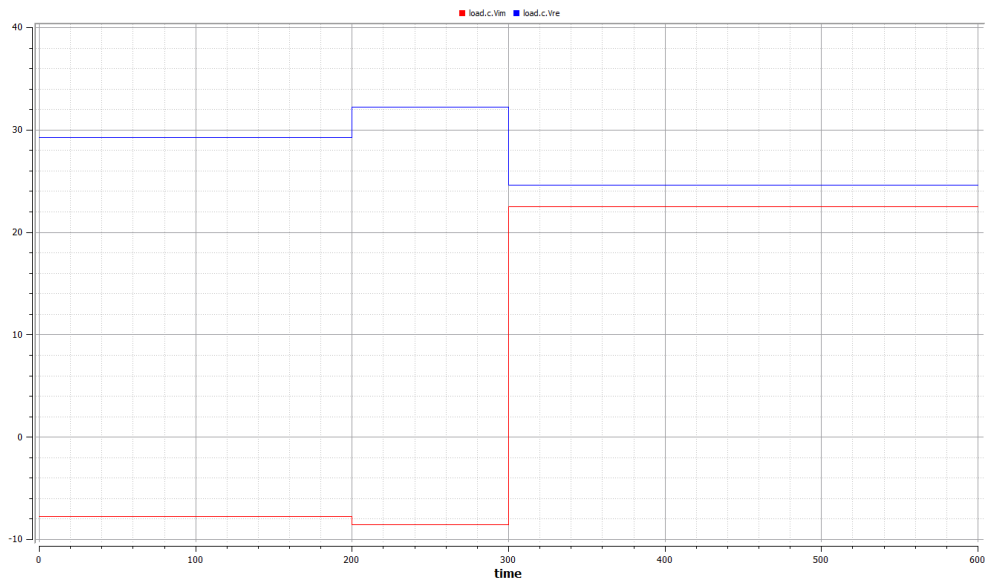


FIG.3.3.9 – inverter test islanded case AC voltage

For the islanded case the inverter is connected to the load directly which is represented by a phasor resistance.

The input phase angle is increased at time 300 from value 1 to be 2, and the input voltage amplitude is increased at the time 200 from value 100 to be 110 in order to feel the effect of changing of inputs on the output response of real voltage, real current, imaginary voltage and imaginary current.

Inverter test connection to grid case:

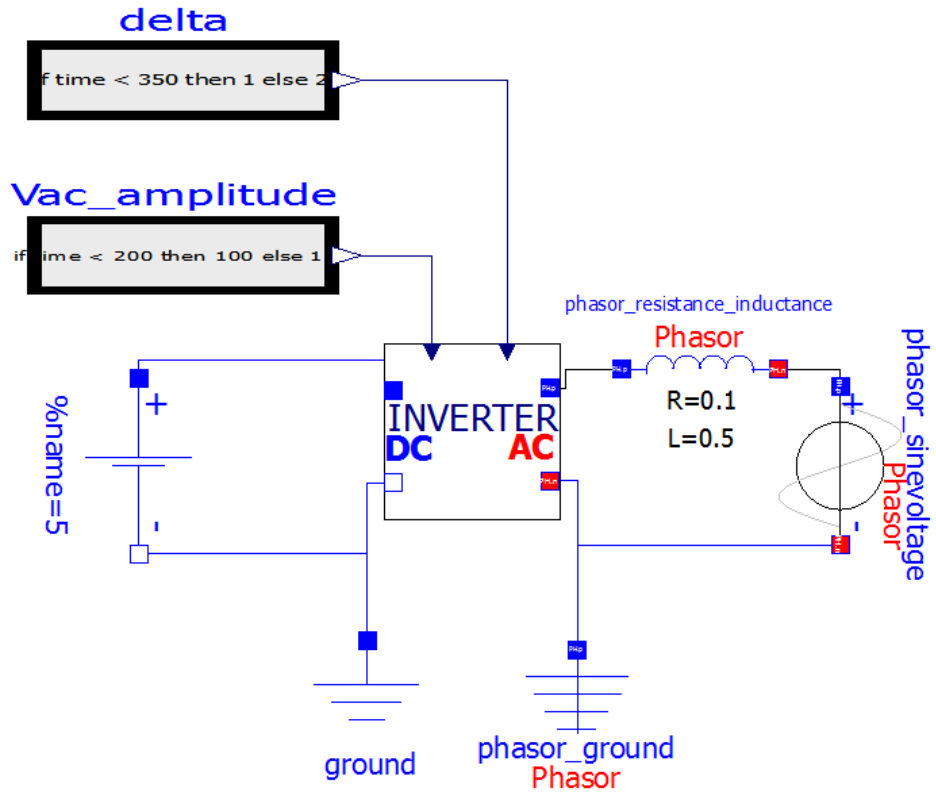


FIG.3.3.10 – inverter test grid case configuration

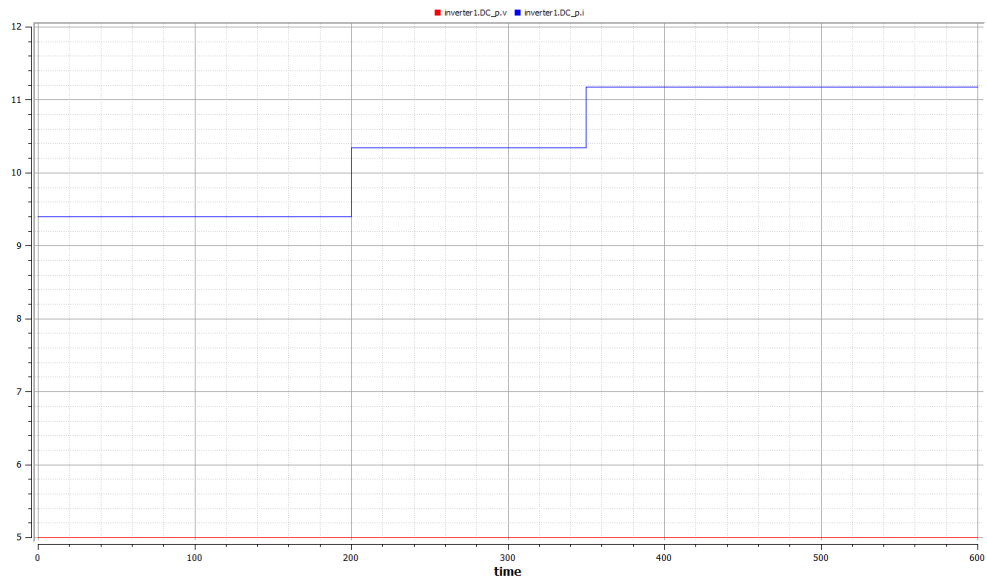


FIG.3.3.11 – inverter test Grid connected case DC input

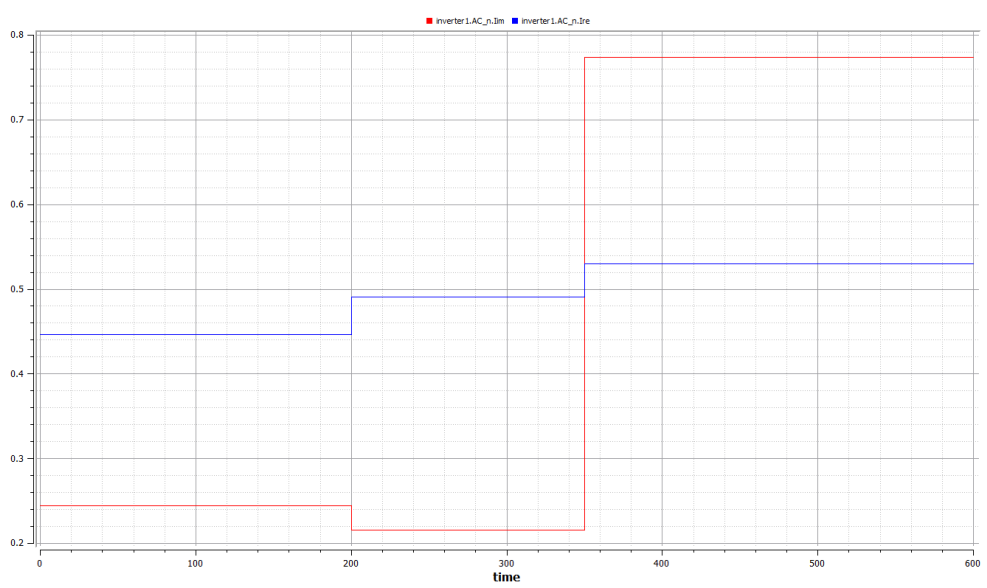


FIG.3.3.12 – inverter test Grid connected case AC current

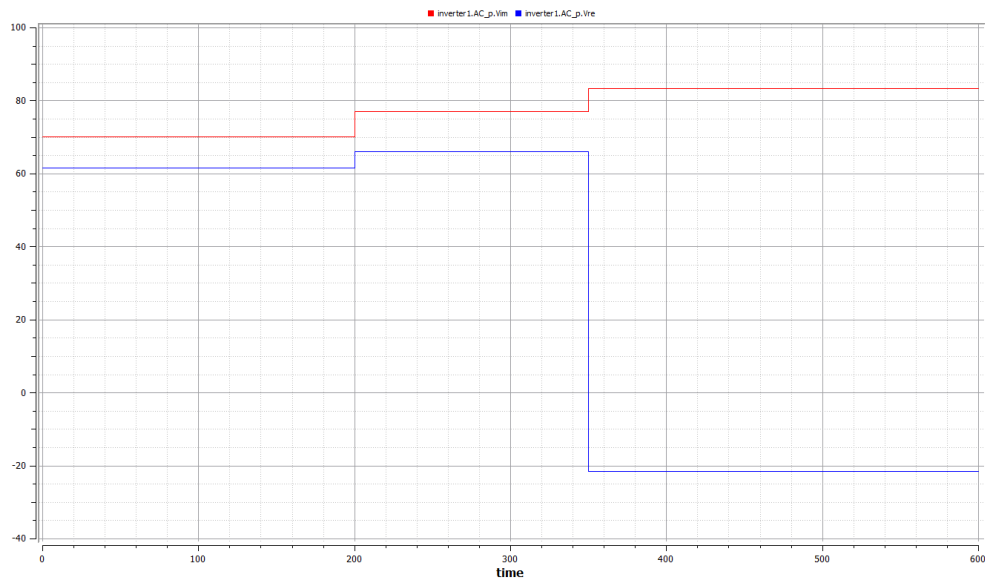


FIG.3.3.13 – inverter test Grid connected case AC voltage

In the grid connected case the same procedures of previous test was applied but the resistive load is replaced with a phasor AC voltage source and small inductance that express the grid and its impedance.

4

CHAPTER FOUR

SIMULATION

EXAMPLES

4.1

Controller

This section presents the background behind the modelling of the controller of a stand-alone PV system.

All power systems must include a control strategy that describes the interactions between its components. The use of battery as a storage form implies thus the presence of a charge controller.

The charge controller is used to manage the energy flow to PV system, batteries and loads by collecting information on the battery voltage and knowing the maximum and minimum values acceptable for the battery voltage. There are two main operating modes for the controller:

- 1) Normal operating condition, when the battery voltage fluctuates between maximum and minimum voltages.
- 2) Overcharge or over-discharge condition, which occur when the battery voltage reaches some critical values.

To protect the battery against an excessive charge, the PV arrays are disconnected from the system, when the terminal voltage increases above a certain threshold V_{\max_off} and when the current required by the load is less than the current delivered by the PV arrays. PV arrays are connected again when the terminal voltage

decreases below a certain value V_{\max_on} . This can be done by using a switch with a hysteresis cycle, as illustrated in FIG.4.1.1.

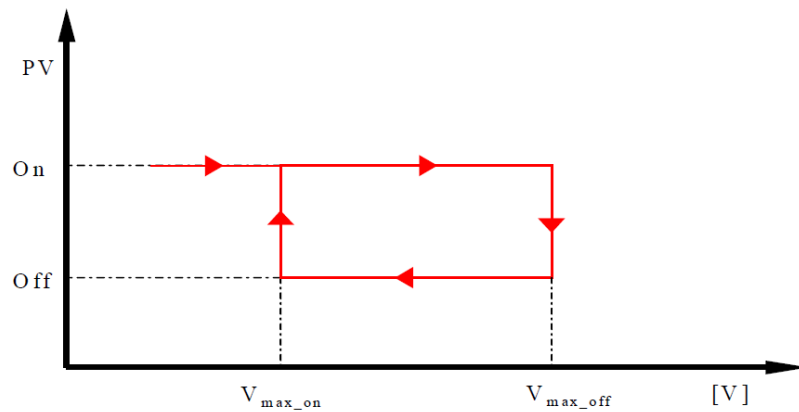


FIG.4.1.1 – operating principle of an overcharge protector

To protect the battery against excessive discharge, the load is disconnected when the terminal voltage falls below a certain threshold V_{\min_off} and when the current required by the load is bigger than the current delivered by the PV arrays. The load is reconnected to the system when the terminal voltage is above a certain value V_{\min_on} , using a switch with a hysteresis cycle, as shown in FIG.4.1.2.

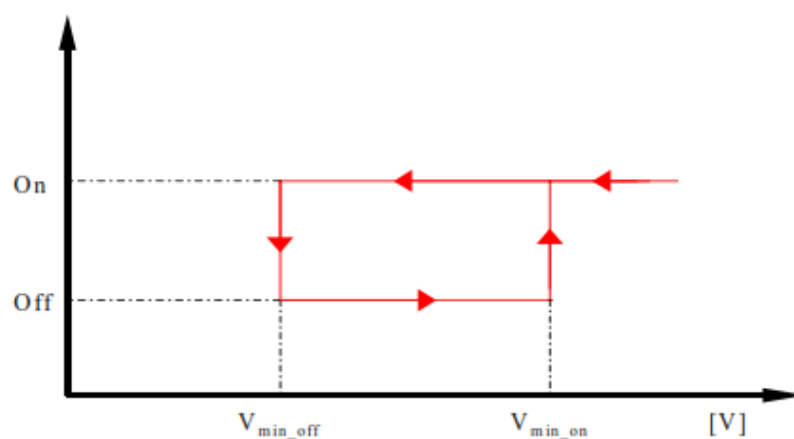


FIG.4.1.2 – operating principle of an discharge protector

The switches may either be electromechanical (relay, contactors, etc.) or solid state (bipolar transistors, MOSFET's, etc.) – see (Lorenzo, 1994).

The steps in the modelling of the controller process are summarized in Table below. [3]

	Constraint	Command
(1)	If $V > V_{max_off}$ and $I_{load} < I_{pv}$	Disconnect PV arrays from the system
(2)	If command (1) is done and $V < V_{max_on}$	Reconnect PV arrays to the system
(3)	If $V < V_{min_off}$ and $I_{load} > I_{pv}$	Disconnect the load from the system
(4)	If command (3) is done and $V > V_{min_on}$	Reconnect the load to the system

Summary of controller process – Table

4.1.1. MPPT techniques: Necessity and classification

4.1.1.1. Need of MPPT

The efficiency of PV system can be improved if the PV array is operated intentionally at MPP, irrespective of varying atmospheric conditions. This can be done by properly matching PV source with the load for any weather condition, to achieve maximum power generation. The technique by which the maximum power point on the P–V curve is been tracked electrically, MPP is located and maximum power is extracted for different environment conditions is called maximum power point tracking (MPPT). There are two ways by which maximum power can be extracted from PV array they are: Mechanical tracking and Electrical tracking (MPPT).

Mechanical tracking is a physical tracking process in which orientation of PV panel is changed at a pre-calculated and pre-defined angle throughout day along with the position of sun. The orientation of PV panel is also changed with months and seasons throughout year. This change in orientation can be manual or automatic. Electrical tracking (MPPT) is a process in which I-V curve of the panel is tracked for MPP. Usually power electronics devices are used in renewable energy power generation as electrical trackers. They can track the MPP in order to achieve maximum efficiency and can also convert DC power to AC power as required by stand-alone system or grid so as to comply with power quality requirements of the power system.

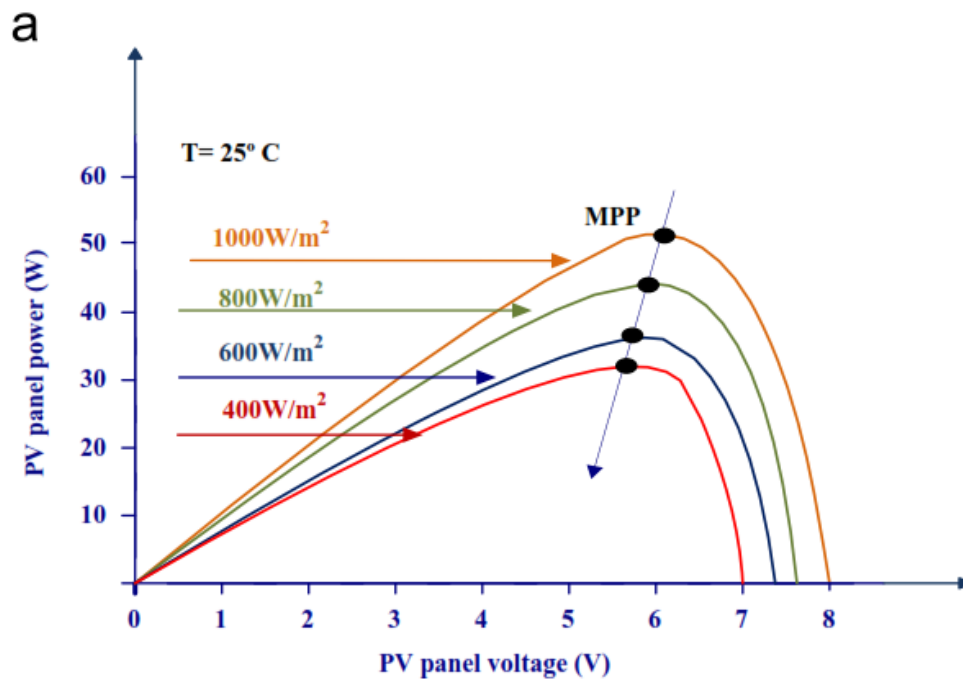


FIG.4.1.3.a – P-V characteristics at constant temperature and different insulations

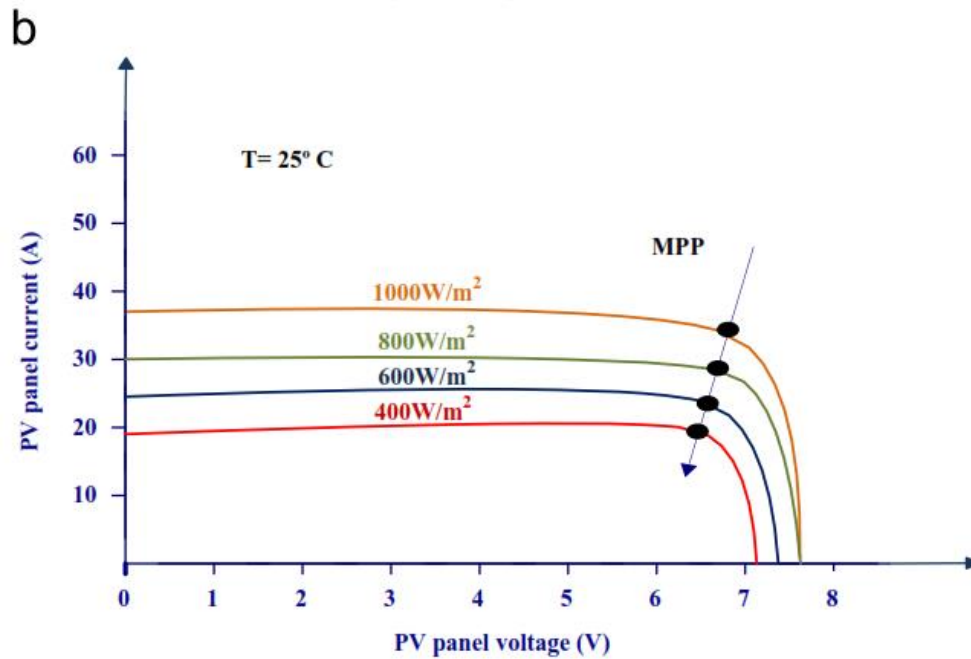


FIG.4.1.3.b – I-V characteristics at constant temperature and different insulations.

A power converter device mostly, DC/DC(buck/boost/buck–boost type) converter along with inverter (two-stage conversion) or inverter alone (single-stage conversion) as shown in FIG.4.1.4 is used in between the PV module and the load (stand-alone or grid) to achieve MPPT. These converters use some algorithm, to ensure that the PV module always operates at its MPP these algorithms are called MPPT techniques. A digital controller (microcontroller or DSP) is used to control the converter, to implement these algorithms and perform the function of MPPT. To extract maximum power from PV system a number of MPPT methods (electrical) have been proposed in literature ^[13-14].

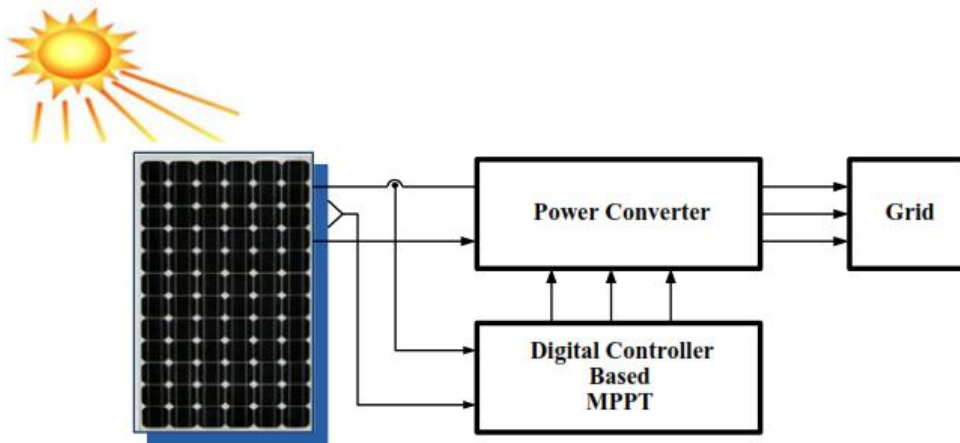


FIG.4.1.4 – Block diagram of MPPT controller for photovoltaic system

4.1.1.2. Classification of MPPT techniques

There are different ways of classifying MPPT techniques, some based on the number of variables used to track MPP like one variable or two variable methods, and some based on the type of techniques used to track MPP. The different MPPT control techniques in this thesis are classified into broadly three groups: Offline (indirect), Online (direct) and other techniques, mainly on the basis of parameters required to track MPP. FIG.4.1.5 depicts classification of different MPPT techniques.

Offline control techniques usually use technical data of PV panels to estimate the MPP. These data includes prior information like, I-V and P-V curves of the panels for different climatic conditions, different mathematical models etc. of PV panels.

Online (direct) methods on the other hand use real time, PV voltages and/or current measurements for tracking MPP. These methods do not require the measurement of temperature and solar irradiance and also the PV array model. The offline methods

are cost effective but performance wise less effective than online and other methods. Other methods include either modification or combination of these methods or methods based on indirect calculations.

4.1.2. Review of various MPPT techniques

4.1.2.1. Voltage (open circuit voltage) and current (short circuit current) based MPPT.

Voltage-and current-based MPPT are also called mathematical computational methods ^[13]. In this method, the non-linear I–V characteristics of solar panels are modelled, which are true for different atmospheric conditions. In both the methods, system requires a DC/DC converter which operates in buck or boost mode. The driver circuit for this converter and also the shunt and the series switch is controlled by a microcontroller or DSP ^[13-15].

The process of sampling of short circuit current or open circuit voltage, computing of maximum current or maximum voltage and adjusting the duty cycle is repeated to track MPP.

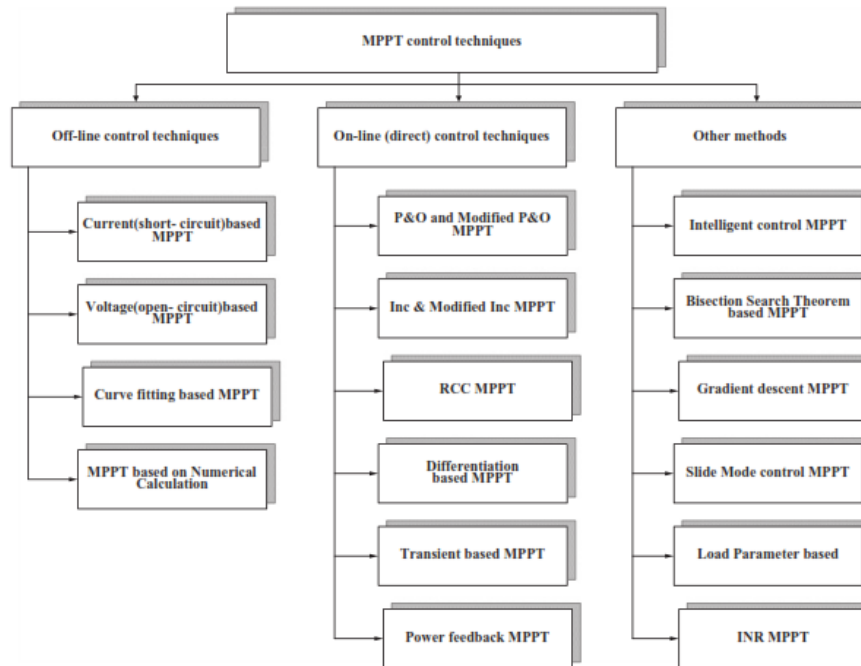


FIG.4.1.5 – Classification of MPPT techniques

4.1.2.1.1. Current (short-circuit) based MPPT

$$I_{MPP} \cong K_{mi} I_{sc} \quad (1)$$

Eq. (1) is the basis of current based technique. I_{MPP} and I_{sc} are PV panel current during MPP and short circuit condition resp. K_{mi} is proportionality constant called current factor its value varies from 0.7 to 0.9 depending upon cell material and characteristic of panel used [13]. Where [13] did not take into account the temperature dependency in the above equation, since K_{mi} is not always constant, but varies with the surface conditions of the PV panel.

Eq. (1) is plotted in FIG.4.1.6. Hardware consists of a shunt switch (power electronic) for measurement of short-circuit current by short circuiting the panel. The I_{MPP} can be computed by using

proportional controller after a hold circuit whose coefficient is K_{mi} . Short-circuit current of the panel (I_{sc}) is sampled periodically and from Eq. (1) once K_{mi} is known, I_{MPP} can be calculated for different sampled values of I_{sc} . The duty cycle of DC/DC converter is increased or decreased so that output current becomes equal to I_{MPP} .

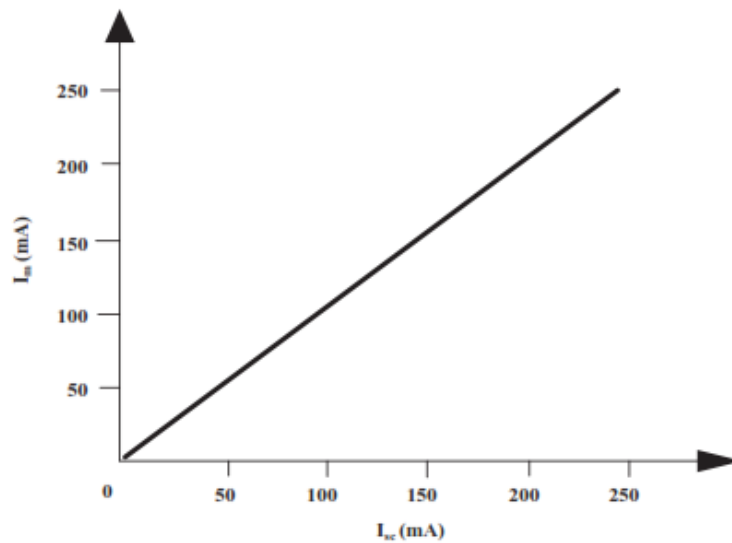


FIG.4.1.6 – Plot pertaining to Eq. (1)

4.1.2.1.2. Voltage (open-circuit) based MPPT

The maximum power point voltage V_{MPP} and open circuit voltage V_{OC} have a linear dependence for different solar radiation and operating temperatures. This is the key to develop voltage MPPT technique. Eq. (2) gives relation between V_{MPP} and V_{OC} .

$$V_{MPP} \cong K_{mv} V_{OC} \quad (2)$$

Where K_{mv} is called voltage factor and its value ranges from 0.7 to 0.95 depending upon the characteristics of the PV panel (FIG.4.1.7). In voltage based method, a series switch placed in

between panel and converter, does the measurement of open circuit voltage. The MPPT momentarily sets the PV array current to zero by open circuit and measure V_{oc} then V_{MPP} is calculated according to Eq. (1). The MPPT controller then, controls the duty cycle to obtain load voltage equals to V_{MPP} . This process is repeated periodically to get maximum power.

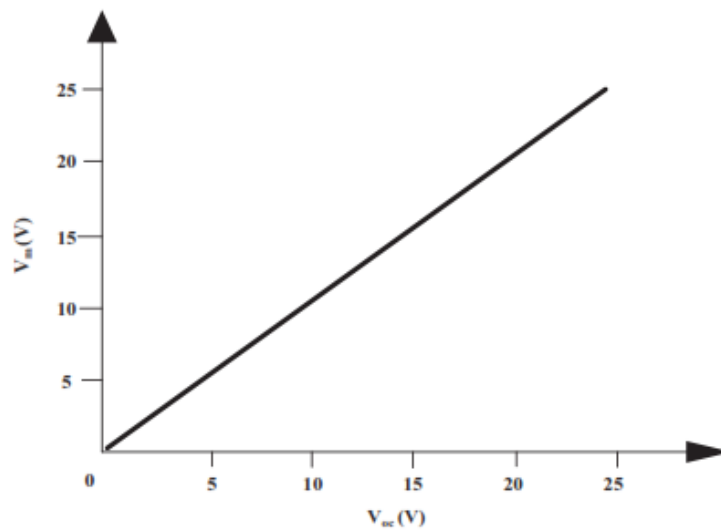


FIG.4.1.7 – Plot pertaining to Eq. (2)

Tracking speed of both techniques are high, as no derivatives are required to be calculated, sensors required are less and are practical method for MPP estimation. But major problem with both the techniques is loss of power during sampling of short circuit current and open circuit voltage. The current based method requires hardware which is more complicated and expensive as shunt switch is required and has more losses as compared to voltage based method, hardware of same rating.

Accuracy of current based technique is more compared to voltage based technique whereas, voltage based technique is more efficient and has fewer losses. The advantage of this method is

that it is simple and economic and uses only one feedback loop, but disadvantage is that it is not effective in varying temperature and insolation conditions also this method cannot be applied in the battery energy storage system. This method is used in case where insolation does not changes much for example satellite system.

4.1.2.2. Look-up table method

This is one of the offline methods of tracking MPP. In this method prior knowledge of PV panel material, technical data, panel characteristics at different environmental conditions are required and are stored. Then the PV panel output current I_{PV} and output voltage V_{PV} are sensed power is calculated and compared with those of stored values to track MPP and operating point is shifted to new maximum power point. Thus large amount of data is required to be stored before actually tracking MPP and system requires a large memory capacity to store prior data. Also, system becomes complex for varying atmospheric conditions. This method is not very accurate method of MPP tracking, number of sensors required is more and also speed of this method is slow.

4.1.2.3. Curve- fitting-based MPPT

The curve-fitting techniques is an offline technique where PV panel characteristics, technical data and other manufacturing details are required, also mathematical model and equations describing the output characteristics are decided in advance. This method is based on different models of PV panels and uses mathematical equations for these models. Based on the mathematical model and equations used, the voltage corresponding to MPP is calculated and the operating point on the characteristics of the panel is moved to track the MPP. One of

such model, where PV panel characteristic is given by Eq. (3) where α , β , γ , and δ are coefficients determined by sampling k values of PV panel output voltage V_{PV} , PV current I_{PV} and output power P_{PV} . Once these coefficients are calculated the voltage at MPP can be calculated by using Eq. (4) and MPP can tracked.

$$P_{PV} = \alpha V_{PV}^3 + \beta V_{PV}^2 + \gamma V_{PV} + \delta \quad (3)$$

At Maximum power point, $dP_{PV}/dV_{PV} = 0$

$$V_{MPP} = \frac{-\beta \pm \sqrt{\beta^2 - 3\alpha\gamma}}{3\alpha} \quad (4)$$

The advantage of this method is its simplicity, as no differentiations are to be calculated but disadvantage is that it requires prior knowledge of the PV model, mathematical equations and parameter dependence on cell material and specifications. Also, it requires large memory as the number of calculations is large. Speed is less as large computation time is required to calculate α , β , γ , and δ for different environmental conditions.

4.1.2.4. The perturb and observe method (P&O) and modified P&O MPPT

P&O is an iterative method of MPPT tracking. It senses the panel operating voltage periodically calculates and compares the PV output power with that of the previous power, then the operating voltage is changed by changing the duty ratio and change in the direction of power is observed to track MPP.

The sign of change in power is used, if the power increases by increasing voltage then the operating voltage is further perturbed in the same direction as shown in FIG.4.1.8, this process continues till $dP/dV=0$. As soon as the MPP is reached, the

voltage oscillates around the MPP, instead of being stably positioned on it, as voltage perturbation continues at MPP also. This is one of the biggest disadvantages of this method. Also, as the voltage is perturbed periodically considerable power loss takes place.

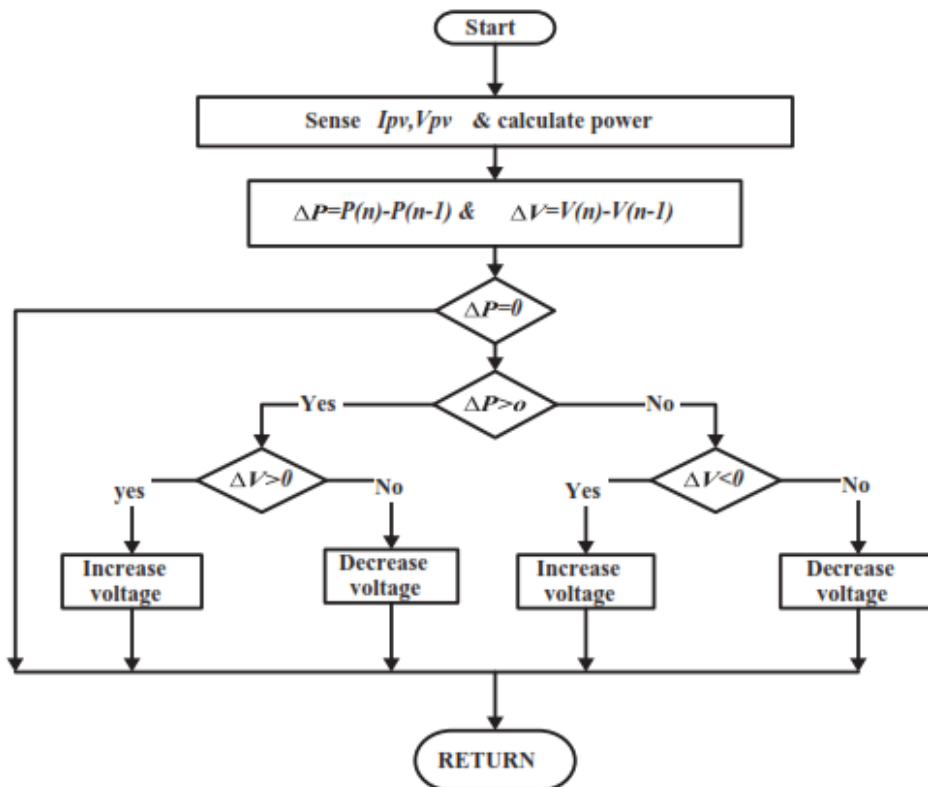


FIG.4.1.8 – Flow chart of P&O algorithm

So this method does not gives good results under rapidly changing atmospheric conditions as shown in P-V curve in FIG.4.1.9, also speed of this method is slow as it tracks the MPP in several steps. However, this method has an advantage of not requiring solar panel characteristics.

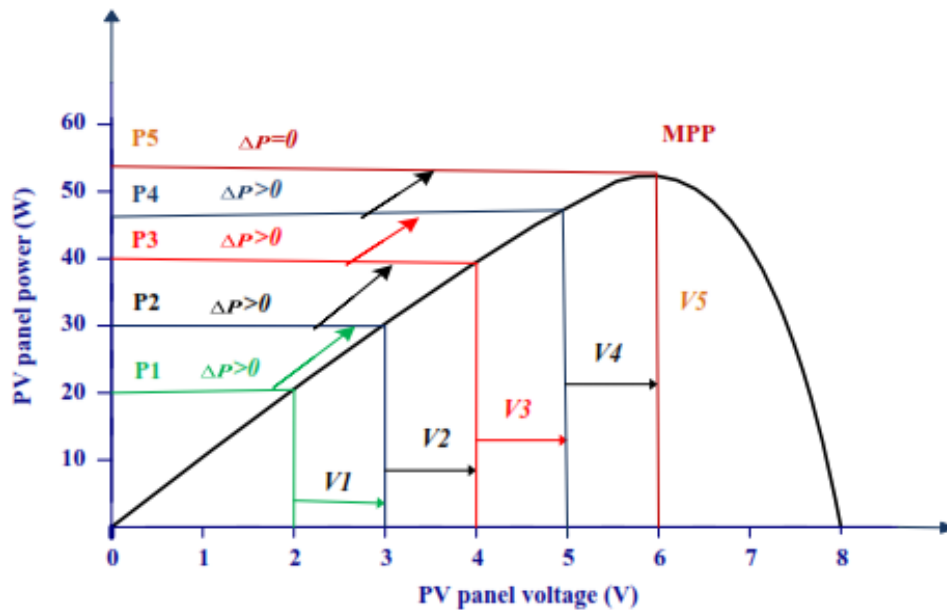


FIG.4.1.9 – P-V Curve for P&O algorithm

As shown in FIG.4.1.8, PV panel output voltage V_{PV} and output current I_{PV} are sensed. Then power is calculated $P(n)$ and compared with the power measured in the previous sample $P(n-1)$, in order to get ΔP . Then according to the sign of ΔP and ΔV , the duty cycle of the converter is changed to track MPP as summarized below.

- If the value of ΔP is zero, the system is working at MPP and no change in duty cycle is required as shown in FIG.4.1.9.
- If the value of $\Delta P > 0$ and $\Delta V > 0$, the operating point is located on the left of MPP and duty cycle is to be increased to increase the voltage so as to reach MPP.
- If the value of $\Delta P < 0$ and $\Delta V < 0$, the operating point is toward right of MPP and duty cycle must be decreased to reach MPP.

- If the value of $\Delta P < 0$ and $\Delta V < 0$, the operating point is towards left of MPP and duty cycle is to be increased to reach MPP.
- And if the value of $\Delta P < 0$ and $\Delta V > 0$, the operating point is towards right of MPP and duty cycle this time is to be decreased to reach MPP.

The conventional P&O technique tracks the MPP by perturbing the PV panel voltage or current and moves the control variable towards the MPP with fixed step size as in FIG.4.1.10. The fixed step size tracking have certain disadvantages like slow speed and large steady state oscillations. If large steps are chosen, it will result in faster dynamics but steady state oscillations also increases and efficiency decreases. On the other hand if small steps are chosen dynamics will slow down. So to overcome this problem of fixed steps, adaptive (modified) P&O algorithms are used which uses adaptive step size to increase tracking speed and reduce steady state oscillations.

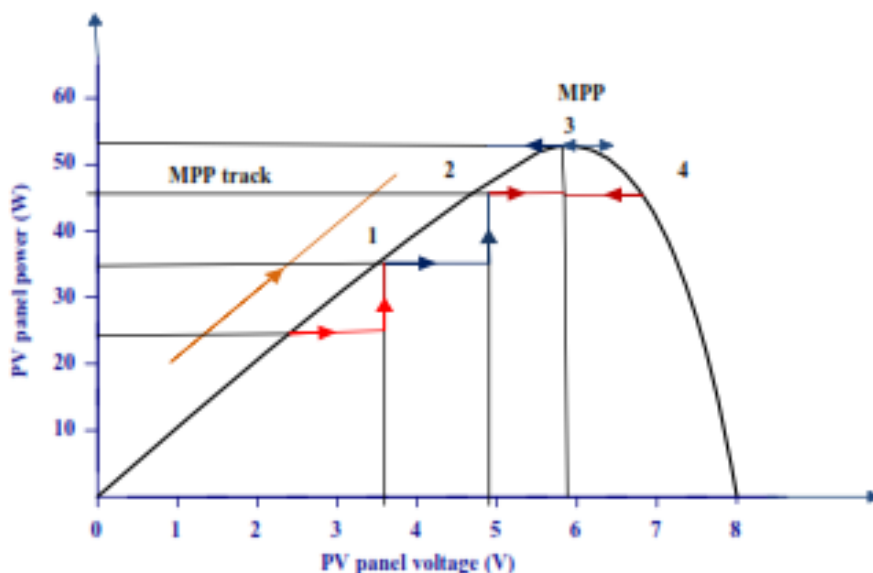


FIG.4.1.10 – Implementation of P&O method, showing oscillations around MPP

4.1.2.5. Incremental conductance method (INC) and modified INC MPPT

INC technique is widely used MPPT technique. The disadvantage of P&O method, of oscillation of operating point around MPP during changing environmental conditions can be eliminated in INC method by comparing the instantaneous panel conductance (I_{PV}/V_{PV}) with the incremental panel conductance (dI_{PV}/dV_{PV}). The voltage of MPP is tracked to satisfy $dP_{PV}/dV_{PV} = 0$, which is MPP. INC based algorithm is advantageous over other conventional methods because it is easy to implement, high tracking speed and better efficiency.

Output power from solar panel is: P_{PV} PV array output power

$$P_{PV} = V_{PV} I_{PV} \quad (5)$$

Differentiating Eq. (5) with respect to V_{PV} gives

$$dP_{PV}/dV_{PV} = I_{PV} + V_{PV} (dI_{PV}/dV_{PV}) \quad (6)$$

This equation is the basis of INC algorithm as shown in P-V curve FIG.4.1.11, at MPP

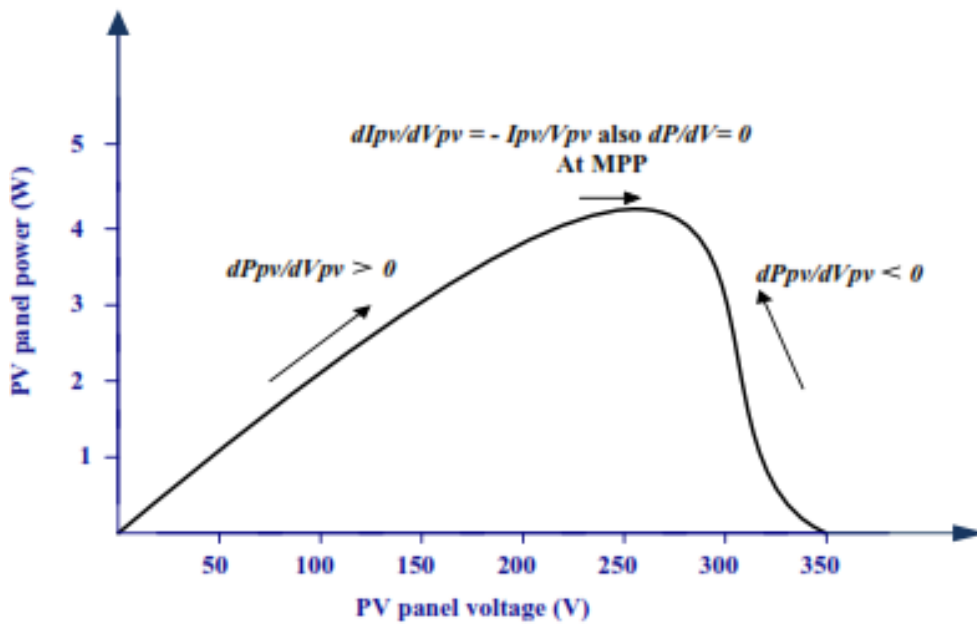


FIG.4.1.11 – P-V Curve for INC MPPT

$$dP_{PV}/dV_{PV} = 0 \quad (7)$$

$$dI_{PV}/dV_{PV} = -I_{PV}/V_{PV} \quad (8)$$

If the operating point is on the right of the power curve then we have

$$dP_{PV}/dV_{PV} < 0 \quad (9)$$

If the operating point is on the left of the power curve then we have

$$dP_{PV}/dV_{PV} > 0 \quad (10)$$

In this algorithm the present and previous values of the solar panel voltage and current are sensed and are used to calculate the values of dI_{PV} and dV_{PV} . The algorithm is as shown in FIG.4.1.12 for current based incremental conductance MPPT, similar algorithm exists for voltage based control where voltage is

sensed compared and changed. Hardware required is as shown in FIG.4.1.13 (a)

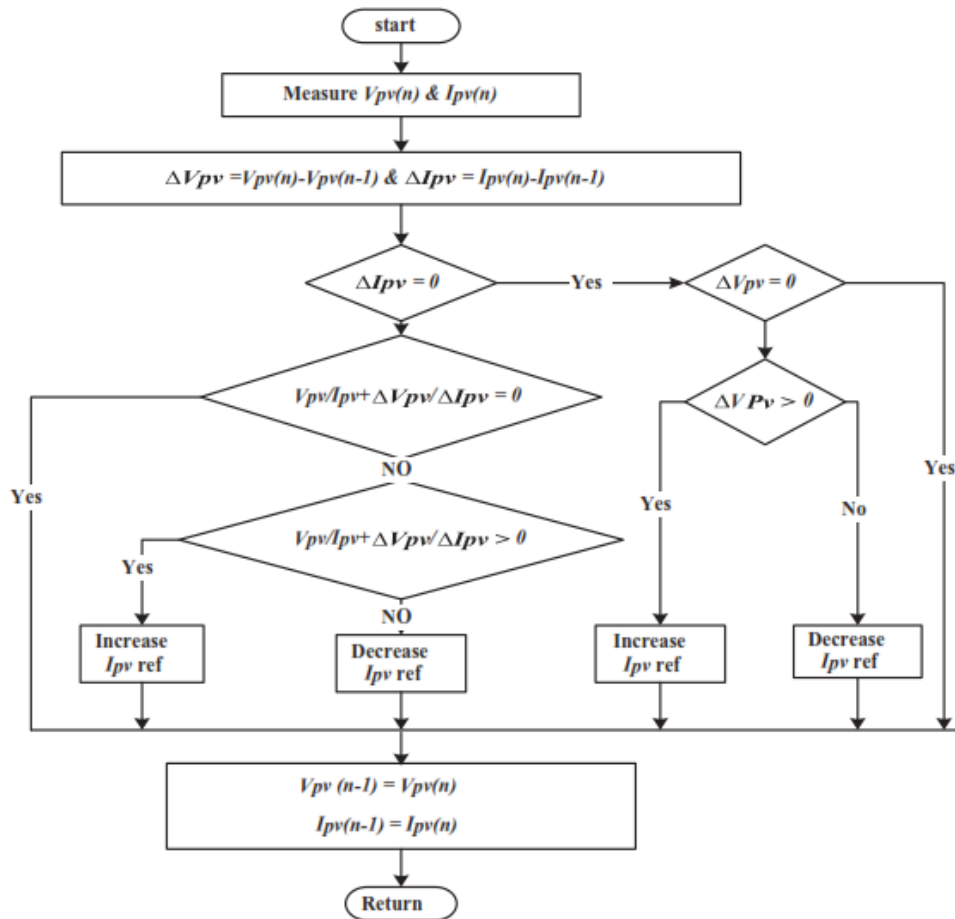


FIG.4.1.12 – Flow chart of INC method

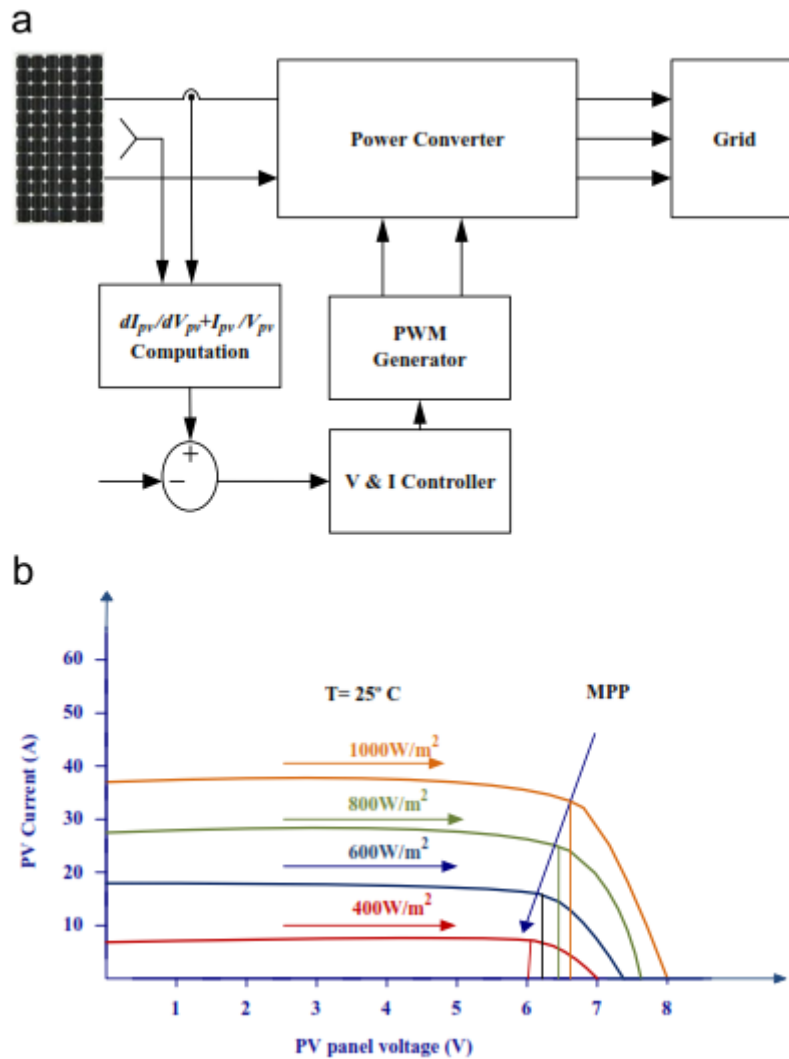


FIG.4.1.13 – (a) Hardware required for INC MPPT. (b) I-V curve for INC MPPT.

If $dV_{PV}=0$ and $dI_{PV} =0$, then there is no change in atmospheric conditions and the MPPT is still operating at MPP where $dP_{PV}/dV_{PV}=0$, reference voltage is equal to maximum voltage for this atmospheric condition and is not changed that is there is no perturbation until a change in current is sensed.

- If $dV_{PV} =0$ and $dI_{PV} >0$, if the amount of insolation increases, the PV power increases raising the MPP voltage.

This requires the MPPT to increase the operating voltage to track the MPP as shown in FIG.4.1.13 (b).

- On the other hand if $dI_{PV} < 0$, decrease in insolation lowers the PV power and also lowering the MPP voltage and this requires the MPPT to decrease the PV array operating voltage.
- If $dP_{PV}/dV_{PV} > -I_{PV}/V_{PV}$, then $dP_{PV}/dV_{PV} > 0$, and the PV array operating point is to the left of the MPP on the P–V curve. Thus, the PV panel voltage is to be increased to reach the MPP.
- Similarly, if $dI_{PV}/dV_{PV} < -I_{PV}/V_{PV}$, then $dP_{PV}/dV_{PV} < 0$ and the PV panel operating point lie to the right of the MPP on the P–V curve and the voltage must be reduced to reach the MPP.

The duty cycle of the DC/DC converter is changed accordingly which changes the PV operating voltage to track the MPP.

The problem of fixed small or large steps can be resolved, if MPPT with variable step size is used, where the algorithm changes the step size automatically according to the PV array characteristics as suggested in the variable step size (Modified) INC MPPT algorithm. If the operating point is far from MPP, the step size is increased, which enables fast tracking ability, if the operating point is near to the MPP, the step size becomes very small so that the oscillations are reduced contributing to higher efficiency. This technique gives very good results during rapidly changing atmospheric conditions with minimal oscillations and a good compromise between dynamic and steady state response. [9]

4.2

Islanded load Simulation example

In this simulation example a configuration of several components were set together to represent the actual connection between PV module, battery, inverter and the islanded loads as shown in the FIG.4.2.1 below.

The PV module "cell 2 lines series" has an input solar radiation "Qrad1", the positive pin is connected to the "PV_Switch" to enable controlling the connection of the PV module to the battery and inverter, the negative pin is grounded and the heat port is connected through a thermal connector to a fixed temperature source representing the environment temperature.

The battery model as described before in chapter 2.3 is connected to ground through the negative pin, "PV_Switch" and "Battery_Switch" through the positive pin, and the heat port is also connected through a thermal connector to a fixed temperature source representing the environment temperature.

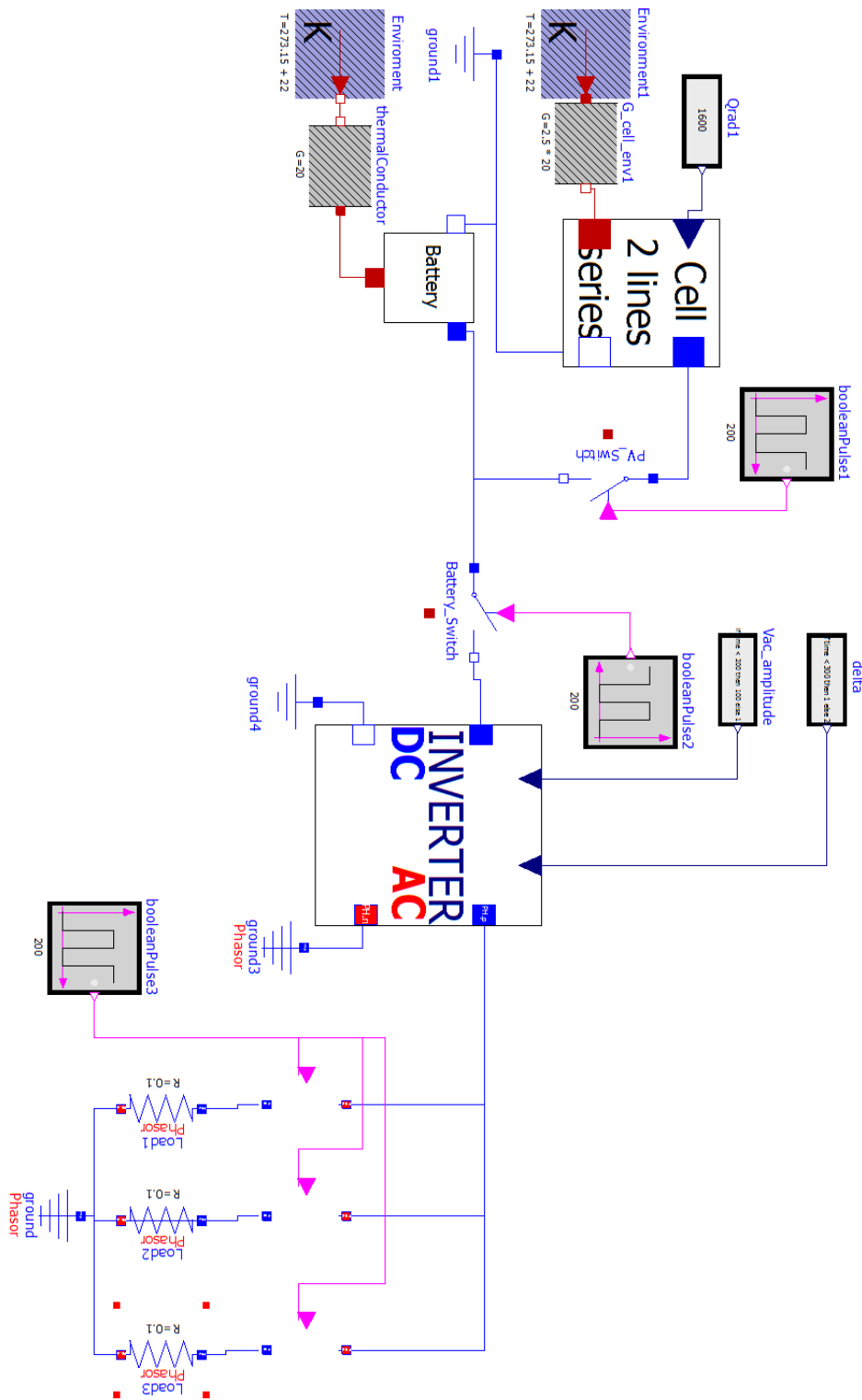


FIG.4.2.1 - Islanded load control test case configuration

The inverter model takes the DC input to DC positive Pin from the "Battery_switch" that controls the DC input power from Battery and PV module, the DC negative pin is connected to ground, Inverter inputs are connected to the phase angle "delta" and the amplitude value of the voltage "Vac_amplitude" so it can give the controlled output voltage across its positive and negative AC pins, the AC negative pin is connected to a phasor ground described in chapter 3.3 as all the AC terminals in this thesis are treated in a phasor form to be easy for the Modelica compiler to simulate in a short time, and the AC positive pin is connected to the load through Phasor switches.

The Islanded load is represented by three phasor resistances to act as an AC load and feed by power that comes from the inverter through the controlled phasor switches of each phasor resistance, and the other side is connected to the phasor ground.

The switches are manipulated to control the connection of each model to the other parts of the islanded network for more control and they are also existing in real life expressed by the circuit breaker of each component that controls the connection of this part to the network or isolate it in case of fault or maintenance.

In this simulation example, the Boolean pulse sources are used to represent the control signal of opening or closing the switches to connect a model or isolate it from the islanded network.

The "PV_Switch" is usually closed to connect the PV module to the battery to charge it, as long as the PV module is generating power during daylight hours, while the "Battery_Switch" is used to control the connection of generated power to the inverter whenever there is a load to be feed, through closing the "Battery_Switch" the inverter is put to online to feed the load with

the assigned voltage through the inverter inputs (voltage amplitude and phase angle), and the last three phasor switches of the islanded load are used to control the connection of loads to the network as usually not all the loads are switched together all the time; so representing it in these three separate phasor resistances gives the availability of simulating load variation in the network for more realistic simulation of the network.

For more clear simulation results, showing the change in response according to each input change; the value of inverter input amplitude voltage was increased at time 100 and the inverter input phase angle was increased at time 200.

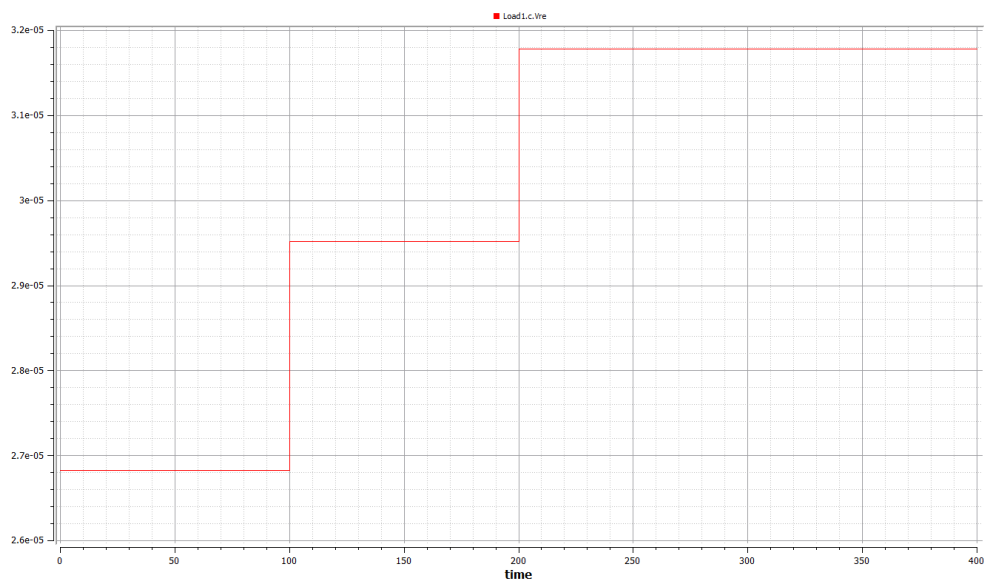


FIG.4.2.2 – Islanded load test real voltage

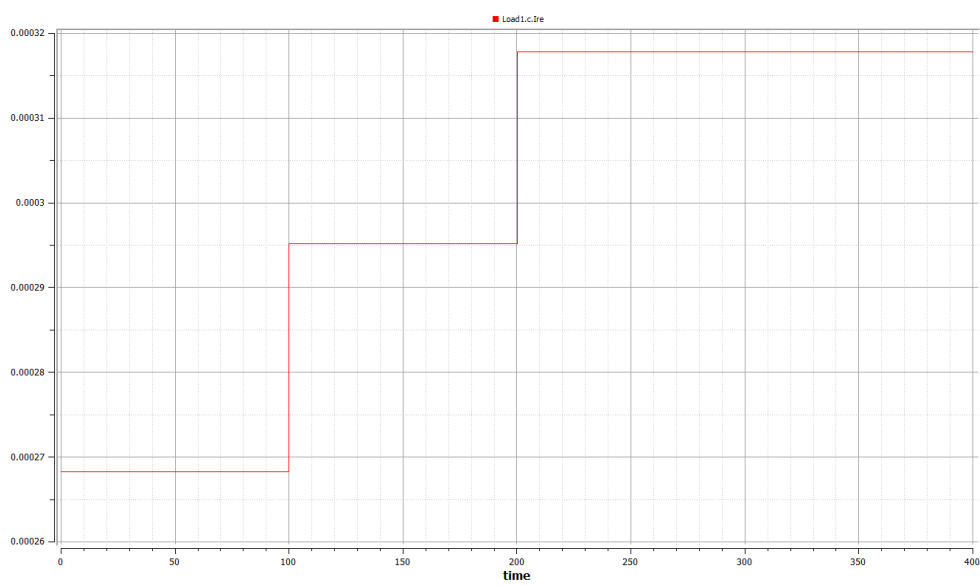


FIG.4.2.3 – Isolated load test real current

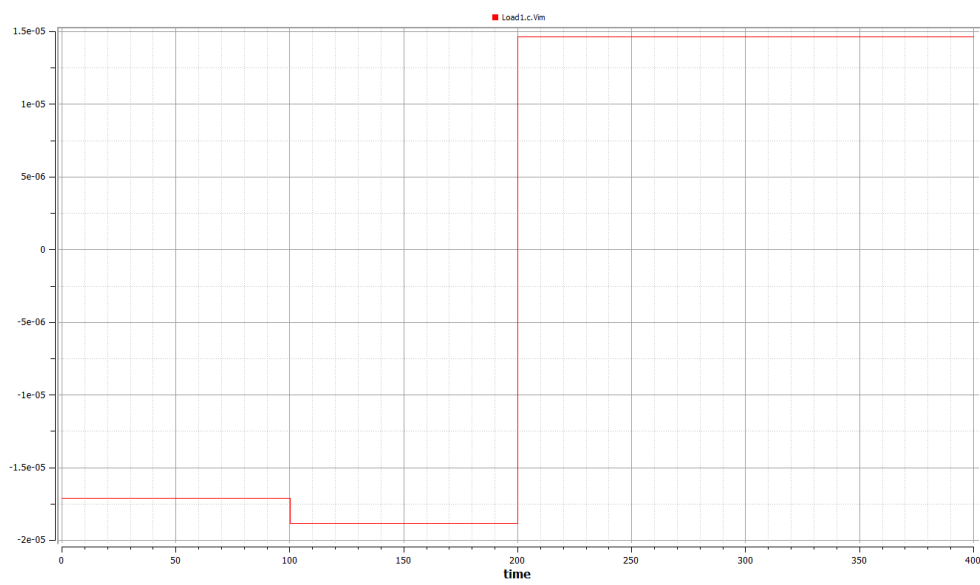


FIG.4.2.4 – Isolated load test imaginary voltage

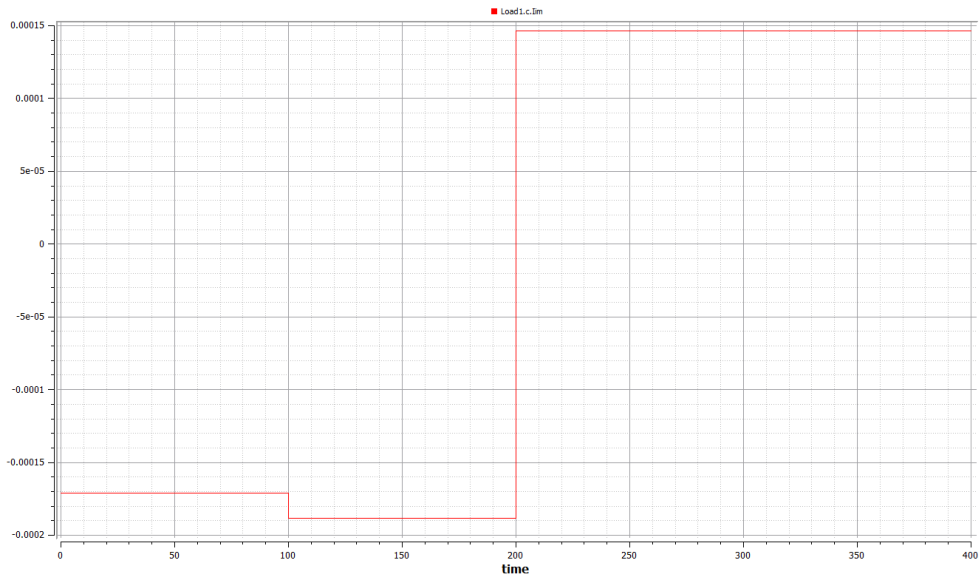


FIG.4.2.5 – Islanded load test imaginary current

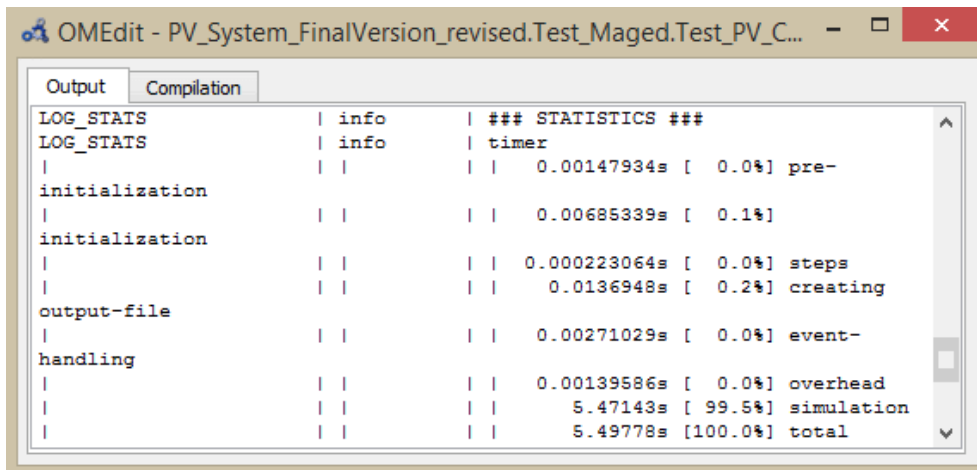


FIG.4.2.6 – Islanded load test simulation time

The effect of changing the voltage amplitude had its influence on the corresponding change in the output real and imaginary voltages and currents. As shown in the above figures 4.2.2,3,4,5 the results of the real and imaginary voltages and currents show a similar behaviour as the inverter test results in chapter 3.3, as

expected because the output of the inverter is directly connected to the load without any other influence in between.

And we can see in the FIG.4.2.6 the total simulation time of the whole test (5.49sec.) that indicates the saves of compiler simulation time due to the reasonable approximations mentioned in each individual model component.

4.3

Grid connected Simulation example

In the Grid connected simulation example the same configuration of PV module, Battery, Inverter and load are used as in the previous example of chapter 4.2, but in this example a new component is added as shown in FIG.4.3.1 below, as to connect the load to be fed from the grid whenever the PV generation is not available or to connect the PV generated power to the grid when the generated power is more than the connected load and this is done through adding a phasor commutating switch between the inverter, the grid and the load to allow always the connection of 2 terminals only out of the three, and this is expressed in reality by the Automatic transfer switch "ATS" which is always used when there are multiple sources feeding the same load.

The manual control of the ATS of the commutating switch in this example is done by the Boolean pulse source for simple simulation purposes, while in reality more complicated control scheme is used to control the ATS and a lot of factors has to be considered before synchronization with the grid as manipulating the inverter output voltage and frequency.

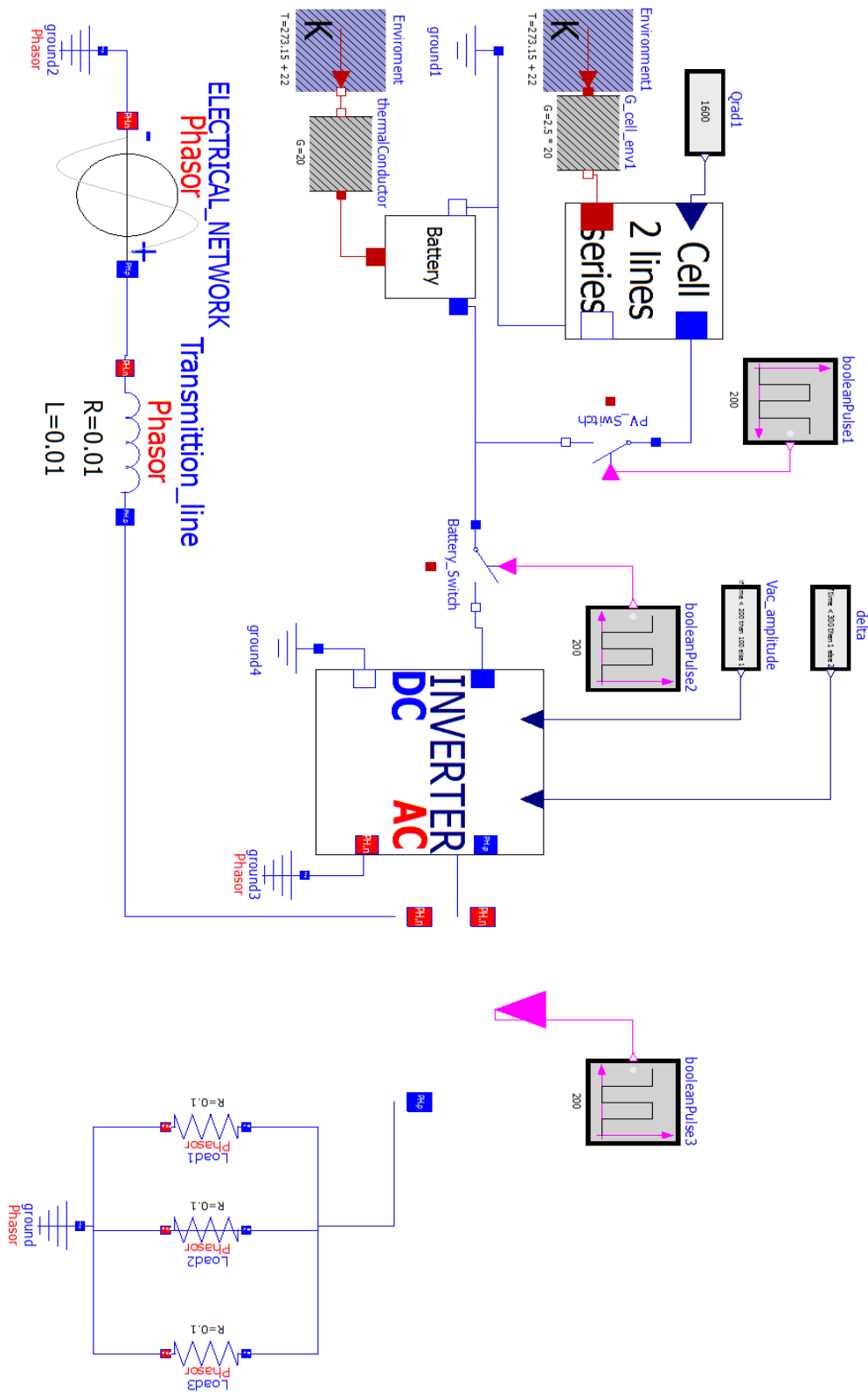


FIG.4.3.1 – Grid connected control test case configuration

For more clear simulation results, showing the change in response according to each input change; the value of inverter input amplitude voltage was increased at time 100, the inverter input phase angle was increased at time 200 and the commutating switch position was changed at time 300 to change the feeding of the load from the PV generation to be fed by the Electrical network.

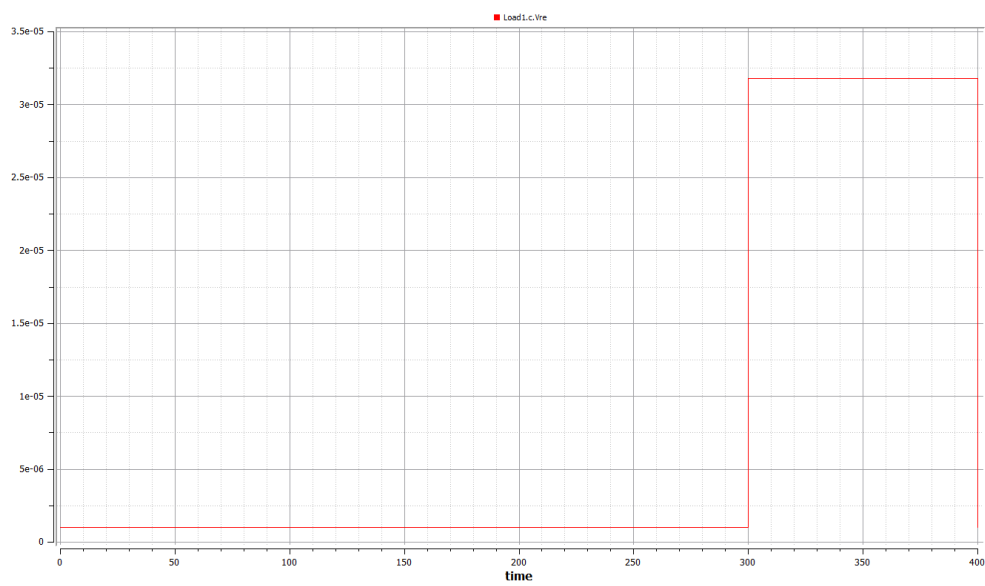


FIG.4.3.2 – Grid connected test real voltage

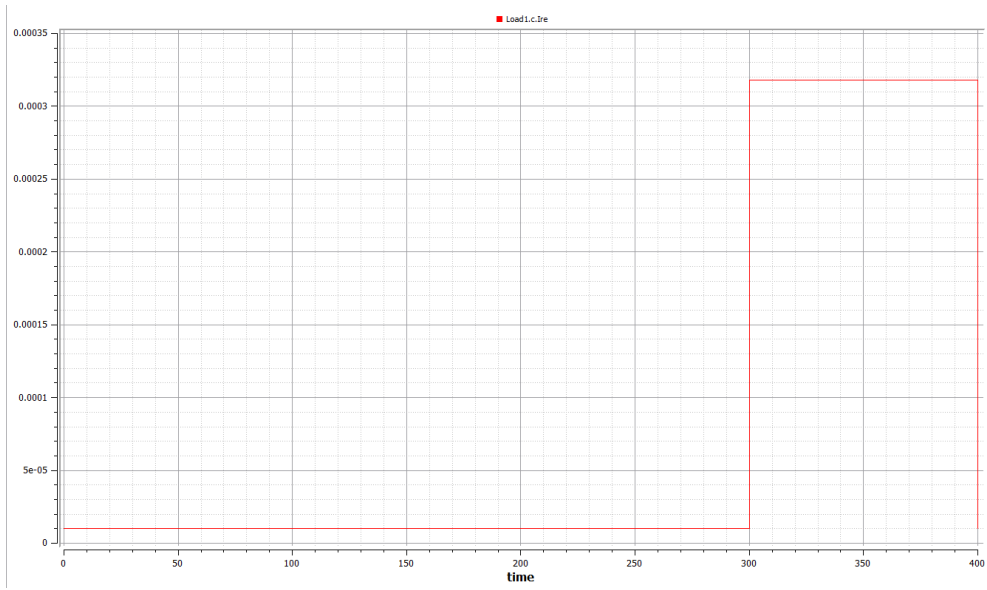


FIG.4.3.3 – Grid connected test real current

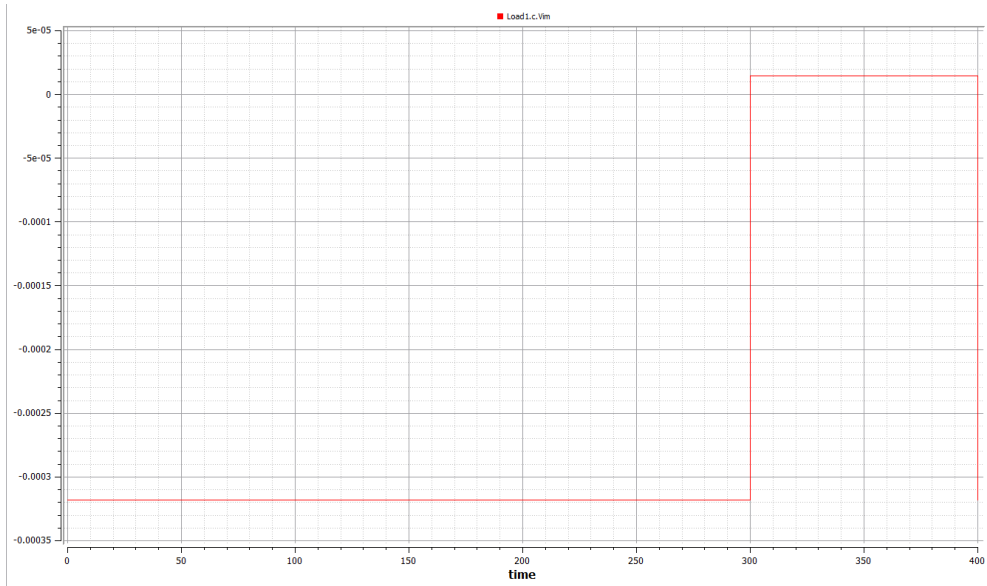


FIG.4.3.4 – Grid connected test imaginary voltage

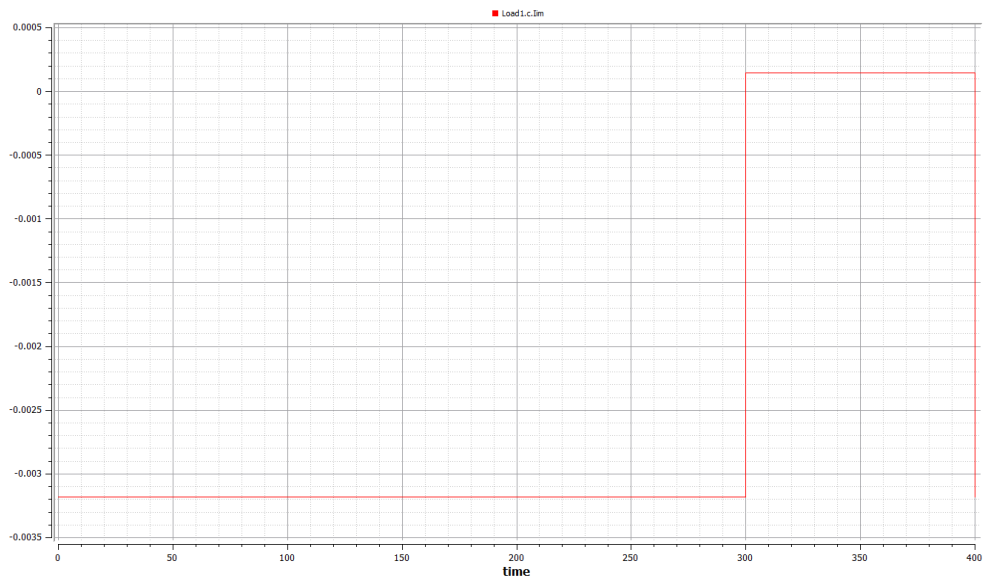


FIG.4.3.5 – Grid connected test imaginary current

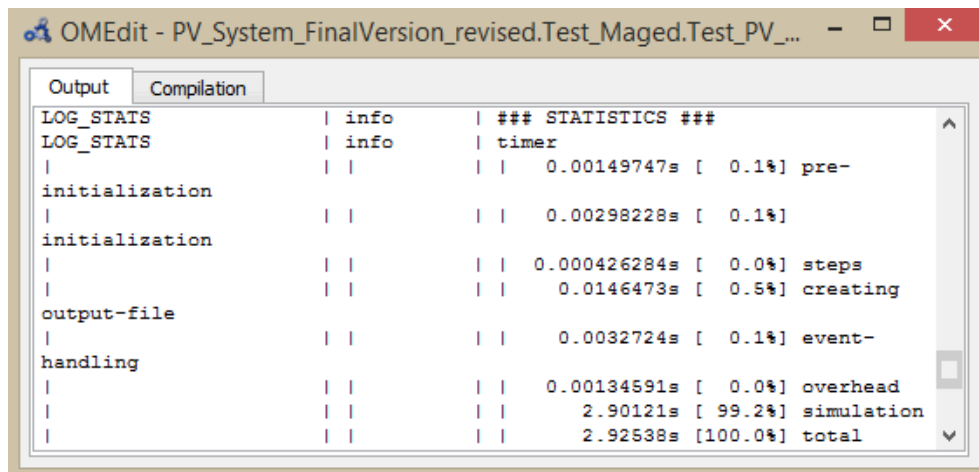


FIG.4.3.6 – Grid connected test simulation time

In the above figures 4.3.2,3,4,5 the change in the real and imaginary voltages and currents of the phasor load at time 300 reflects the change of the power source from the PV system to the Grid after according to the commutator switch control signal. Also FIG.4.3.6 shows the total simulation time of 2.9 seconds.

5

CHAPTER FIVE

CONCLUSION AND
FUTURE WORKS

CONCLUSION AND FUTURE WORKS

Generalized models for PV system and its control were developed and verified in Modelica language, which allow the future research to build more detailed models and change the parameters to expand its functionality to match other types of the models easily. A library of mathematical models were developed for each individual element of a PV system, namely solar cells, battery, inverter, phasor loads, simulation and control models for both cases standalone and connected to grid systems. The modules have been designed in the form of Modelica block library. The masked icons make the block model more user-friendly and dialog boxes let the user configure easily the designed PV system modules.

The validation of these mathematical models was performed through the comparison between the simulation results and the theoretical analysis acquired from literature. The validation of each individual component model has concluded the following remarks:

PV module model: reflects in a significant way the effect of change in solar radiation and ambient temperature on the I-V characteristic curve of the solar cell. The approximation of the I-V curve into equivalent two line equations saved the compiler calculation time and increased the efficiency of the simulation but

also I-V curve could be introduced to the model in the form of table values for more detailed interpolation and easier MPPT control. Also using the heat port was important in studying the heat transfer which gives more accuracy for the model to calculate the actual temperature of the cell and how it can be used in research to improve the energy optimization of the PV cell.

Battery: it reflects properly the influence of the temperature on the battery dynamics as the battery voltage, internal resistance and maximum capacity. Modelling based on the use of electric equivalent circuit models mixed with black box approach gives the model the balance between simplicity, efficiency and adequacy for short and long term simulations. The V-SOC curves were also approximated to second degree polynomial to closely match the real curves and increase the simulation efficiency, saving compiler calculation time. And for future works the polynomial could be introduced as data tables from practical data sheets to match the exact curves or other battery types.

Inverter: the efficiency and performance of renewable energy sources can be increased by the development of the control structures of the grid connected inverters. An input DC power converted to output AC power with a prescribed efficiency and controlled according to the input variables defining the voltage amplitude and phase was an easy and simple structure imitates the major behaviour of the inverter. The phasor study of AC components saved the energy of the compiler from going through complex equations.

And through implementing these individual components models it was noticed that some points is needed to be revealed in future works such as:

- A better understanding and modelling of the non-linear dynamics of the battery. More battery tests are necessary to get more information about how to improve the model relation between state of charge and battery voltage dynamics. Besides the influence of the temperature on the battery and its aging.
- Control structures equipped with protection algorithms for the battery against excess discharge at the inverter side and overcharging of the battery from the PV module side.
- A further analysis of the PV module regarding the simulated efficiency of the modules, the approximated cell temperature and the PV module's performance sensitivity like real life conditions and ageing of the cells.
- Tests viewed for the whole PV system not as individual components.

LIST OF FIGURES

CHAPTER ONE

FIG 1.4.1	Block diagram of a general control scheme of PV system	7
-----------	--	---

CHAPTER TWO

FIG 2.1.1	Model for a single solar cell	12
FIG 2.1.2.a	PV cell I-V curve at different solar radiation.....	13
FIG 2.1.2.b	PV cell I-V curve at different temperature	14
FIG 2.1.3	Typical solar cell I-V curve	14
FIG 2.1.4	Influence of ambient radiation (a) and cell temperature (b) on the cell characteristics	17
FIG 2.1.5	Series (a) and parallel (b) connection of identical cells.....	18
FIG 2.1.6	PV module consists of NPM parallel branches, each of NSM solar cells in series.....	19
FIG 2.1.7	Nominal and standard conditions	20
FIG 2.2.1	Battery schematic diagram.....	23
FIG 2.2.2	Influence of ambient radiation on the cell	25
FIG 2.2.3	A simplified electric equivalent network model of a cell (neglecting the parasitic reactions).....	26
FIG 2.3.1	Connection of the inverter.....	29
FIG 2.3.2	General structure for synchronous controller	33
FIG 2.3.3	Two-level three-phase inverter configuration.....	35
FIG 2.3.4	Six active vectors and two null vectors in SVM...	35
FIG 2.3.5	SVM switching patterns for sector 1.....	37

FIG 2.3.6	Basic structure of a PLL system for grid synchronization.....	38
-----------	---	----

CHAPTER THREE

FIG 3.1.1	TQ/IV curve Modelica icon.....	41
FIG 3.1.2	TQ/IV curve Modelica diagram	42
FIG 3.1.3	Cell 2 lines Modelica icon.....	44
FIG 3.1.4	Cell 2 lines char Modelica diagram.....	45
FIG 3.1.5	IV-Curve.....	47
FIG 3.1.6	Cell 2 lines Modelica icon.....	49
FIG 3.1.7	Cell 2 lines Modelica diagram.....	49
FIG 3.1.8	Cell 2 lines parameters	50
FIG 3.1.9	BP 3125 datasheet	51
FIG 3.1.10	cell 2 lines test configuration	51
FIG 3.1.11	Cell 2 lines output current	52
FIG 3.1.12	Cell 2 lines output voltage.....	52
FIG 3.1.13	Cell 2 lines output power.....	53
FIG 3.1.14	Cell Series output current.....	54
FIG 3.1.15	Cell Series output voltage	54
FIG 3.1.16	Cell Series output power	55
FIG 3.1.17	Cell parallel output current.....	55
FIG 3.1.18	Cell parallel output voltage.....	56
FIG 3.1.19	Cell parallel output power	56
FIG 3.1.20	Cell Heat port temperature.....	57
FIG 3.2.1	Battery Modelica icon	58
FIG 3.2.2	Battery Modelica diagram.....	59
FIG 3.2.3	V-SOC-curve	60
FIG 3.2.4	Battery Parameters	63
FIG 3.2.5	Battery capacity vs temperature	64
FIG 3.2.6	Battery voltage vs temperature	64
FIG 3.2.7	Battery internal resistance vs temperature	65

FIG 3.2.8	Battery test configuration.....	65
FIG 3.2.9	Battery charging current	66
FIG 3.2.10	Battery discharging current	67
FIG 3.2.11	Battery heat port temperature	67
FIG 3.3.1	Phasor pins	69
FIG 3.3.2	Phasor pins variables'	69
FIG 3.3.3	inverter Modelica icon	69
FIG 3.3.4	inverter Modelica diagram	70
FIG 3.3.5	inverter parameters	71
FIG 3.3.6	inverter test islanded case configuration	72
FIG 3.3.7	inverter test islanded case DC input	73
FIG 3.3.8	inverter test islanded case AC current.....	73
FIG 3.3.9	inverter test islanded case AC voltage	74
FIG 3.3.10	inverter test grid case configuration	75
FIG 3.3.11	inverter test Grid connected case DC input.....	76
FIG 3.3.12	inverter test Grid connected case AC current	76
FIG 3.3.13	inverter test Grid connected case AC voltage	77

CHAPTER FOUR

FIG 4.1.1	operating principle of an overcharge protector ...	80
FIG 4.1.2	operating principle of a discharge protector	80
FIG 4.1.3.a	P-V characteristics at constant temperature and different insulations.....	82
FIG 4.1.3.b	I-V characteristics at constant temperature and different insulations.....	83
FIG 4.1.4	Block diagram of MPPT controller for photovoltaic system	84
FIG 4.1.5	Classification of MPPT techniques	86
FIG 4.1.6	Plot pertaining to Eq. (1).....	87
FIG 4.1.7	Plot pertaining to Eq. (2).....	88
FIG 4.1.8	Flow chart of P&O algorithm	91

FIG 4.1.9	P-V Curve for P&O algorithm	92
FIG 4.1.10	Implementation of P&O method, showing oscillations around MPP.....	93
FIG 4.1.11	P-V Curve for INC MPPT	95
FIG 4.1.12	Flow chart of INC method.....	96
FIG 4.1.13.a	Hardware required for INC MPPT	97
FIG 4.1.13.b	I-V curve for INC MPPT	97
FIG 4.2.1	Islanded load control test case configuration ...	100
FIG 4.2.2	Islanded load test real voltage	102
FIG 4.2.3	Islanded load test real current	103
FIG 4.2.4	Islanded load test imaginary voltage	103
FIG 4.2.5	Islanded load test imaginary current	104
FIG 4.2.6	Islanded load test simulation time.....	104
FIG 4.3.1	Grid connected control test case configuration .	107
FIG 4.3.2	Grid connected test real voltage.....	108
FIG 4.3.3	Grid connected test real current.....	109
FIG 4.3.4	Grid connected test imaginary voltage	109
FIG 4.3.5	Grid connected test imaginary current	110
FIG 4.3.6	Grid connected test simulation time.....	110

REFERENCES

- [1] Huan-Liang Tsai, Ci-Siang Tu, and Yi-Jie Su, Development of Generalized Photovoltaic model using matlab-simulink.
- [2] Jihad Bou Merhi, Jana Chalak, and Joya Zeitouny, Estimation of Battery Internal Parameters.
- [3] Anca D. Hansen, Poul Sørensen, Lars H. Hansen and Henrik Bindner, Models for a stand-alone PV system.
- [4] S. W. Angrist, , Direct Energy Conversion, Allyn and Bacon, Inc., 4th edition, 1982, pp. 177-227.
- [5] J. C. H. Phang, D. S. H. Chan, and J. R. Philips, "Accurate analytical method for the extraction of solar cell model parameters," Electronics Letters, vol. 20, no. 10, 1984, pp.406-408.
- [6] Massimo Ceraolo, Tarun Huria, Rechargeable lithium battery energy storage systems for vehicular applications, PHD thesis.
- [7] R. A. Huggins, "*Advanced batteries: materials science aspect*", Springer, 2008. ISBN 0-3877-6423-2
- [8] Abdelhalim Zekry, A. Alshazly, A. Abdelrahman, *Simulation and implementation of grid-connected inverters*, International Journal of Computer Applications (0975 – 8887), Volume 60– No.4, December 2012.
- [9] Pallavee Bhatnagar, R.K. Nema, Maximum power point tracking control techniques; State-of-the-art in photovoltaic applications.
- [10] Z.M. Salameh, M.A. Casacca, W.A. Lynch, "A Mathematical Model for Lead-Acid Batteries", IEEE Trans. Energy Conversion, vol. 7, issue 1, pp. 93-97, Mar. 1992, doi:10.1109/60.124547.
- [11] M. Chen, G.A. Rincon-Mora, "Accurate electrical battery model capable of predicting Runtime and I_V Performance," IEEE Trans. Energy Conversion, vol. 21, no. 2, pp. 504-511, Jun. 2006, doi:10.1109/TEC.2006.874229
- [12] Ceraolo, M., "New Dynamical Models of Lead-Acid Batteries", IEEE Trans. Power Systems, vol. 15, no. 4, pp. 1184-1190, Nov. 2000, doi:10.1109/59.898088.
- [13] Kobayashi K, Takano I, Sawada Y. A study on a two stage maximum power point tracking control of a photovoltaic system under partially shaded insolation conditions. In: IEEE Power Engineering Society General Meeting 2612–2617. 2003.
- [14] Al Nabulsi A, Dhaouadi R. Efficiency optimization of a DSP-based standalone PV system using fuzzy logic and dual-MPPT control. IEEE Transactions on Industrial Informatics 2012;8(3):573–84.

[15] Kashif Ishaque, Zainal Salam, A review of maximum power point tracking techniques of PV system for uniform insolation and partial shading condition.

[16] Olaf Enge, Christoph Clauß, Peter Schneider, Peter Schwarz, Quasi-stationary AC Analysis using Phasor description With Modelica.

[17] Hakan Doğan Parıldar, Alberto Ieva, mixed time & phasor domain modelling of electric networks For simulation efficiency.